THE UNIVERSITY OF MICHIGAN

INDUSTRY PROGRAM OF THE COLLEGE OF ENGINEERING

THE EFFECT OF LONGITUDINAL OSCILLATIONS ON FLUID FLOW AND HEAT TRANSFER FROM VERTICAL SURFACES IN FREE CONVECTION

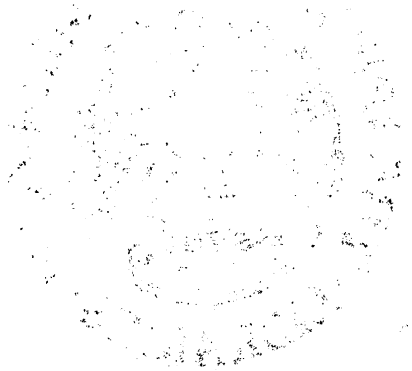

Siavash Eshghy

May, 1963

IP-621

ACKNOWLEDGMENTS

The author wishes to express his sincere gratitude to Professor Vedat S. Arpaci, Chairman of the Doctoral Committee, under whose direction this work was performed. Gratitude is extended to Professor John A. Clark, project supervisor and Director of the Heat Transfer and Thermodynamics Laboratory. The writer is grateful to Professors Arthur G. Hansen, Robert C. Juvinall and Ruel V. Churchill for their interest and cooperation.

The research reported herein is part of the research program on heat transfer of unsteady flows of the Aeronautical Research Laboratory, Office of Aerospace Research of the United States Air Force whose support is acknowledged. The assistance of Dr. M. G. Scherberg of this Laboratory is appreciated.

The research support of the National Science Foundation, Grant No. 9386, and the fellowship support of the Iranian Ministry of Education, are gratefully acknowledged.

Many thanks go to Mrs. Norlene Martin, Mrs. Alice DeRienzo, and to the Industry Program of the College of Engineering for their help in the preparation of the manuscript.

TABLE OF CONTENTS

TABLE OF CONTENTS (CONT'D)

LIST OF FIGURES

LIST OF FIGURES (CONT'D)

LIST OF FIGURES (CONT'D)

LIST OF FIGURES (CONT'D)

NOMENCLATURE

a	Thermal diffusivity of the fluid
A	Amplitude of oscillation
$A_1 \ldots A_5$	Functions of Prandtl number
A_T	Total heat transfer area
B	Coefficient of η in the second approximation velocity profile
B_1	Coefficient of η_θ in the second approximation temperature profile
$C_1 \ldots C_5$	Functions of Prandtl number
$D_1 \ldots D_3$	Functions of Prandtl number
E_n	Notation defined as being 'i' when n is odd and '1' when n is even
f	Friction factor
fr	Frequency, cycles per unit time
$F(\eta)$	η dependency of steady free-convection stream function
g	Gravitational acceleration
$G(\Delta)$	A polynomial function of Δ
Gr_x	Grashof number, $\beta g \theta_w x^3/\nu^2$
Gr_ℓ	Grashof number, $\beta g \theta_w \ell^3/\nu^2$
h	Coefficient of heat transfer
$H(\eta)$	Dimensionless temperature function in steady free convection
i	Positive square root of -1, $\sqrt{-1}$
k	Thermal conductivity
K	A constant
ℓ	Characteristic length
n	Dummy integer in the series

Nu_x	Local Nusselt number, hx/k
Nu_ℓ	Average Nusselt number, $\frac{1}{k}\int_0^\ell h\,dx$
p	Fluid pressure
Pr	Prandtl number of the fluid
q	Rate of heat transfer
Re_x	Reynolds number, $U_\infty x/\nu$
Re_ℓ	Reynolds number, $U_\infty \ell/\nu$
$S(\Delta)$	A polynomial function of Δ
t	Time variable
T	Temperature of the fluid
u	x-directional velocity of the fluid
$U(t)$	Potential flow function
U_o	Coefficient of $\epsilon \cos \omega t$ in the expression for $U(t)$
U_∞	Uniform velocity outside the boundary layer
v	y-directional velocity of the fluid
$V(\Delta)$	A polynomial function of Δ
$V_o(x)$	Velocity function in the steady-state integral solution, $\beta g \Theta_w \delta^2/6\nu$
$\bar{V}_o$	A constant defined as $\beta g \Theta_w/6\nu$
$W(\Delta)$	A polynomial function of Δ
x	Distance along the plate
$X(\Delta)$	A polynomial function of Δ
y	Distance perpendicular to the wall
$Y(\Delta)$	A polynomial function of Δ
$Z(\Delta)$	A polynomial function of Δ

Greek Letters

$\alpha_o \ldots \alpha_{11}$	Functions of Prandtl number
β	Coefficients of volume expansivity at constant pressure
$\beta_1 \ldots \beta_9$	Functions of Prandtl number
γ_n	Coefficients of the series solution for B
δ	Velocity boundary layer thickness
δ_Θ	Thermal boundary layer thickness
δ_{ij}	Kronecker delta
Δ	Ratio of boundary layer thicknesses, δ_Θ/δ
ϵ	$\lvert U(t)\rvert/u_{o_{max}}$
ϵ_m	Emissivity of the radiating surface
η	Steady-state similarity parameter, y/δ
η_Θ	Steady-state similarity parameter, y/δ_Θ
Θ	Temperature difference, $T - T_\infty$
λ_n	Coefficients of the series solution for B_1
μ	Viscosity of the fluid
ν	Kinematic viscosity of the fluid
ξ	Dimensionless boundary layer thickness, δ/ℓ
π_1	A dimensionless number, $\beta g \Theta_w \ell^2/\nu U_o$
π_2	A dimensionless number, $\beta g \Theta_w \delta^2/\nu U_o$
ρ	Fluid density
σ	The Stefan-Boltzmann constant
τ_w	Shear stress at the wall
φ	Phase angle
ψ	Steady-state stream function

ω	Circular frequency, radiants per unit time
ω^*	Frequency parameter, $\omega\delta^2/\nu$
Ω	Dimensionless frequency, $\omega\ell^2/\nu$

Subscripts

W	Condition at the wall (y = 0)
∞	Condition outside the boundary layer
o	First approximation
1	Second approximation
2	Third approximation
20	Steady component of the third approximation
21	Oscillating component of the third approximation

LIST OF COMPLEX QUANTITIES

B

B_1

f_1

f_{21}

h_1

Nu_1

Nu_{21}

u_1

u_{21}

v_1

v_{21}

Θ_1

Θ_{21}

τ_{w1}

CHAPTER I

INTRODUCTION

Much work has been published on the analytical treatment of problems in steady as well as unsteady laminar free convection. Schmidt and Beckmann, 1930,[1] S. Ostrach, 1952,[2] E. M. Sparrow and J. L. Gregg, 1956[3] and 1958,[4] Finston, 1956,[5] Millsaps and Pohlhausen, 1958[6] and some others have obtained analytical solutions for steady heat transfer from vertical plates and cylinders, each using a different condition at the wall. Yang, 1960,[7] lists possible similarity (exact) solutions for the steady free convection flow and heat transfer as follows:

1. From a vertical flat plate with
   a. Prescribed constant surface temperature
   b. Surface temperature varying with any power of a linear function of x.
   c. Surface temperature varying with an exponential function of x.
2. From a vertical circular cylinder with surface temperature varying linearly with x.

In the above four cases, the restrictions are imposed only on surface temperature, however, for each case, one can find the similar restrictions on the surface heat flux. Sugawara and Michiyoshi, 1951[8] obtained approximate solutions, valid for small time, for momentum and energy equations in the case of a step change in the surface temperature of a vertical flat plate. Siegel, 1958[9] treated both the above case and that

of a step change in surface heat flux; he used integral techniques on the boundary-layer form of momentum and energy equations. Their work was followed by a few unsteady exact solutions in which similarity techniques were used exclusively. Yang,[7] presents possible unsteady exact solutions obtainable by the similarity technique. These are:

1. For the case of a vertical flat plate.
   a. Unsteady free convection with surface temperature varying inversely as a linear combination of x and t.
   b. Surface temperature varying directly with a linear function of x and inversely with the square of a linear function of t.
   c. Uniform but unsteady surface temperature variation at large distance x.
2. For the case of a vertical circular cylinder, uniform but unsteady surface temperature at large values of x.

In all of the above cases, the cause of the transient is some unsteady thermal condition at the wall. Chung and Anderson, 1961[10] treat the case of free convection from a vertical plate and a horizontal cylinder in which Grashof number is an arbitrary function of time. The solution obtained applies when either the uniform wall temperature or the acceleration field is arbitrarily time dependent. Their analytical approach is a combination of similarity and successive approximation techniques.

In recent years much attention has been focused on unsteady convection heat transfer caused by flow oscillations. This can be achieved either by mechanical oscillation of the heat transfer surface or the

super-position of a sound field on the external flow. Lighthill, 1954[11] calculated the response of laminar skin friction and heat transfer from an oscillating arbitrary cylinder. Illingworth, 1958[12] treated the case of a heated flat plate with zero incidence in a low speed stream containing a progressive sound wave. His calculations are for a compressible fluid with a potential flow of the following form

$$U(x,t) = U_0\left[1+\epsilon\cos\left(\omega t - \frac{M}{M+1}\cdot\frac{\omega x}{U_0}\right)\right]$$

where M is the Mach number of the mean flow. He carries only two approximations and obtains limiting solutions for both large and small frequencies. Kestin, et al., 1961[13] analysed the same problem for an incompressible fluid with a potential flow of the form

$$U(x,t) = U_0\left[1+\epsilon\cos\omega\left(\frac{x}{U_0}-t\right)\right].$$

They calculate the first three approximations for the case of small frequency ω. Considering the third approximation in their calculation, they obtain the net change in heat transfer and skin friction to be negative and positive, respectively.

In the above two cases, the effect of gravity has been neglected such that the heat transfer mechanism is only forced convection. Schoenhals and Clark, 1962[14] present an analytical treatment of the effect of transverse wall vibrations on free-convective flow and heat transfer from a vertical flat plate. They carry the first two approximations for the case of an incompressible fluid. Blankenship[15] extended Schoenhal's work and carried the third approximation for both finite as well as infinite plate.

The problem of free-convective flow and heat transfer from a vertical plate oscillating in its own plane and in the direction of a force field, has apparently remained untreated.

A limited number of experimental measurements have been made of the average heat transfer coefficient. Chamberlin[16] oscillated an open-end vertical cylinder in air and found no noticeable change in the free convective heat transfer. Spratt, et al.[17] studied the effect of strong sound fields on free convective heat transfer from a horizontal cylinder and found substantial increases in heat transfer. Holman, et al.,[18] introducing artificial oscillation in free convective flow along a flat plate, found no change in the steady heat transfer. Soehngen and Holman,[19] studying the effect of sound fields on free convective heat transfer from a horizontal cylinder, conclude that for low intensities there is no change in heat transfer but for high intensities substantial increases are noticed.

In the present research, the problem of free-convective heat transfer and fluid flow from a vertical flat plate oscillating in its own plane has been given analytical treatment. An experimental program has been conducted. Measurements of the mean coefficient of heat transfer from an oscillating cylinder with large diameter have been made. This system adequately models a flat plate.

CHAPTER II

THEORETICAL ANALYSIS

Statement of the Problem

The analytical model is shown in Figure 1. It consists of a thin flat plate extending from 0 to ∞ in x direction and from $-\infty$ to $+\infty$ in z direction. The plate has a uniform temperature T_w which is greater (for g being in the -x direction) than that of the ambient at rest, signified by T_∞. The plate oscillates harmonically in its own plane and in the direction of an external (gravitational) force field. It is desired to determine analytical expressions for the rate of heat transfer and the wall shear stress.

Formulation of the Problem

The following assumptions have been made in the formulation of the problem described above:

a. The flow is laminar - this will restrict the upper limit of Reynolds number.

b. The boundary-layer approximations are valid - this will restrict the lower limit of Reynolds number.

c. The properties of the fluid are taken to be constant except for the thermally induced density variations which give rise to a buoyancy term in the momentum equation (c.f. Reference 1)

d. Viscous dissipation and other compressibility effects are neglected.

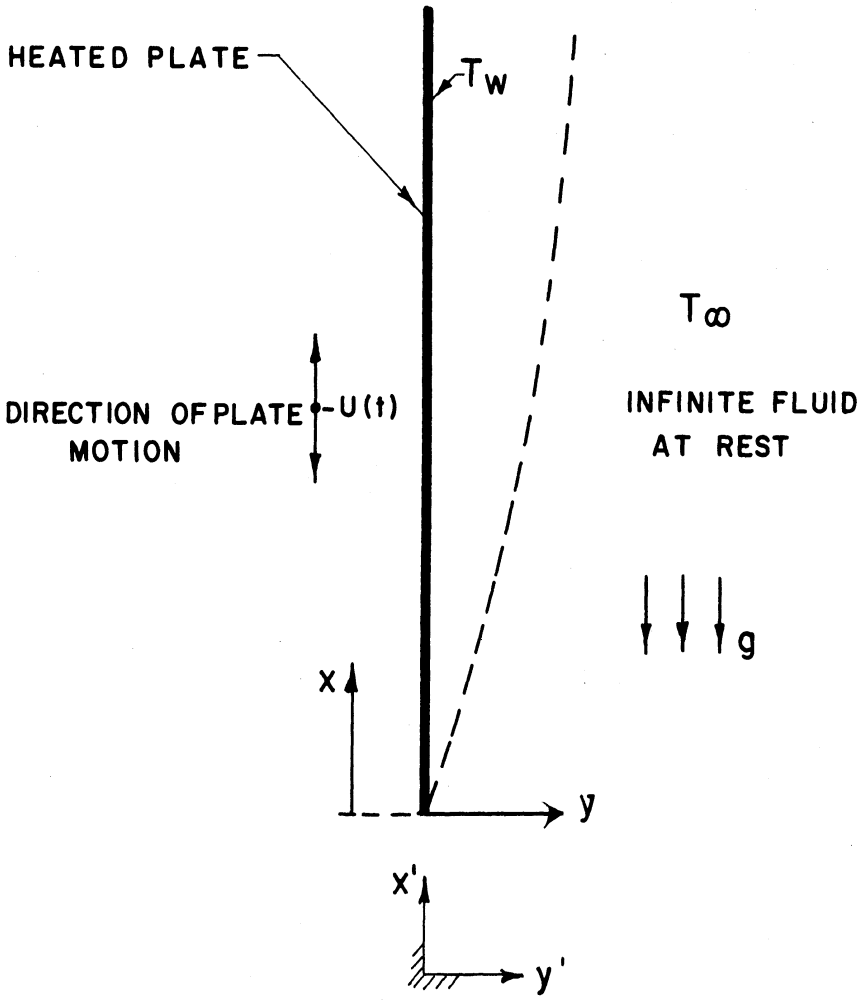

Figure 1. Analytical Model.

Based on the foregoing assumptions and with respect to a reference frame fixed to the plate, the momentum, continuity and energy equations, and the appropriate boundary conditions are:

$$\frac{\partial u}{\partial t} + u\frac{\partial u}{\partial x} + v\frac{\partial u}{\partial y} = \nu\frac{\partial^2 u}{\partial y^2} + \beta g\theta + \frac{dU}{dt} \qquad (1)$$

$$u(x,0,t) = v(x,0,t) = 0$$

$$u(x,\infty,t) = U(t)$$

$$\frac{\partial u}{\partial x} + \frac{\partial v}{\partial y} = 0 \qquad (2)$$

$$\frac{\partial \theta}{\partial t} + u\frac{\partial \theta}{\partial x} + v\frac{\partial \theta}{\partial y} = \alpha\frac{\partial^2 \theta}{\partial y^2} \qquad (3)$$

$$\theta(x,0,t) = \theta_w$$

$$\theta(x,\infty,t) = 0$$

The same formulation would be obtained for a fixed plate in an oscillating potential flow. This fact has been demonstrated in Appendix I. Equations (1), (2), and (3) must now be solved simultaneously for u, v, and θ. Considering that a similarity solution does not exist* and Equation (1) is nonlinear, a linearization process must be carried out if the problem is to be approached analytically. Assuming ϵ to be a positive number less than unity, the velocity of the potential flow can be specified as

$$U(t) = \epsilon U_0 \cos \omega t \quad , \qquad (4)$$

* The possibility of a similarity solution, in its classical sense, was investigated but no suitable transformation was found that would reduce the partial differential equations to ordinary differential equations.

where U_o is assumed a constant independent of frequency of the plate oscillation. The order of magnitude of U_o, as a reference velocity, is assumed the same as the maximum velocity of steady free convection at a distance $x = \ell$. Introduction of ϵ into the expression for $U(t)$, is the first step towards perturbation of the governing differential equations, which is a well-known technique of linearization. The quantities u, v, and Θ are perturbed around their steady state values, i.e., the case where $\epsilon = 0$.

Perturbation of the Differential Equations

Considering the nature of $U(t)$ expressed in Equation (4), the following forms may be assumed for the functions involved.

$$u(x,y,t) = u_o(x,y) + \epsilon u_1^*(x,y,t) + \epsilon^2 u_2(x,y,t) \tag{5}$$

$$v(x,y,t) = v_o(x,y) + \epsilon v_1^*(x,y,t) + \epsilon^2 v_2(x,y,t) \tag{6}$$

$$\theta(x,y,t) = \theta_o(x,y) + \epsilon \theta_1^*(x,y,t) + \epsilon^2 \theta_2(x,y,t) \tag{7}$$

Substituting Equations (5), (6), (7), and (4) into Equations (1), (2), and (3), and arranging according to the powers of ϵ and neglecting terms of the order of ϵ^3 and higher, results in

First Approximation, ϵ^0

$$u_0\frac{\partial u_0}{\partial x} + v_0\frac{\partial u_0}{\partial y} = \beta g\theta_0 + \nu\frac{\partial^2 u}{\partial y^2}$$

$$u_0(x,0) = v_0(x,0) = 0 \quad ; \quad u_0(x,\infty) = 0 \tag{8}$$

$$\frac{\partial u_0}{\partial x} + \frac{\partial v_0}{\partial y} = 0 \tag{9}$$

$$u_0\frac{\partial \theta_0}{\partial x} + v_0\frac{\partial \theta_0}{\partial y} = \alpha\frac{\partial^2 \theta_0}{\partial y^2}$$

$$\theta_0(x,0) = \theta_w \quad ; \quad \theta_0(x,\infty) = 0 \tag{10}$$

The above equations which are the formulation of steady laminar free convection from a vertical flat plate, have been solved and tabulated for eight different Prandtl numbers by Ostrach.(2)

Second Approximation, ϵ^1

$$\frac{\partial}{\partial t}\left[u_1^* - U_0\cos\omega t\right] + u_0\frac{\partial u_1^*}{\partial x} + v_0\frac{\partial u_1^*}{\partial y} + \frac{\partial u_0}{\partial x}u_1^* +$$

$$\frac{\partial u_0}{\partial y}v_1^* - \beta g\theta_1^* - \nu\frac{\partial^2 u_1^*}{\partial y^2} = 0 \tag{11}$$

$$u_1^*(x,0,t) = v_1^*(x,0,t) = 0 \quad ; \quad u_1^*(x,\infty,t) = U_0\cos\omega t$$

$$\frac{\partial u_1^*}{\partial x} + \frac{\partial v_1^*}{\partial y} = 0 \tag{12}$$

$$\frac{\partial \theta_1^*}{\partial t} + u_0 \frac{\partial \theta_1^*}{\partial x} + v_0 \frac{\partial \theta_1^*}{\partial y} - \alpha \frac{\partial^2 \theta_1^*}{\partial y^2} + \frac{\partial \theta_0}{\partial x} u_1^* + \frac{\partial \theta_0}{\partial y} v_1^* = 0 \tag{13}$$

$$\theta_1^*(x,0,t) = \theta_1^*(x,\infty,t) = 0$$

Third Approximation, ϵ^2

$$\frac{\partial u_2}{\partial t} + u_0 \frac{\partial u_2}{\partial x} + \frac{\partial u_0}{\partial x} u_2 + v_0 \frac{\partial u_2}{\partial y} + \frac{\partial u_0}{\partial y} v_2 - \nu \frac{\partial^2 u_2}{\partial y^2} -$$

$$\beta g \theta_2 + u_1^* \frac{\partial u_1^*}{\partial x} + v_1^* \frac{\partial u_1^*}{\partial y} = 0 \tag{14}$$

$$u_2(x,0,t) = v_2(x,0,t) = 0$$

$$\frac{\partial u_2}{\partial x} + \frac{\partial v_2}{\partial y} = 0 \tag{15}$$

$$\frac{\partial \theta_2}{\partial t} + u_0 \frac{\partial \theta_2}{\partial x} + u_2 \frac{\partial \theta_0}{\partial x} + v_0 \frac{\partial \theta_2}{\partial y} + \frac{\partial \theta_0}{\partial y} v_2 - \alpha \frac{\partial^2 \theta_2}{\partial y^2} +$$

$$u_1^* \frac{\partial \theta_1^*}{\partial x} + v_1^* \frac{\partial \theta_1^*}{\partial y} = 0 \tag{16}$$

$$\theta_2(x,0,t) = 0$$

In all the above equations, u_1^*, u_2, Θ_1^* and Θ_2 are functions of time t, as well as x and y. If solutions are sought for large values of time

where the effects of initial transients have died out, the initial conditions become immaterial and the time dependency of the functions may be predicted. The periodic term $U_0 \cos \omega t$ appearing in Equation (11) suggests that all the first approximation functions are also time wise periodic functions with the same frequency ω. In effect, the solutions thus sought will be steady periodic in nature.

For mathematical convenience, use is made of the imaginary exponential functions in the following manner.

$$
\begin{aligned}
U(t) &= \mathcal{R}\left\{ \epsilon U_0 e^{i\omega t} \right\} = \epsilon U_0 \cos \omega t \quad , \\
u_1^*(x,y,t) &= \mathcal{R}\left\{ u_1(x,y) e^{i\omega t} \right\} \quad , \\
v_1^*(x,y,t) &= \mathcal{R}\left\{ v_1(x,y) e^{i\omega t} \right\} \quad , \\
\theta_1^*(x,y,t) &= \mathcal{R}\left\{ \theta_1(x,y) e^{i\omega t} \right\} \quad ,
\end{aligned}
\tag{17}
$$

where $\mathcal{R}$ denotes the real value of the complex quantity in the brackets. The new functions u_1, v_1 and θ_1 are now complex quantities and independent of t. Substituting (17) into (11), (12), and (13), and observing that the symbol $\mathcal{R}$ appears in front of every term, it is concluded that since $\mathcal{R}$ is a linear operator (the sum of real values is the real value of the sum), it can be dropped out of the equations. All terms are now linear in $e^{i\omega t}$ which can also be dropped out. In this manner, time dependency is omitted from the differential equations and time-independent equations and the boundary conditions are obtained for the second

approximation

$$i\omega(u_1 - U_o) + u_o \frac{\partial u_1}{\partial x} + v_o \frac{\partial u_1}{\partial y} + \frac{\partial u_o}{\partial x} u_1 + \frac{\partial u_o}{\partial y} v_1 -$$

$$\beta g \theta_1 - \nu \frac{\partial^2 u_1}{\partial y^2} = 0 \qquad (18)$$

$$u_1(x,0) = v_1(x,0) = 0 \quad ; \quad u_1(x,\infty) = U_o$$

$$\frac{\partial u_1}{\partial x} + \frac{\partial v_1}{\partial y} = 0 \qquad (19)$$

$$i\omega\theta_1 + u_o \frac{\partial \theta_1}{\partial x} + v_o \frac{\partial \theta_1}{\partial y} - a \frac{\partial^2 \theta_1}{\partial y^2} +$$

$$\frac{\partial \theta_o}{\partial x} u_1 + \frac{\partial \theta_o}{\partial y} v_1 = 0 \qquad (20)$$

$$\theta_1(x,0) = \theta_1(x,\infty) = 0$$

Substituting Equations (17) into (14), results in,

$$\frac{\partial u_2}{\partial t} + u_o \frac{\partial u_2}{\partial x} + \frac{\partial u_o}{\partial x} u_2 + v_o \frac{\partial u_2}{\partial y} + \frac{\partial u_o}{\partial y} v_2 -$$

$$\beta g \theta_2 - \nu \frac{\partial^2 u_2}{\partial y^2} = -\mathcal{R}\left\{ u_1 e^{i\omega t} \right\} \cdot \mathcal{R}\left\{ \frac{\partial u_1}{\partial x} e^{i\omega t} \right\} - \qquad (21)$$

$$\mathcal{R}\left\{ v_1 e^{i\omega t} \right\} \cdot \mathcal{R}\left\{ \frac{\partial u_1}{\partial y} e^{i\omega t} \right\}$$

The terms on the right of Equation (21), can each be reduced into a time-independent term and a harmonic term in the following manner.

$$\mathcal{R}\left\{u_1 e^{i\omega t}\right\} = u_{1R}\cos\omega t - u_{1I}\sin\omega t \ ,$$

$$\mathcal{R}\left\{v_1 e^{i\omega t}\right\} = v_{1R}\cos\omega t - v_{1I}\sin\omega t \ ,$$

where u_{1R} and u_{1I} are the real part and the imaginary part of u_1 respectively. v_{1R} and v_{1I}, similarly, correspond to the real part and imaginary part of the complex quantity v_1. Then,

$$\mathcal{R}\left\{u_1 e^{i\omega t}\right\}\cdot\mathcal{R}\left\{\frac{\partial u_1}{\partial x} e^{i\omega t}\right\} = u_{1R}\frac{\partial u_{1R}}{\partial x}\cos^2\omega t + u_{1I}\frac{\partial u_{1I}}{\partial x}\sin^2\omega t - \frac{1}{2}\left(u_{1R}\frac{\partial u_{1I}}{\partial x} + u_{1I}\frac{\partial u_{1R}}{\partial x}\right)\sin 2\omega t \ . \qquad (21a)$$

Considering that,

$$\sin^2\omega t \equiv \frac{1}{2}(1-\cos 2\omega t)$$

$$\cos^2\omega t \equiv \frac{1}{2}(1+\cos 2\omega t) \ ,$$

Equation (21a) reduces to

$$\mathcal{R}\left\{u_1 e^{i\omega t}\right\}\cdot\mathcal{R}\left\{\frac{\partial u_1}{\partial x} e^{i\omega t}\right\} = \frac{1}{2}\left(u_{1R}\frac{\partial u_{1R}}{\partial x} + u_{1I}\frac{\partial u_{1I}}{\partial x}\right) +$$

$$\frac{1}{2}\left[\left(u_{1R}\frac{\partial u_{1R}}{\partial x} - u_{1I}\frac{\partial u_{1I}}{\partial x}\right)\cos 2\omega t -\right.$$

$$\left.\left(u_{1R}\frac{\partial u_{1I}}{\partial x} + u_{1I}\frac{\partial u_{1R}}{\partial x}\right)\sin 2\omega t\right] .$$

This can be further reduced by the use of the following identities

$$\bar{u}_1\frac{\partial u_1}{\partial x} + u_1\frac{\overline{\partial u_1}}{\partial x} \equiv 2\left(u_{1R}\frac{\partial u_{1R}}{\partial x} + u_{1I}\frac{\partial u_{1I}}{\partial x}\right) ,$$

and

$$\mathcal{R}\left\{u_1\frac{\partial u_1}{\partial x} e^{2i\omega t}\right\} \equiv \left(u_{1R}\frac{\partial u_{1R}}{\partial x} - u_{1I}\frac{\partial u_{1I}}{\partial x}\right)\cos 2\omega t -$$

$$\left(u_{1R}\frac{\partial u_{1I}}{\partial x} + u_{1I}\frac{\partial u_{1R}}{\partial x}\right)\sin 2\omega t ,$$

to its final form

$$\mathcal{R}\left\{u_1 e^{i\omega t}\right\}\cdot\mathcal{R}\left\{\frac{\partial u_1}{\partial x} e^{i\omega t}\right\} = \tag{21b}$$

$$\frac{1}{4}\left(\bar{u}_1\frac{\partial u_1}{\partial x} + u_1\frac{\overline{\partial u_1}}{\partial x}\right) + \frac{1}{2}\mathcal{R}\left\{u_1\frac{\partial u_1}{\partial x} e^{2i\omega t}\right\} ,$$

where the superscript bar (—) denotes the complex conjugate. The term

$$\mathcal{R}\left\{ v_1 e^{i\omega t} \right\} \cdot \mathcal{R}\left\{ \frac{\partial u_1}{\partial y} e^{i\omega t} \right\} ,$$

can also be reduced, in a similar manner, to its final form

$$\mathcal{R}\left\{ v_1 e^{i\omega t} \right\} \cdot \mathcal{R}\left\{ \frac{\partial u_1}{\partial y} e^{i\omega t} \right\} = \tag{21c}$$

$$\frac{1}{4}\left(\bar{v}_1 \frac{\partial u_1}{\partial y} + v_1 \frac{\overline{\partial u_1}}{\partial y} \right) + \frac{1}{2}\mathcal{R}\left\{ v_1 \frac{\partial u_1}{\partial y} e^{2i\omega t} \right\}$$

Substituting Equations (21b) and (21c) into (21) results in

$$\frac{\partial u_2}{\partial t} + u_0 \frac{\partial u_2}{\partial x} + \frac{\partial u_0}{\partial x} u_2 + v_0 \frac{\partial u_2}{\partial y} + \frac{\partial u_0}{\partial y} v_2 - \nu \frac{\partial^2 u_2}{\partial y^2} - \beta g \theta_2 = u_{10} + \mathcal{R}\left\{ u_{11} e^{2i\omega t} \right\} , \tag{22}$$

where

$$u_{10} = -\frac{1}{4}\left(\bar{u}_1 \frac{\partial u_1}{\partial x} + u_1 \frac{\overline{\partial u_1}}{\partial x} + \bar{v}_1 \frac{\partial u_1}{\partial y} + v_1 \frac{\overline{\partial u_1}}{\partial y} \right) ,$$

and,

$$u_{11} = -\frac{1}{2}\left(u_1 \frac{\partial u_1}{\partial x} + v_1 \frac{\partial u_1}{\partial y} \right) .$$

Inspection of Equation (22) reveals that, if it is to be satisfied uniquely, for large values of time, then the quantities u_2, v_2 and θ_2

must have the following forms

$$u_2(x,y,t) = u_{20}(x,y) + \mathcal{R}\left\{ u_{21}(x,y)\, e^{2i\omega t} \right\}$$

and,

$$v_2(x,y,t) = v_{20}(x,y) + \mathcal{R}\left\{ v_{21}(x,y)\, e^{2i\omega t} \right\} \tag{23}$$

and,

$$\theta_2(x,y,t) = \theta_{20}(x,y) + \mathcal{R}\left\{ \theta_{21}(x,y)\, e^{2i\omega t} \right\}$$

in order to comply with $u_{10} + \mathcal{R}\{u_{11}e^{2i\omega t}\}$ in Equation (22). It is obvious from Equation (22) that unless u_{10} is identically zero, the functions u_2, Θ_2 and v_2 cannot be purely harmonic. Conditions of Equations (23) are such that Equations (15) and (16) are also identically satisfied in time domain. Substituting Equations (23) into (14), (15) and (16) and separating the terms with the symbol $\mathcal{R}$ and without, the following sets of equations are obtained for the third approximation.

a. Non-Oscillatory Components

$$u_0 \frac{\partial u_{20}}{\partial x} + \frac{\partial u_0}{\partial x} u_{20} + v_0 \frac{\partial u_{20}}{\partial y} + \frac{\partial u_0}{\partial y} v_{20} - \beta g \theta_{20} - \nu \frac{\partial^2 u_{20}}{\partial y^2} +$$

$$\frac{1}{4}\left(u_1 \frac{\overline{\partial u_1}}{\partial x} + \overline{u_1} \frac{\partial u_1}{\partial x} + v_1 \frac{\overline{\partial u_1}}{\partial y} + \overline{v_1} \frac{\partial u_1}{\partial y} \right) = 0 \tag{24}$$

$$u_{20}(x,0) = v_{20}(x,0) = 0$$

$$\frac{\partial u_{20}}{\partial x} + \frac{\partial v_{20}}{\partial y} = 0 \tag{25}$$

$$u_0 \frac{\partial \theta_{20}}{\partial x} + v_0 \frac{\partial \theta_{20}}{\partial y} - a \frac{\partial^2 \theta_{20}}{\partial y^2} + u_{20} \frac{\partial \theta_0}{\partial x} + v_{20} \frac{\partial \theta_0}{\partial y} +$$

$$\frac{1}{4}\left(u_1 \frac{\overline{\partial \theta_1}}{\partial x} + \overline{u_1} \frac{\partial \theta_1}{\partial x} + v_1 \frac{\overline{\partial \theta_1}}{\partial y} + \overline{v_1} \frac{\partial \theta_1}{\partial y} \right) = 0 \tag{26}$$

$$\theta_{20}(x,0) = 0$$

b. Oscillatory Components

$$2i\omega u_{21} + u_0 \frac{\partial u_{21}}{\partial x} + \frac{\partial u_0}{\partial x} u_{21} + v_0 \frac{\partial u_{21}}{\partial y} + \frac{\partial u_0}{\partial y} v_{21} - \nu \frac{\partial^2 u_{21}}{\partial y^2} -$$

$$\beta g \theta_{21} + \frac{1}{2}\left(u_1 \frac{\partial u_1}{\partial x} + v_1 \frac{\partial u_1}{\partial y} \right) = 0 \tag{27}$$

$$u_{21}(x,0) = v_{21}(x,0) = u_{21}(x,\infty) = 0$$

$$\frac{\partial u_{21}}{\partial x} + \frac{\partial v_{21}}{\partial y} = 0 \tag{28}$$

$$2i\omega \theta_{21} + u_0 \frac{\partial \theta_{21}}{\partial x} + v_0 \frac{\partial \theta_{21}}{\partial y} - a \frac{\partial^2 \theta_{21}}{\partial y^2} + u_{21} \frac{\partial \theta_0}{\partial x} + v_{21} \frac{\partial \theta_0}{\partial y} +$$

$$\frac{1}{2}\left(u_1 \frac{\partial \theta_1}{\partial x} + v_1 \frac{\partial \theta_1}{\partial y} \right) = 0 \tag{29}$$

$$\theta_{21}(x,0) = \theta_{21}(x,\infty) = 0$$

Solutions of the Differential Equations

Analytical treatment of Equations (18) - (20), (24) - (26) and (27) - (29), in their present form, is very unlikely to produce the solutions desired. It is, however, possible to obtain solutions valid for limited ranges of some of the variables and parameters involved. One such parameter, is the frequency ω. It is mathematically possible, for large values of this parameter, to evaluate the order of magnitude of the terms in the differential equations. This would suggest that solutions be attempted for two regions, namely, the large ω region and the small ω region. In each of the above mentioned regions, it is sometimes necessary to subdivide the already limited range of ω, into subregions of small y and large y. This subdivision, however, does not affect substantially the accuracy of the results obtained for heat transfer and shear stress at the wall, considering that these quantities themselves are evaluated at the wall.

Large ω Solutions for the Second Approximation

It can be shown that in Equation (18) which is linear in u_1 but nonhomogeneous,

$$u_1 \equiv O\left[u_1 \right] \quad ,$$

$$\frac{\partial u_1}{\partial y} = O\left[\omega^{1/2} u_1 \right] \quad ,$$

and

$$\frac{\partial^2 u_1}{\partial y^2} = O\left[\omega\, u_1 \right] \quad ,$$

when ω becomes substantially large. Rewriting Equation (18) with the

order of magnitude of each term written beneath it, one obtains,

$$i\omega u_1 + u_o\frac{\partial u_1}{\partial x} + v_o\frac{\partial u_1}{\partial y} + \frac{\partial u_o}{\partial x}u_1 + \frac{\partial u_o}{\partial y}v_1 - \nu\frac{\partial^2 u_1}{\partial y^2} = \beta g\theta_1 + i\omega U_o$$

$$[\omega u_1] \quad [u_1] \quad [\omega^{1/2}u_1] \quad [u_1] \quad [\omega^{-1}u_1] \quad [\omega u_1] \quad .$$

Comparing the linear terms and retaining the ones with the highest order of magnitude namely $[\omega u_1]$, results in

$$i\omega u_1 - \nu\frac{\partial^2 u_1}{\partial y^2} = \beta g\theta_1 + i\omega U_o \quad .$$

The nonhomogeneous terms, however, should be compared not to the linear terms but to themselves. It is now physically obvious that since the cause of transient (which produces θ_1) is mechanical, in nature, rather than thermal, $\beta g\theta_1$ may be neglected, for large ω, compared to $i\omega U_o$. Therefore,

$$i\omega u_1 - \nu\frac{\partial^2 u_1}{\partial y^2} = i\omega U_o$$

$$u_1(x,0) = 0 \qquad (30)$$

$$u_1(x,\infty) = U_o \quad ,$$

is the governing momentum equation within the limits of the foregoing assumptions. The solution of Equation (30) may readily be obtained in the form

$$u_1 = U_o\left(1 - e^{-y\sqrt{\frac{i\omega}{\nu}}}\right) \quad , \qquad (31)$$

and furthermore, $v_1 = 0$ from continuity considerations. Evaluating the order of magnitude of terms in Equation (20), in the same manner as above, one obtains the following

$$i\omega\theta_1 + u_o\frac{\partial\theta_1}{\partial x} + v_o\frac{\partial\theta_1}{\partial y} - a\frac{\partial^2\theta_1}{\partial y^2} = -u_1\frac{\partial\theta_o}{\partial x} - v_1\frac{\partial\theta_o}{\partial y}$$

$$[\omega\theta_1] \quad [\theta_1] \quad [\omega^{1/2}\theta_1] \quad [\omega\theta_1] \quad .$$

Neglecting the terms whose order of magnitude is smaller than $[\omega\theta_1]$ and considering that $v_1 = 0$, one obtains the governing energy equation and its appropriate boundary conditions for the second approximation as

$$i\omega\theta_1 - a\frac{\partial^2\theta_1}{\partial y^2} = -u_1\frac{\partial\theta_o}{\partial x}$$

$$\theta_1(x,0) = \theta_1(x,\infty) = 0 \quad . \tag{32}$$

The general solution to Equation (31) is readily obtainable, however, the particular solution will involve the function $\theta_o(x,y)$ which is available in tabulated form and therefore cannot be operated on analytically. This may be overcome by approximating the exact value of θ_o by its tangent at the wall, for small values of y, in the form

$$\theta_o(x,y) \cong \theta_w + \left(\frac{\partial\theta_o}{\partial y}\right)_w \cdot y$$

then,

$$\frac{\partial\theta_o}{\partial x} = y\frac{d}{dx}\left(\frac{\partial\theta_o}{\partial y}\right)_w = y\left(\frac{\partial^2\theta_o}{\partial y\,\partial x}\right)_w \quad . \tag{33}$$

Considering that $(\frac{\partial \Theta_o}{\partial y})_w$ is independent of y, $\frac{\partial \Theta_o}{\partial x}$ expressed in Equation (33) is now explicit in y and can readily be operated on with respect to y. Then the solution of Equation (32), near the wall, is

$$\theta_1(x,y) = \frac{iU_o}{a\omega}\left(\frac{\partial^2 \theta_o}{\partial y \partial x}\right)_w \left\{ ay\left(1 - \frac{Pr}{Pr-1} e^{-y\sqrt{\frac{i\omega}{\nu}}}\right) + \right.$$

$$\left. \frac{2i\nu}{(Pr-1)^2}\sqrt{\frac{i\nu}{\omega}}\left(e^{-y\sqrt{\frac{i\omega}{a}}} - e^{-y\sqrt{\frac{i\omega}{\nu}}}\right)\right\} . \qquad (34)$$

Away from the wall (near the edge of the boundary layer), as Lighthill[11] points out, $\frac{\partial^2 \theta_1}{\partial y^2}$ may be neglected compared to $i\omega\theta_1$ and thus a solution is obtained for $\theta_1(x,y)$ valid for large values of y, as

$$\theta_1(x,y) = \frac{iU_o}{\omega} \cdot \frac{\partial \theta_o}{\partial x}\left(1 - e^{-y\sqrt{\frac{i\omega}{\nu}}}\right) . \qquad (35)$$

Small ω Solutions for the Second Approximation

In the preceding section asymptotic solutions were obtained for large values of frequency ω. In order to estimate the range of validity of these asymptotic expressions, it seems essential to attempt solutions that would be valid for the other extreme, namely small values of frequency. When such solutions are compared with each other, it is usually possible

to estimate, by observation, the vicinity of the point of transition of one limiting solution to the other.

Solutions will be obtained for Equations (18), (19) and (20), for the case of small values of frequency ω, using integral techniques.

The integral procedure adopted in this work requires an integral solution of the steady state free convection. Although some integral solutions do exist in the literature for the case of steady free convection (c.f. References 20 and 21), an integral solution was derived using fourth order profiles both for temperature θ_o and velocity u_o.

$$u_o = V_o(x)\,\eta^2(\eta-1)(2-\eta)$$
$$\theta_o = \theta_w(1+\eta_\theta)(1-\eta_\theta)^3 \quad , \tag{36}$$

where

$$\eta = \frac{y}{\delta} \quad ,$$
$$\eta_\theta = \frac{y}{\delta_\theta} \quad ,$$

and

$$V_o(x) = \frac{\beta g \theta_w}{6\nu}\delta^2 \quad .$$

Equations (36) already satisfy the appropriate boundary conditions, second order smoothness on the edge of the boundary, and the following conditions obtained from Equations (8) and (10) for $y = 0$ (at the wall)

and namely,

$$\nu\left(\frac{\partial^2 u_o}{\partial y^2}\right)_w = -\beta g \theta_w$$
$$\alpha\left(\frac{\partial^2 \theta_o}{\partial y^2}\right)_w = 0 \qquad (37)$$

Defining $\Delta \equiv \delta_\theta/\delta$, there are two unknowns to be found, δ and Δ. These will be found by satisfying the integrated form of Equations (8) and (10) over the thickness of the boundary layer,

$$\frac{d}{dx}\int_0^\infty u_o^2\, dy = -\nu\left(\frac{\partial u_o}{\partial y}\right)_w + \beta g \int_0^\infty \theta_o\, dy \quad , \qquad (38)$$

and

$$\frac{d}{dx}\int_0^\infty u_o \theta_o\, dy = -\alpha\left(\frac{\partial \theta_o}{\partial y}\right)_w \quad . \qquad (39)$$

The following value is obtained for δ.

$$\delta = 5.9\left[(1.8\Delta - 1)\frac{\nu^2 x}{\beta g \theta_w}\right]^{1/4} \qquad (40)$$

Here Δ satisfies

$$378\,\Delta(1.8\Delta - 1)G(\Delta) = \frac{5}{Pr} \quad , \qquad (41)$$

where

$$G(\Delta) = \frac{1}{15}\Delta^2 - \frac{1}{14}\Delta^3 + \frac{9}{280}\Delta^4 - \frac{1}{180}\Delta^5 \quad , \ \Delta \leqslant 1$$

$$= \frac{1}{20} - \frac{1}{30}\Delta^{-1} + \frac{1}{140}\Delta^{-3} - \frac{1}{504}\Delta^{-4} \quad , \ \Delta \geqslant 1 \ . \tag{42}$$

The values of Δ have been tabulated as a function of Prandtl number Pr in Appendix II. Figure 2 shows a plot of $Nu_x/(Gr_x)^{1/4}$ versus Prandtl number Pr and a similar plot has been presented in Figure 3 for $u_{max}/\sqrt{\beta g \theta_w x}$. The agreement of these calculations with the exact similarity solution (2) is very good for Prandtl numbers ranging from 0.7 to 200.

A somewhat similar procedure is used for obtaining solutions for Equations (18), (19) and (20). Here it was found convenient to use fifth order profiles for the functions involved. The result is

$$\frac{u_1}{U_o} = 5\eta^4 - 4\eta^5 + B(\eta - 4\eta^4 + 3\eta^5) +$$

$$\frac{i\omega\delta^2}{2\nu}(-\eta^2 + 3\eta^4 - 2\eta^5) + \frac{i\omega\delta^2}{6\nu}B(\eta^3 - 2\eta^4 + \eta^5) + \tag{43}$$

$$\frac{\beta g \theta_w \delta^2}{6\nu U_o \Delta} B_1(-\eta^3 + 2\eta^4 - \eta^5)$$

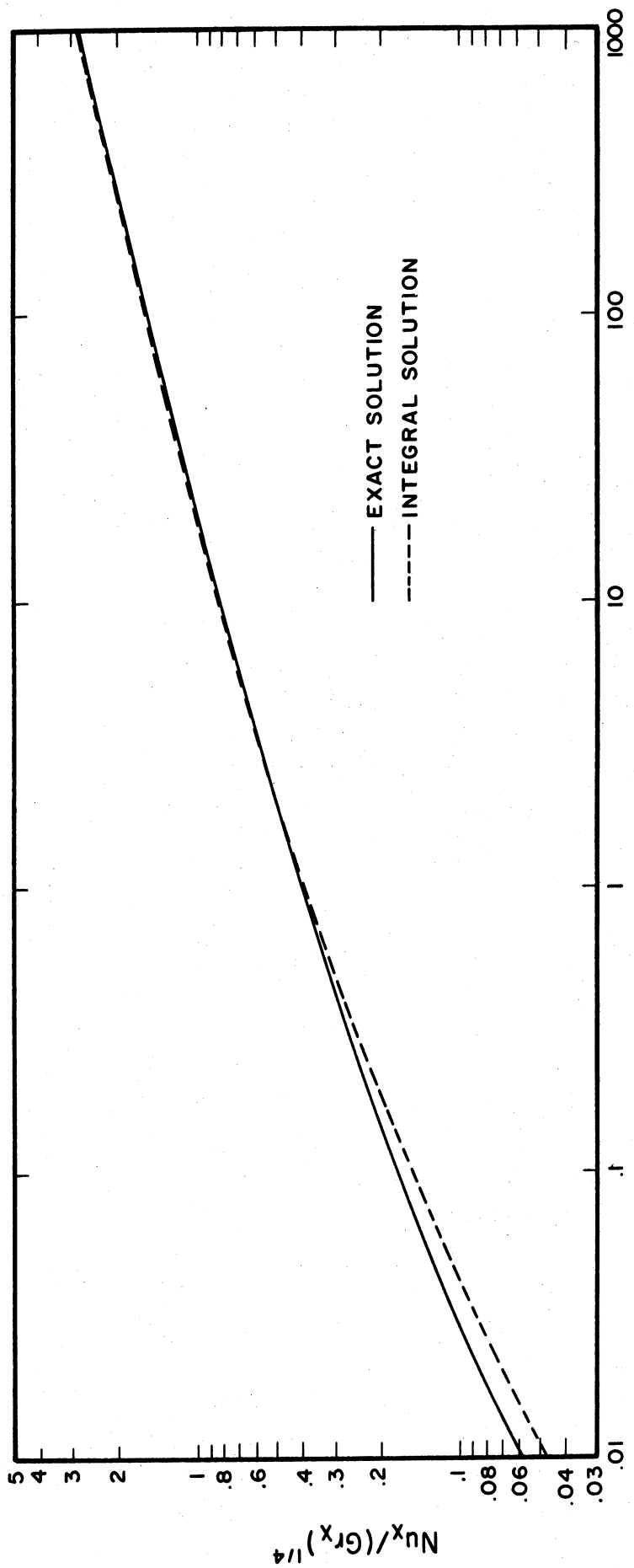

Figure 2. The Steady State Nusselt Number as a Function of Prandtl Number.

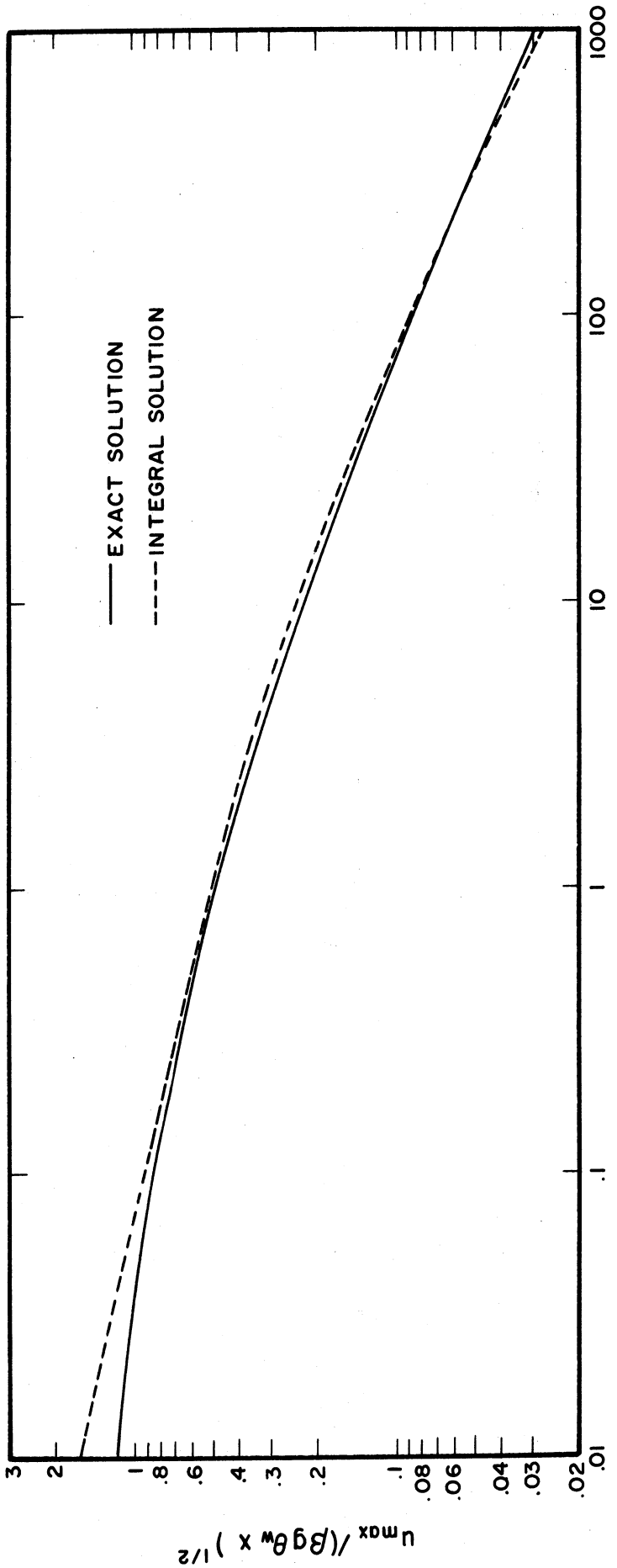

Figure 3. The Steady State Maximum Velocity as a Function of Prandtl Number.

$$\frac{\theta_1}{\theta_w} = B_1\left[\eta_\theta - 4\eta_\theta^4 + 3\eta_\theta^5 + \frac{i\omega\delta^2\Delta^2}{6a}\left(\eta_\theta^3 - 2\eta_\theta^4 + \eta_\theta^5\right)\right] \tag{44}$$

The velocity profile u_1 already satisfies the following conditions:

at $y = \delta$: $\quad u_1 = U_o \quad ; \quad \frac{\partial u_1}{\partial y} = 0$

at $y = 0$: $\quad u_1 = 0 \quad ; \quad \nu\frac{\partial^2 u_1}{\partial y^2} = -i\omega U_o \quad ;$ (45)

$$\nu\frac{\partial^3 u_1}{\partial y^3} = i\omega\frac{\partial u_1}{\partial y} - \beta g\frac{\partial \theta_1}{\partial y} \quad ,$$

where the last two conditions have been derived from Equation (18). On the other hand, the temperature profile θ_1, satisfies,

at $y = \delta$: $\quad \theta_1 = 0 \quad ; \quad \frac{\partial \theta_1}{\partial y} = 0$

at $y = 0$: $\quad \theta_1 = 0 \quad ; \quad \frac{\partial^2 \theta_1}{\partial y^2} = 0 \quad ;$ (26)

$$a\frac{\partial^3 \theta_1}{\partial y^3} = i\omega\frac{\partial \theta_1}{\partial y} \quad ,$$

where the last two conditions have been derived from Equation (20). The unknowns B and B_1 will be determined by satisfying the integrated forms of Equations (18) and (20). The velocities v_o and v_1 have been

eliminated by the use of Equations (9) and (19).

$$i\omega\int_0^\infty (u_1 - U_0)\,dy - \beta g\int_0^\infty \theta_1\,dy + \nu\left(\frac{\partial u_1}{\partial y}\right)_w + 2\frac{d}{dx}\int_0^\infty u_0 u_1\,dy - U_0\frac{d}{dx}\int_0^\infty u_0\,dy = 0 \tag{47}$$

$$i\omega\int_0^\infty \theta_1\,dy + a\left(\frac{\partial \theta_1}{\partial y}\right)_w + \frac{d}{dx}\int_0^\infty (\theta_1 u_0 + \theta_0 u_1)\,dy = 0 \tag{48}$$

Substitution of Equations (43) and (44) into Equation (47) results in the following differential equation:

$$\begin{aligned}
&\nu U_0 \delta^{-1} B - \frac{1}{20} U_0 \overline{V}_0 \frac{d}{dx}(\delta^3) - \beta g \theta_w B_1 \left(\frac{1}{5}\Delta\delta + \frac{1}{360}\frac{i\omega\delta^3\Delta^3}{a}\right) + \\
&i\omega\delta U_0\left(-\frac{2}{3} + \frac{1}{5}B - \frac{1}{30}\frac{i\omega\delta^2}{\nu} + \frac{1}{360}\frac{i\omega\delta^2}{\nu}B - \frac{1}{360}\frac{\beta g\theta_w\delta^2}{\nu U_0\Delta}B_1\right) + \\
&U_0\overline{V}_0\left[\frac{13}{1260}\frac{d}{dx}(\delta^3) + \frac{31}{1260}\frac{d}{dx}(\delta^3 B) - \right. \\
&\frac{1}{3780}\frac{\beta g\theta_w}{\nu U_0\Delta}\frac{d}{dx}(\delta^5 B_1) + \frac{17}{840}\frac{i\omega}{\nu}\frac{d}{dx}(\delta^5) + \\
&\left.\frac{1}{3780}\frac{i\omega}{\nu}\frac{d}{dx}(\delta^5 B)\right] = 0 \quad ,
\end{aligned} \tag{49}$$

where $\overline{V}_0 = \delta^{-2} V_0(x)$.

Equation (49) is the new form of the governing momentum equation. Similarly, the new form of the governing energy equation can be obtained by substitution of Equations (43) and (44) into (48), and namely

$$
\begin{aligned}
& i\omega\Delta\delta B_1\left(\frac{1}{5}+\frac{1}{360}\frac{i\omega}{\alpha}\Delta^2\delta^2\right)+\alpha(\Delta\delta)^{-1}B_1+ \\
& \frac{d}{dx}\Big[U_o Z(\Delta)\delta+U_o W(\Delta)\delta B+\overline{V}_o S(\Delta)\delta^3 B_1+ \\
& \frac{1}{6}Pr\,\overline{V}_o Y(\Delta)\frac{i\omega}{\nu}\delta^5 B_1+U_o X(\Delta)\frac{i\omega}{\nu}\delta^3+ \\
& U_o V(\Delta)\frac{i\omega}{\nu}\delta^3 B\Big]=0 \quad ,
\end{aligned}
\tag{50}
$$

where

$$
\begin{aligned}
S(\Delta) &= \Delta^2\left(\frac{2}{21}-\frac{6}{35}\Delta+\frac{1}{9}\Delta^2-\frac{8}{315}\Delta^3\right) \\
V(\Delta) &= \Delta^4\left(\frac{1}{560}-\frac{1}{540}\Delta+\frac{1}{1890}\Delta^2\right) \\
W(\Delta) &= \Delta^2\left(\frac{1}{15}-\frac{1}{45}\Delta^3+\frac{1}{105}\Delta^4\right) \\
X(\Delta) &= \Delta^3\left(-\frac{1}{84}+\frac{1}{120}\Delta^2-\frac{1}{315}\Delta^3\right) \quad , \Delta\leq 1 \\
Y(\Delta) &= \Delta^4\left(\frac{1}{105}-\frac{1}{56}\Delta+\frac{1}{84}\Delta^2-\frac{1}{360}\Delta^3\right) \\
Z(\Delta) &= \Delta^5\left(\frac{1}{36}-\frac{4}{315}\Delta\right) \quad .
\end{aligned}
\tag{51}
$$

Now, Equations (49) and (50) must be solved simultaneously for B and B_1. However, before attempting this, new dimensionless parameters are introduced, for convenience, and equations are rearranged accordingly. The independent variable x is replaced by the boundary layer thickness $\delta(x)$ and non-dimensionalized by using a characteristic length, ℓ. The new dimensionless quantities are:

$$\xi = \frac{\delta}{\ell}$$

$$\Omega = \frac{\omega \ell^2}{\nu} \tag{52}$$

$$\Pi_1 = \frac{\beta g \theta_w \ell^2}{\nu U_o}$$

By substitution and rearrangement, Equations (49) and (50) become

$$(1 + \alpha_4 i\Omega\xi^2)\frac{dB}{d\xi} + (\alpha_1\xi^{-1} + \alpha_5 i\Omega\xi - \alpha_6\Omega^2\xi^3)B =$$

$$\Pi_1\left[(\alpha_2\xi + \alpha_8 i\Omega\xi^3)B_1 + \alpha_0\xi^2\frac{dB_1}{d\xi}\right] + \tag{53}$$

$$\alpha_3\xi^{-1} + \alpha_9 i\Omega\xi - \alpha_{10}\Omega^2\xi^3 \quad ,$$

and

$$(1 + \beta_4 i\Omega\xi^2)\frac{dB_1}{d\xi} + (\beta_1\xi^{-1} + \beta_5 i\Omega\xi - \beta_6\Omega^2\xi^3)B_1 =$$

$$-\frac{1}{\Pi_1}\left[(\beta_3\xi^{-2} + \beta_7 i\Omega)\frac{dB}{d\xi} + (\beta_3\xi^{-3} + \beta_8 i\Omega\xi^{-1})B + \right. \tag{54}$$

$$\left. \beta_2\xi^{-3} + \beta_9 i\Omega\xi^{-1}\right] \quad ,$$

where α's and β's are functions of Prandtl number alone and are defined in Appendix III.

Since solutions are desired for the case of small values of ω, it seems appropriate to attempt a series expansion of B and B_1 around their quasi-steady values ($\omega = 0$).

The quasi-steady case describes the case of a vertical heated flat plate moving parallel and in the direction of gravitational field, with a uniform velocity ϵU_o. The two velocities will be additive and increases are anticipated both in the rate of heat transfer and the shear stress at the wall. This fact was the criterion for improving the profiles involved. The present profile for velocity u_1 gives a friction factor that when plotted against Pr, will cross the Pr axis around Pr = 500. This will limit the upper limit of Prandtl number for which the following solution will hold. The quasi-steady friction factor and Nusselt number are plotted versus Pr, in Figures 16 and 17 respectively.

In expressing B and B_1 in their corresponding Taylor series expansion, one can write

$$B(\xi, \Omega) = \sum_{n=0}^{\infty} \frac{\Omega^n}{n!} \frac{\partial^{(n)} B(\xi, 0)}{\partial \Omega^n}$$

$$B_1(\xi, \Omega) = \sum_{n=0}^{\infty} \frac{\Omega^n}{n!} \frac{\partial^{(n)} B_1(\xi, 0)}{\partial \Omega^n}$$

This assumes that B and B_1 are continuous functions of Ω with continuous derivatives and that the order of differentiation with respect to Ω and ξ can be interchanged. By differentiating Equations (53)

and (54), n times with respect to Ω and setting $\Omega = 0$. The following generalized equations are obtained:*

$$
\begin{aligned}
& ni\alpha_4 \xi^2 \frac{d}{d\xi}\left[\frac{\partial^{(n-1)} B(\xi,0)}{\partial\Omega^{n-1}}\right] + \frac{d}{d\xi}\left[\frac{\partial^{(n)} B(\xi,0)}{\partial\Omega^{n}}\right] - \\
& n(n-1)\alpha_6 \xi^3 \frac{\partial^{(n-2)} B(\xi,0)}{\partial\Omega^{n-2}} + ni\alpha_5 \xi \frac{\partial^{(n-1)} B(\xi,0)}{\partial\Omega^{n-1}} + \\
& \alpha_1 \xi^{-1} \frac{\partial^{(n)} B(\xi,0)}{\partial\Omega^{n}} = \Pi_1 \Bigg\{ ni\alpha_8 \xi^3 \frac{\partial^{(n-1)} B_1(\xi,0)}{\partial\Omega^{n-1}} + \\
& \alpha_2 \xi \frac{\partial^{(n)} B_1(\xi,0)}{\partial\Omega^{n}} + \alpha_0 \xi^2 \frac{d}{d\xi}\left[\frac{\partial^{(n)} B_1(\xi,0)}{\partial\Omega^{n}}\right]\Bigg\} + \\
& \delta_{on}\alpha_3 \xi^{-1} + \delta_{1n} i\alpha_9 \xi - 2\delta_{2n}\alpha_{10}\xi^3 \quad ,
\end{aligned}
\tag{55}
$$

where δ_{ij} is the Kronecker delta defined as,

$$
\delta_{ij} = \begin{cases} 1 \ , & i = j \\ 0 \ , & i \neq j \end{cases} \quad ,
$$

* It is understood that $\frac{\partial^{(\gamma)}}{\partial\Omega^{\gamma}}$ of any quantity is zero, when $\gamma < 0$ and, the quantity itself, when $\gamma = 0$.

and

$$\frac{d}{d\xi}\left[\frac{\partial^{(n)} B_1(\xi,0)}{\partial\Omega^n}\right] + ni\beta_4\xi^2\frac{d}{d\xi}\left[\frac{\partial^{(n-1)} B_1(\xi,0)}{\partial\Omega^{n-1}}\right] -$$

$$n(n-1)\xi^3\frac{\partial^{(n-2)} B_1(\xi,0)}{\partial\Omega^{n-2}} + ni\beta_5\xi\frac{\partial^{(n-1)} B_1(\xi,0)}{\partial\Omega^{n-1}} +$$

$$\beta_1\xi^{-1}\frac{\partial^{(n)} B_1(\xi,0)}{\partial\Omega^n} = -\frac{1}{\Pi_1}\left\{\delta_{on}\beta_2\xi^{-3} + \delta_{1n}i\beta_9\xi^{-1} + \right. \tag{56}$$

$$ni\beta_7\frac{d}{d\xi}\left[\frac{\partial^{(n-1)} B(\xi,0)}{\partial\Omega^{n-1}}\right] + \beta_3\xi^{-2}\frac{d}{d\xi}\left[\frac{\partial^{(n)} B(\xi,0)}{\partial\Omega^n}\right] +$$

$$\left. ni\beta_8\xi^{-1}\frac{\partial^{(n-1)} B(\xi,0)}{\partial\Omega^{n-1}} + \beta_3\xi^{-3}\frac{\partial^{(n)} B(\xi,0)}{\partial\Omega^n}\right\} .$$

In order to satisfy Equations (55) and (56) simultaneously for all n, the n-th derivatives of B and B_1 with respect to Ω, must have the following forms,

$$\frac{\partial^{(n)} B(\xi,0)}{\partial\Omega^n} = E_n\gamma_n\xi^{2n}$$

$$\frac{\partial^{(n)} B_1(\xi,0)}{\partial\Omega^n} = -\frac{1}{\Pi_1}E_n\lambda_n\xi^{2n-2} , \tag{57}$$

where

$$E_n = \begin{cases} 1, \text{ when } n \text{ is even} \\ i, \text{ when } n \text{ is odd} \end{cases} .$$

When expressions in Equation (57) are substituted into (55) and (56), powers of ξ are eliminated from the equations for $n > 2$ and general expressions are derived for the coefficients of the series solution. When $n = 0$, 1 and 2, one should refer to Equations (55) and (56) and solve the special form of these equations for the values of $n \leq 2$. These general expressions are:

$$\gamma_n = \frac{1}{A_5}\left(A_2 \gamma_{n-2} - A_1 \gamma_{n-1} - A_4 \lambda_{n-1} - A_3 \lambda_n \right)$$

$$\lambda_n = \frac{1}{A_5 C_5 + A_3 C_3}\Big[A_5\left(C_4 \gamma_{n-1} - C_1 \lambda_{n-1} + C_2 \lambda_{n-2} \right) + C_3\left(A_2 \gamma_{n-2} - A_1 \gamma_{n-1} - A_4 \lambda_{n-1} \right)\Big] \quad , \tag{58}$$

where

$$A_1 = -n(-1)^n\left[\alpha_5 + 2(n-1)\alpha_4 \right]$$

$$A_2 = n(n-1)\alpha_6$$

$$A_3 = 2(n-1)\alpha_0 + \alpha_2 \quad , \quad n > 2 \tag{59}$$

$$A_4 = -n(-1)^n \alpha_8$$

$$A_5 = 2n + \alpha_1 \quad ,$$

and

$$C_1 = -n(-1)^n\left[2(n-2)\beta_4 + \beta_5\right]$$

$$C_2 = n(n-1)\beta_6$$

$$C_3 = (2n+1)\beta_3 \qquad (60)$$

$$C_4 = -n(-1)^n\left[2(n-1)\beta_7 + \beta_8\right]$$

$$C_5 = 2(n-1) + \beta_1$$

In terms of γ_n and λ_n, then, the quantities B and B_1 take the following forms.

$$B(\xi,\Omega) = \sum_{n=0}^{\infty} E_n \frac{\Omega^n}{n!}\gamma_n \xi^{2n} = \gamma_0 + i\Omega\gamma_1\xi^2 + \frac{\Omega^2}{2}\gamma_2\xi^4 + i\frac{\Omega^3}{6}\gamma_3\xi^6 + \cdots$$

$$B_1(\xi,\Omega) = -\frac{1}{\pi_1}\sum_{n=0}^{\infty} E_n \frac{\Omega^n}{n!}\lambda_n \xi^{2n-2} = -\frac{1}{\pi_1}\left(\lambda_0\xi^{-2} + i\Omega\lambda_1 + \frac{\Omega^2}{2}\lambda_2\xi^2 + i\frac{\Omega^3}{6}\lambda_3\xi^4 + \cdots\right) \qquad (61)$$

The coefficients γ_n and λ_n have been evaluated for Prandtl numbers 0.757, 1, 10 and 100, using the University of Michigan IBM 7090 Digital Computer. The first few of these coefficients are listed in Appendix IV.

Comparison of the Two Limiting Solutions

The combination of ξ, Ω, and π_1 in the preceding calculations, gives rise to two new dimensionless parameters which are independent of ℓ and namely,

$$\omega^* = \frac{\omega \delta^2}{\nu}$$

and

$$\Pi_2 = \frac{\beta g \theta_w \delta^2}{\nu U_c} \quad .$$

The quantities chosen for comparison are the frequency response of the Nusselt number and the friction factor. These quantities are defined as:

$$Nu_1 \equiv \frac{h_1 \delta}{k} = -\frac{\delta}{\theta_w}\left(\frac{\partial \theta_1}{\partial y}\right)_w$$

$$f_1 \equiv \frac{\tau_{w1}}{\frac{1}{2}\rho U_c^2} = 2\frac{\nu}{U_o^2}\left(\frac{\partial u_1}{\partial y}\right)_w$$

For large values of frequency ω, Nu_1 and f_1 are expressed as:

$$Nu_1 = \frac{1}{\omega}\frac{\delta U_o}{\theta_w}\frac{1+2\sqrt{Pr}}{(1+\sqrt{Pr})^2}\left(\frac{\partial^2 \theta_o}{\partial y \partial x}\right)_w e^{-i\frac{\pi}{2}}$$

(62)

$$f_1 = 2\left(\frac{\omega \nu}{U_o^2}\right)^{1/2} e^{i\frac{\pi}{4}} \quad ,$$

and for small values of frequency,

$$Nu_1 = -\frac{B_1}{\Delta} = \frac{1}{\Delta \Pi_2} \sum_{n=0}^{\infty} \frac{E_n}{n!} \lambda_n \omega^{*n}$$

$$f_1 = \frac{2\nu}{\delta U_o} B = \frac{2\nu}{\delta U_o} \sum_{n=0}^{\infty} \frac{E_n}{n!} \gamma_n \omega^{*n} \qquad (63)$$

From the above equations, the quasi-steady values can be deduced as

$$(Nu_1)_{\omega=0} = \frac{\lambda_o}{\Delta \Pi_2}$$

$$(f_1)_{\omega=0} = \frac{2\nu \gamma_o}{\delta U_o} \quad . \qquad (64)$$

The quantities in Equations (63) are complex whereas the ones in (64) are real. Therefore, it is appropriate to normalize the quantities in Equation (63) with respect to their corresponding values in (64) and plot the amplitude and phase angle of each quantity as functions of frequency ω^*, for different values of Prandtl number.

One of the terms in Equations (62) is the steady function $\left(\frac{\partial^2 \theta_o}{\partial y \partial x}\right)_w$ that can be obtained from the numerical solution of Ostrach[2] in the following manner. In Reference 2, θ_o is expressed as

$$\theta_o = \theta_w H(\eta) \quad ,$$

where

$$\eta = C y x^{-1/4} \quad ,$$

and

$$C = \left(\frac{\beta g \theta_w}{4\nu^2}\right)^{1/4} \quad .$$

Then it follows that,

$$\left(\frac{\partial \theta_o}{\partial y}\right)_w = C\,\theta_w\,H'(0)\,x^{-1/4}$$

$$\left(\frac{\partial^2 \theta_o}{\partial y\,\partial x}\right)_w = -\frac{1}{4}\,C\,\theta_w\,H'(0)\,x^{-5/4} =$$

$$-\frac{1}{4\sqrt{2}}\,H'(0)\,(Gr_x)^{1/4}\,\frac{\theta_w}{x^2} \quad .$$

After necessary substitution and rearrangement, the following expressions are obtained for the normalized Nusselt number and friction factor frequency responses.

$$\frac{Nu_1}{(Nu_1)_{\omega=0}} = \alpha_{11}\,\omega^{*-1}\,e^{-i\frac{\pi}{2}} \quad \text{, for large values of } \omega^*$$

$$= \frac{1}{\lambda_o}\sum_{n=0}^{\infty}\frac{E_n}{n!}\,\lambda_n\,\omega^{*n} \quad \text{, for small values of } \omega^* \qquad (65)$$

$$\frac{f_1}{(f_1)_{\omega=0}} = \frac{1}{\gamma_o}\,\omega^{*1/2}\,e^{i\frac{\pi}{4}} \quad \text{, for large values of } \omega^*$$

$$= \frac{1}{\gamma_o}\sum_{n=0}^{\infty}\frac{E_n}{n!}\,\gamma_n\,\omega^{*n} \quad \text{, for small values of } \omega^* \text{ ,} \qquad (66)$$

where α_{11} is a function of Prandtl number and is defined in Appendix III. Defining φ_{f_1} as the phase angle of the friction factor and φ_{Nu_1} as the phase angle of Nusselt number and the amplitude of each quantity by placing it between "absolute value" signs ($|\ |$), they can be expressed as follows:

(a) for large values of ω^*

$$\begin{aligned} \varphi_{f_1} &= 45^\circ \\ \frac{|f_1|}{(f_1)_{\omega=0}} &= \frac{1}{\gamma_0}\,\omega^{*1/2} \\ \varphi_{Nu_1} &= -90^\circ \\ \frac{|Nu_1|}{(Nu_1)_{\omega=0}} &= \alpha_{11}\,\omega^{*-1} \end{aligned} \tag{67}$$

and (b) for small values of ω^*

$$\varphi_{f_1} = \tan^{-1}\left\{\frac{\sum_{n=0}^{\infty}\frac{\gamma_{2n+1}}{(2n+1)!}\,\omega^{*2n+1}}{\sum_{n=0}^{\infty}\frac{\gamma_{2n}}{(2n)!}\,\omega^{*2n}}\right\} \tag{68}$$

$$\frac{|f_1|}{(f_1)_{\omega=0}} = \frac{1}{\gamma_0}\left\{\left[\sum_{n=0}^{\infty}\frac{\gamma_{2n}}{(2n)!}\,\omega^{*2n}\right]^2 + \left[\sum_{n=0}^{\infty}\frac{\gamma_{2n+1}}{(2n+1)!}\,\omega^{*2n+1}\right]^2\right\}^{1/2}$$

$$\varphi_{Nu_1} = \tan^{-1}\left\{\frac{\sum_{n=0}^{\infty}\frac{\lambda_{2n+1}}{(2n+1)!}\,\omega^{*2n+1}}{\sum_{n=0}^{\infty}\frac{\lambda_{2n}}{(2n)!}\,\omega^{*2n}}\right\} \qquad \text{(68 cont'd)}$$

$$\frac{|Nu_1|}{(Nu_1)_{\omega=0}} = \frac{1}{\lambda_0}\left\{\left[\sum_{n=0}^{\infty}\frac{\lambda_{2n}}{(2n)!}\,\omega^{*2n}\right]^2 + \left[\sum_{n=0}^{\infty}\frac{\lambda_{2n+1}}{(2n+1)!}\,\omega^{*2n+1}\right]^2\right\}^{1/2}.$$

Figures 4 and 5 show plots of amplitude ratios versus ω^* for Pr = 0.757. This is the Prandtl number that makes $\Delta = 1$ and is the lower limit of Pr in the small frequency analysis. Figures 6 and 7 show the variation of phase angles with the frequency parameter ω^*. In Figure 6 the two limiting curves intersect at a frequency ω_o^* and in Figure 7 at ω_1^*. These two frequencies, however, are identical for Pr = 0.757 where the two boundary layers (velocity and thermal) are equal and different for other values of Pr. Careful inspections of Figures 4 through 15 indicates that the frequency ω_o^* is a good criterion for estimating the range of validity of the two limiting solutions. It appears that $2\,\omega_o^*$ may be used as the lower limit of the large frequency solution and $1/2\,\omega_o^*$ as the upper limit of the small frequency solution.

Figure 18 shows that ω_o^* is a decreasing function of Prandtl number. This is the most important conclusion drawn from the small frequency calculations. This criterion will be extended to the large

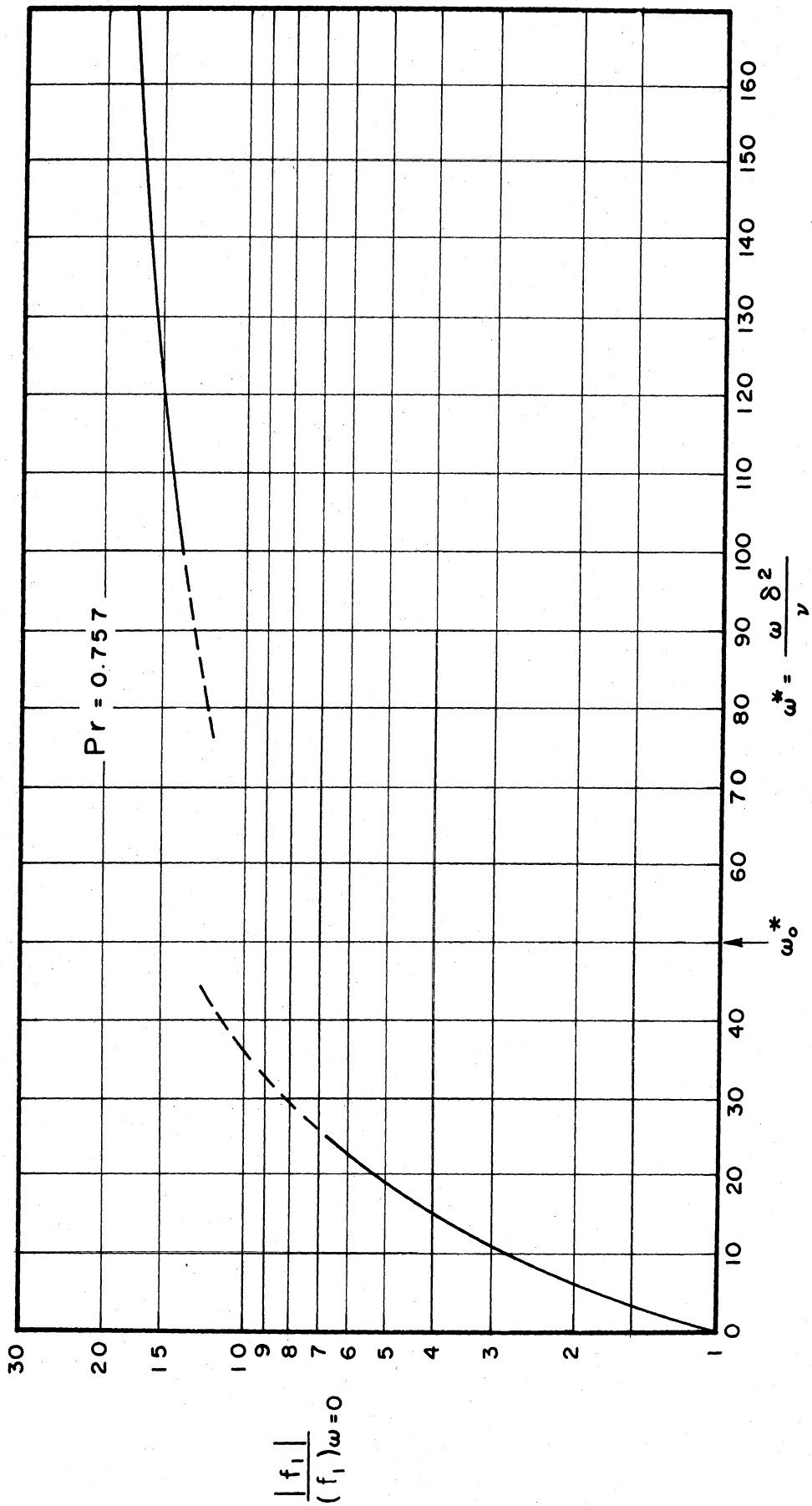

Figure 4. Amplitude Ratio of Friction Factor as a Function of ω^*.

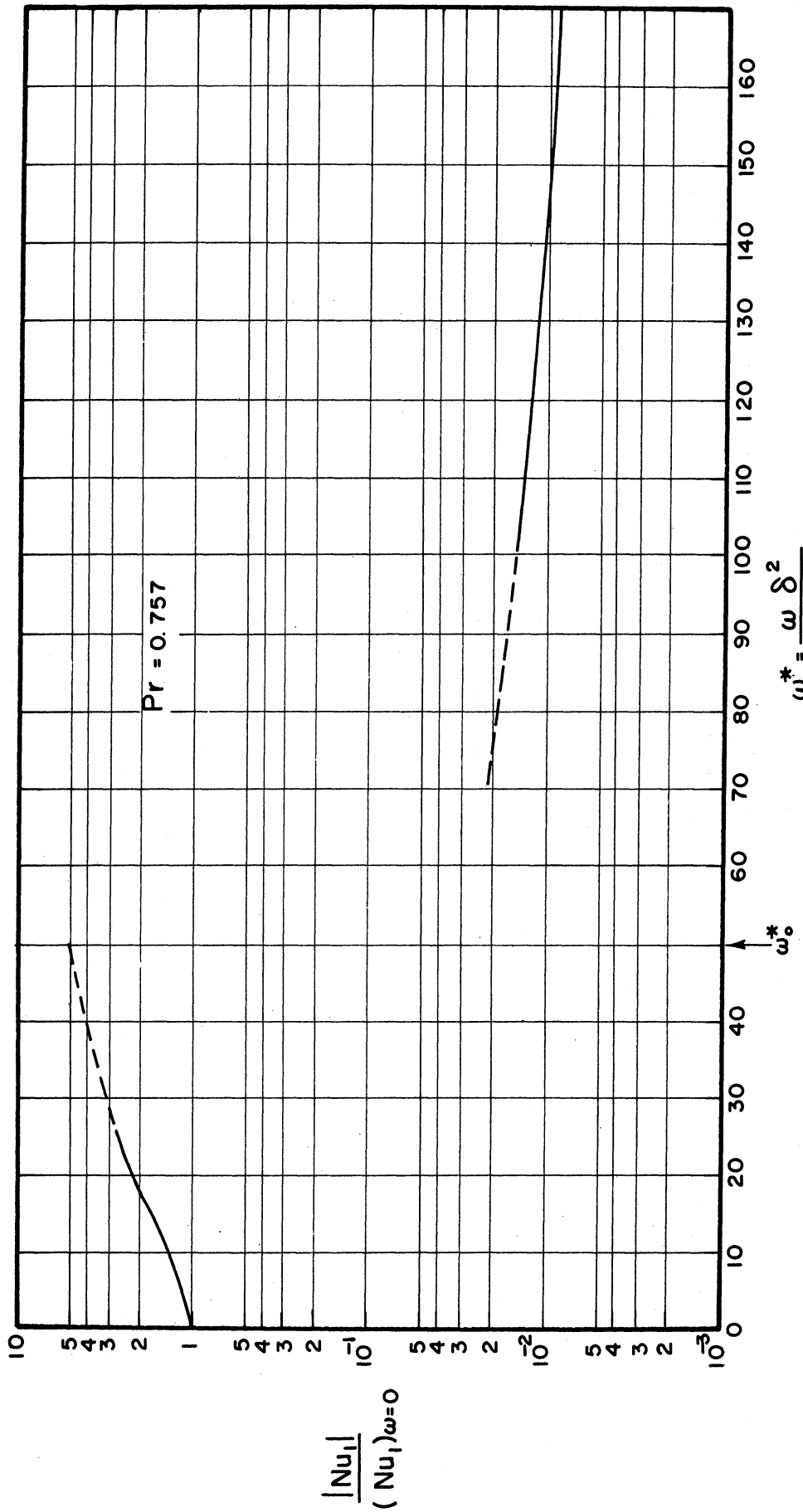

Figure 5. Amplitude Ratio of Nusselt Number as a Function of ω^*.

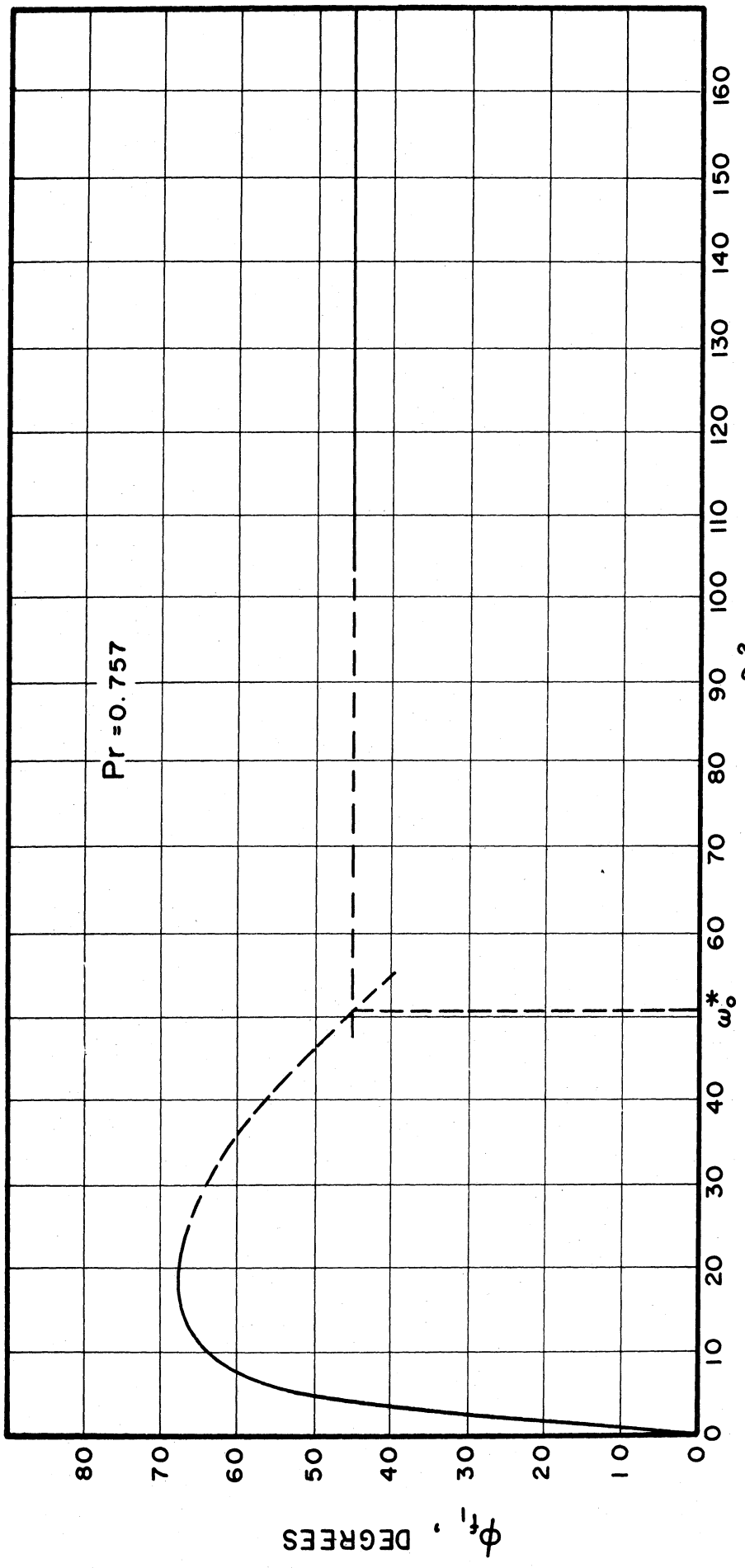

Figure 6. Phase Angle of the Friction Factor as a Function of ω^*.

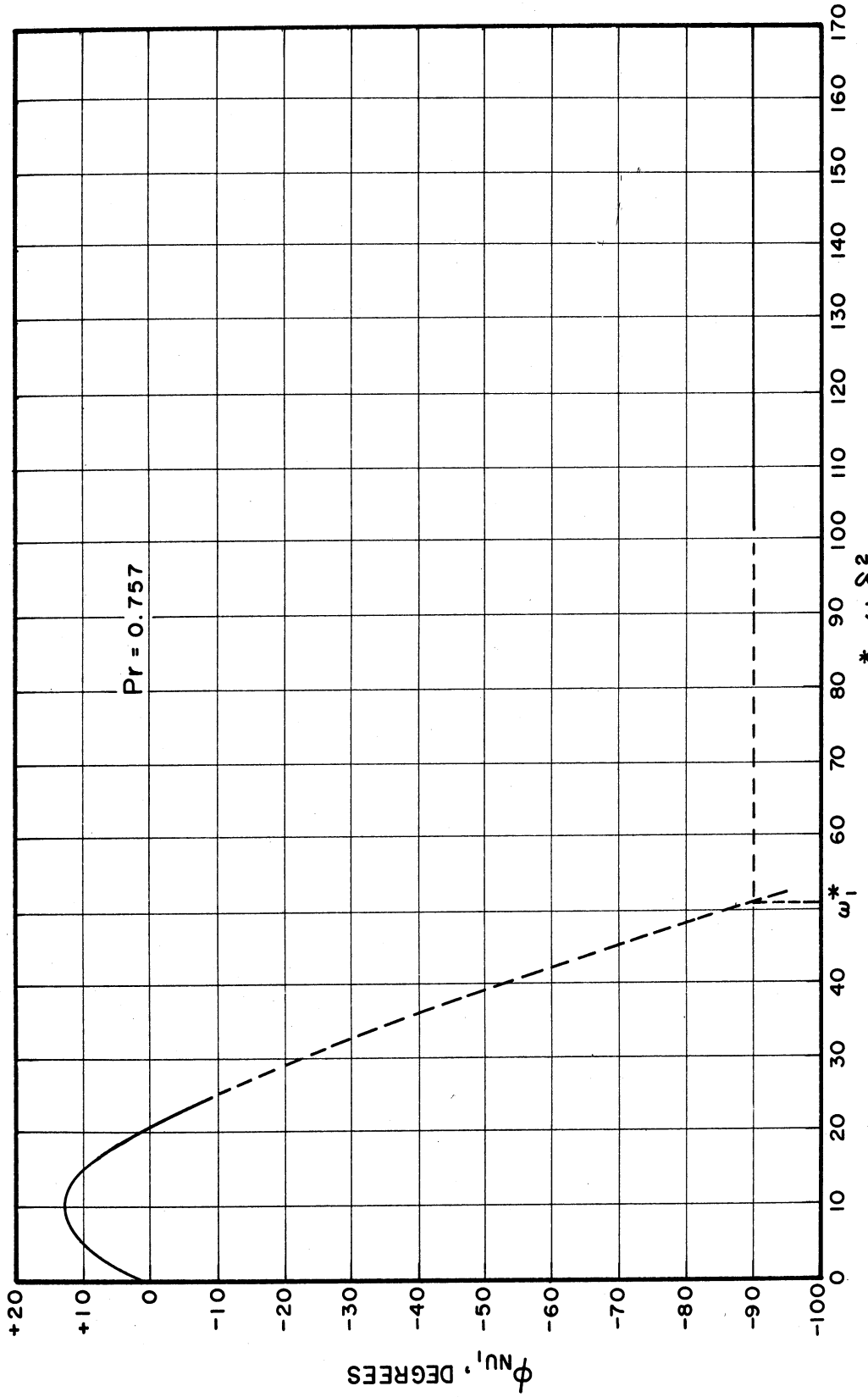

Figure 7. Phase Angle of the Nusselt Number as a Function of ω^*.

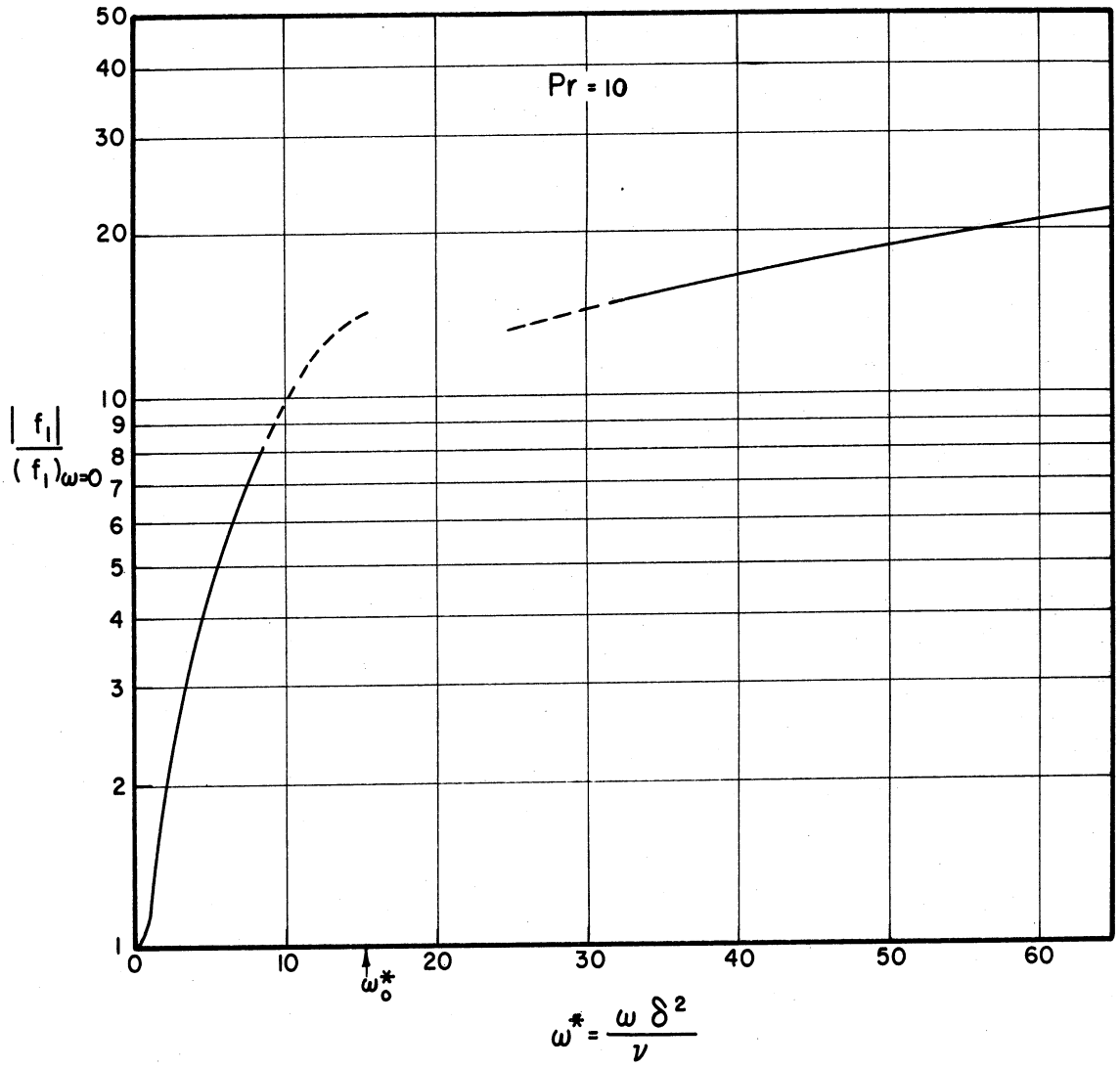

Figure 8. Amplitude Ratio of the Friction Factor as a Function of ω^*.

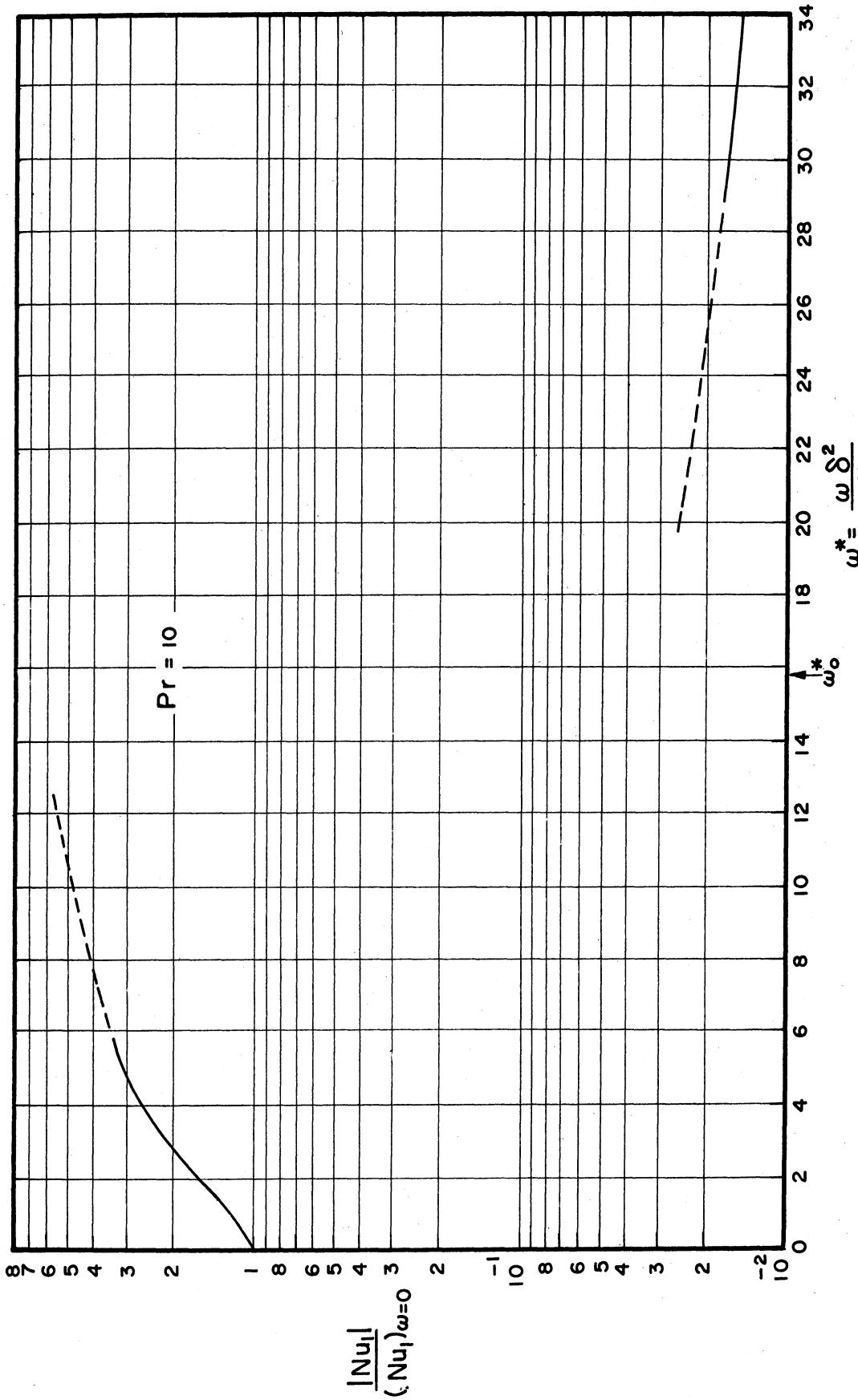

Figure 9. Amplitude Ratio of the Nusselt Number as a Function of ω^*.

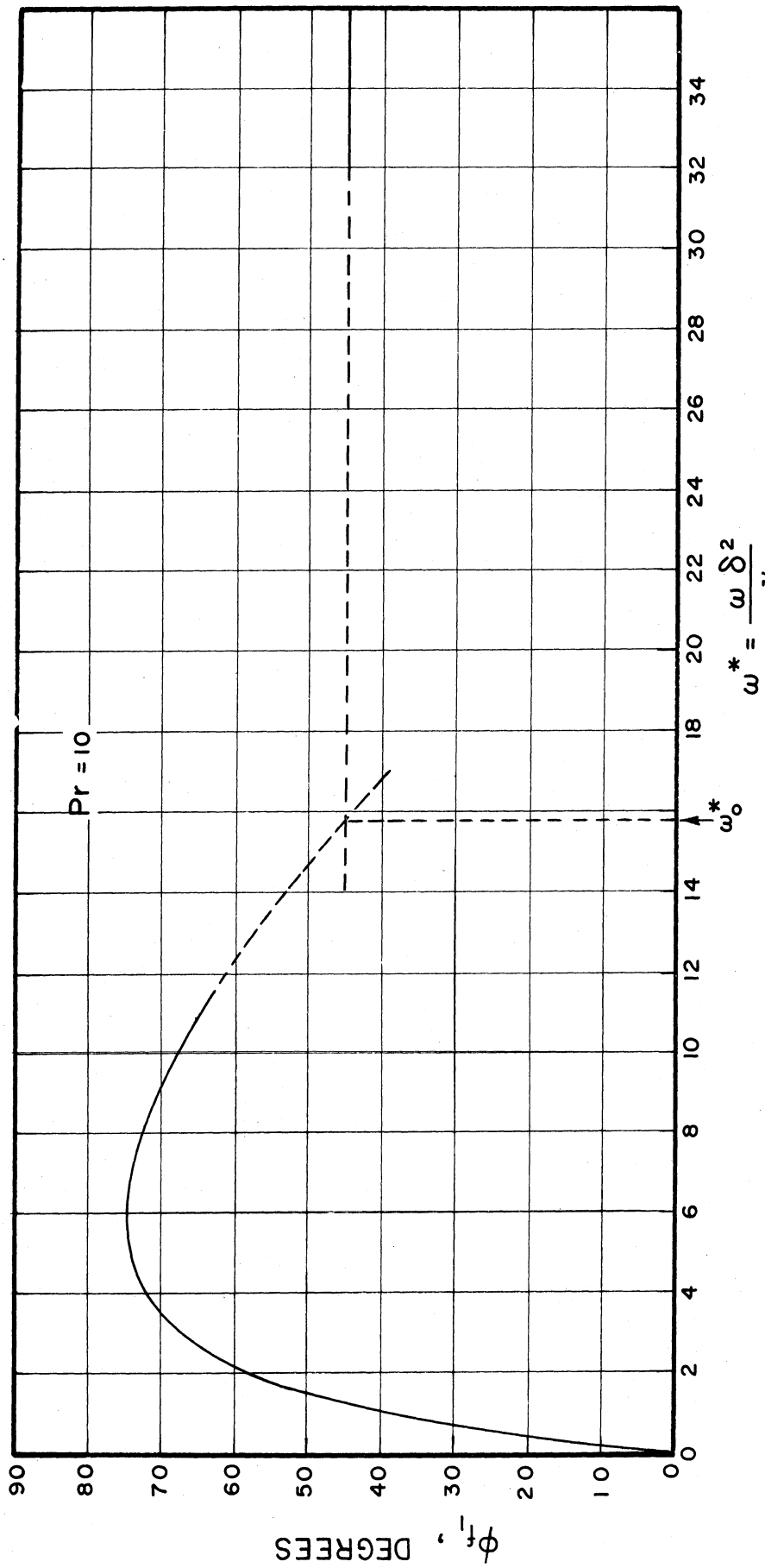

Figure 10. Phase Angle of the Friction Factor as a Function of ω^*.

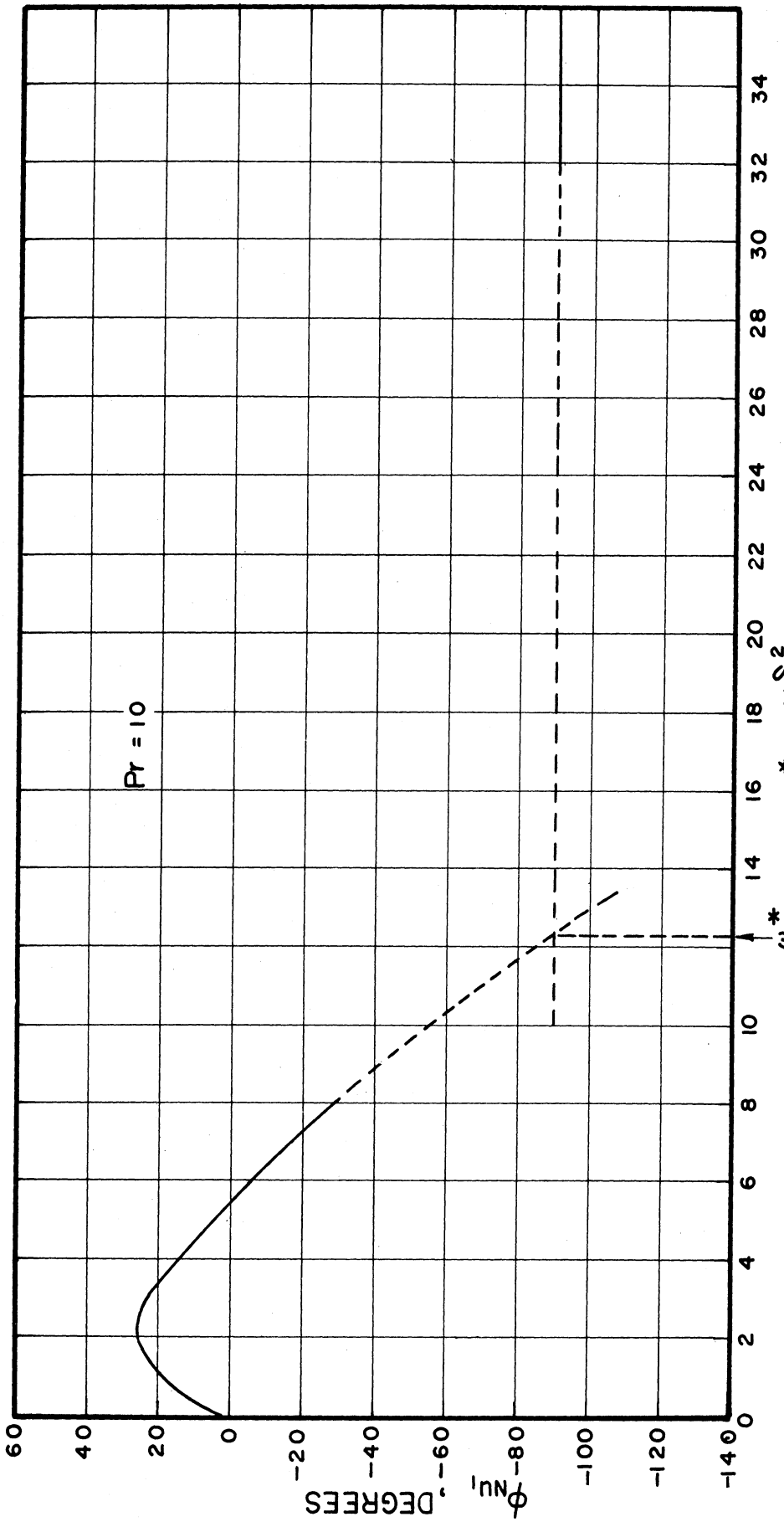

Figure 11. Phase Angle of the Nusselt Number as a Function of ω^*.

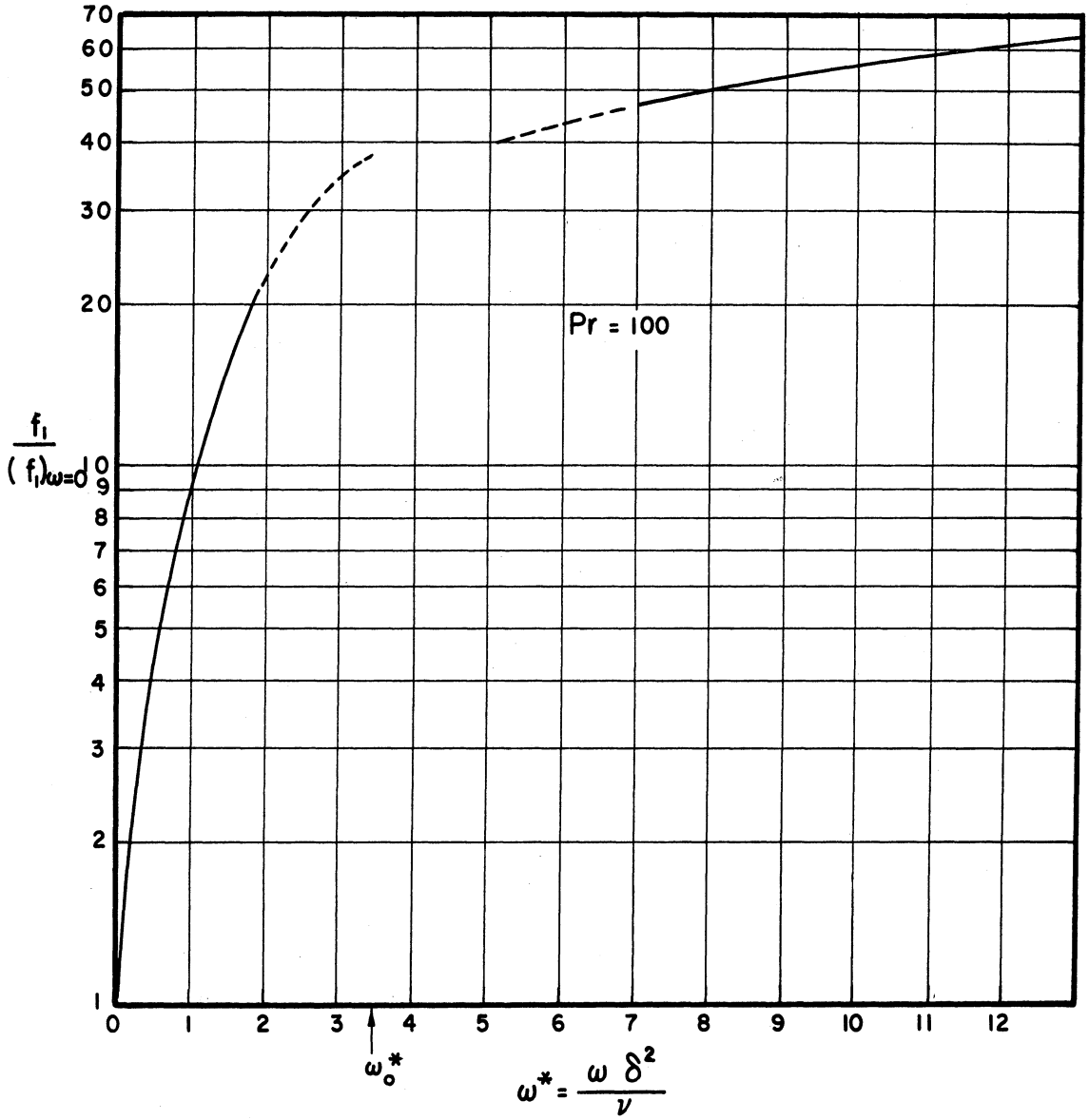

Figure 12. Amplitude Ratio of the Friction Factor as a Function of ω^*.

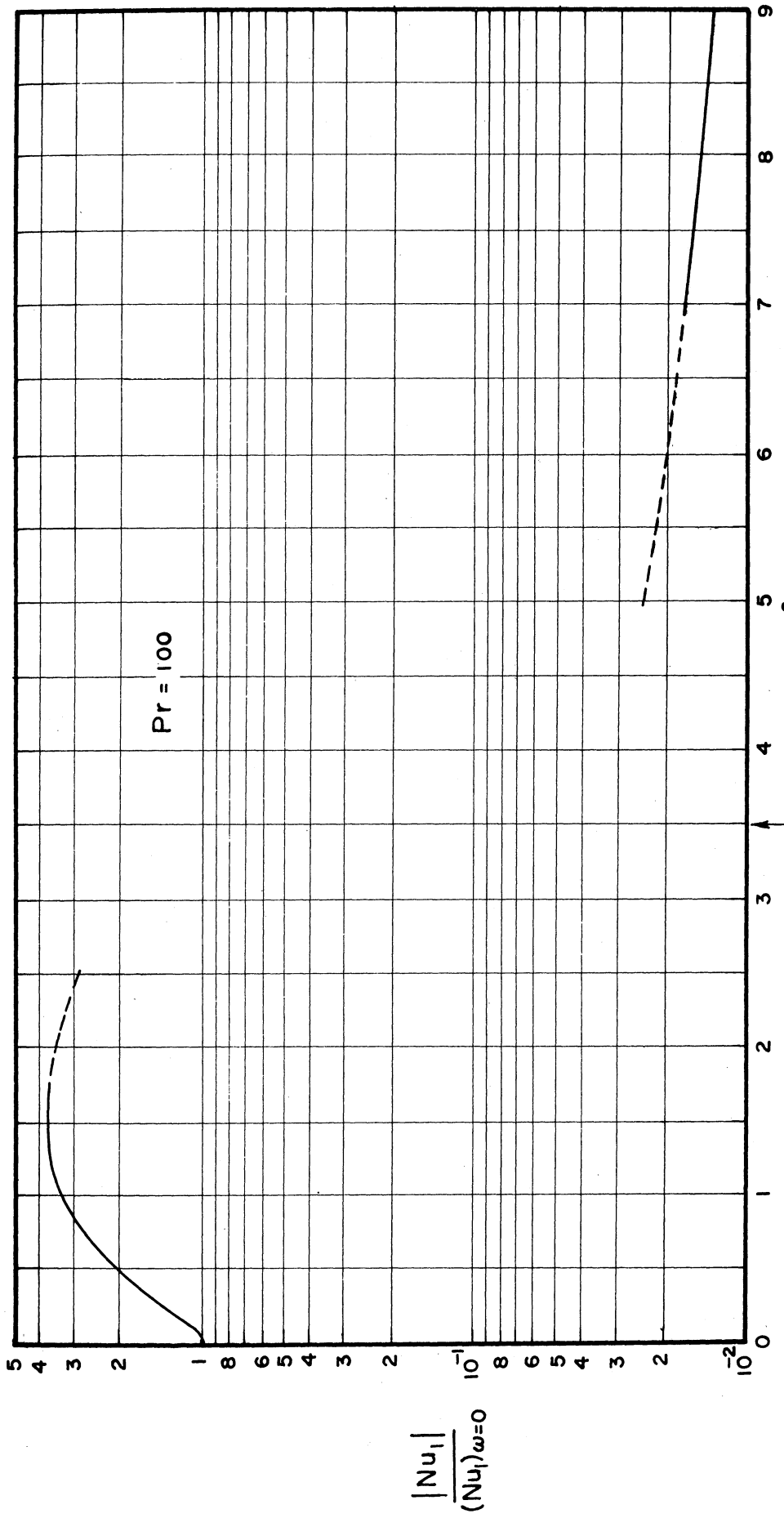

Figure 13. Amplitude Ratio of the Nusselt Number as a Function of ω^*.

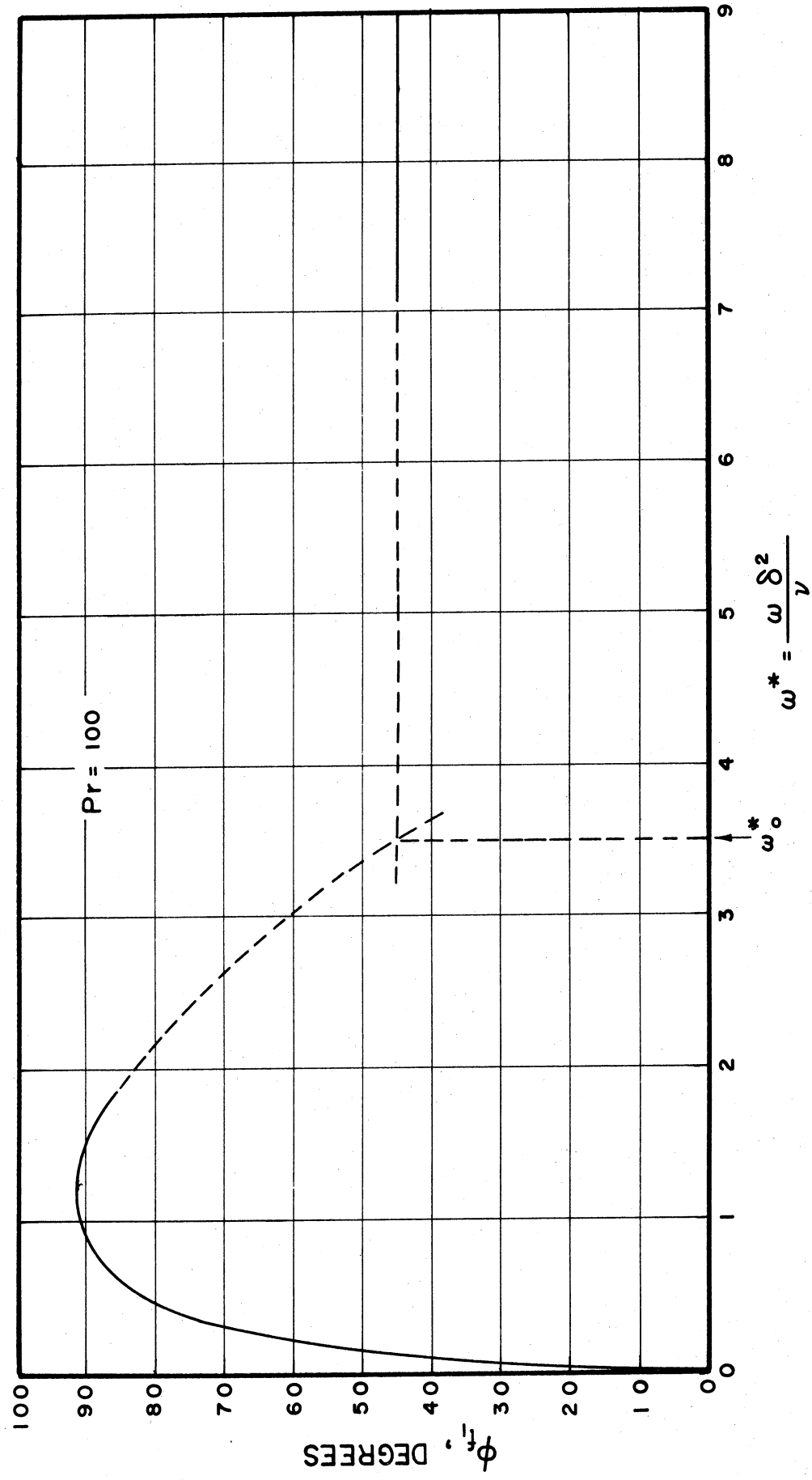

Figure 14. Phase Angle of the Friction Factor as a Function of ω^*.

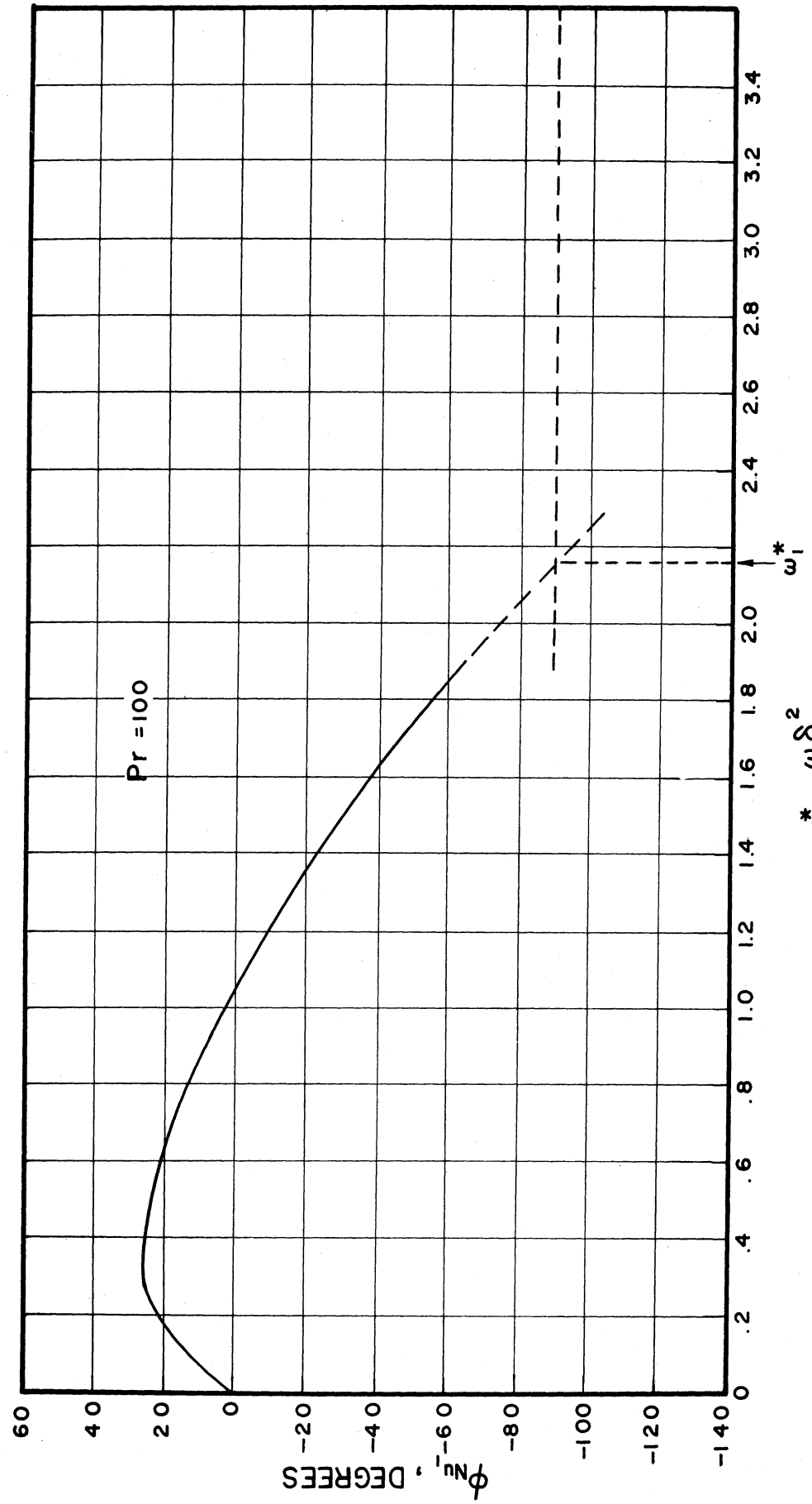

Figure 15. Phase Angle of the Nusselt Number as a Function of ω^*.

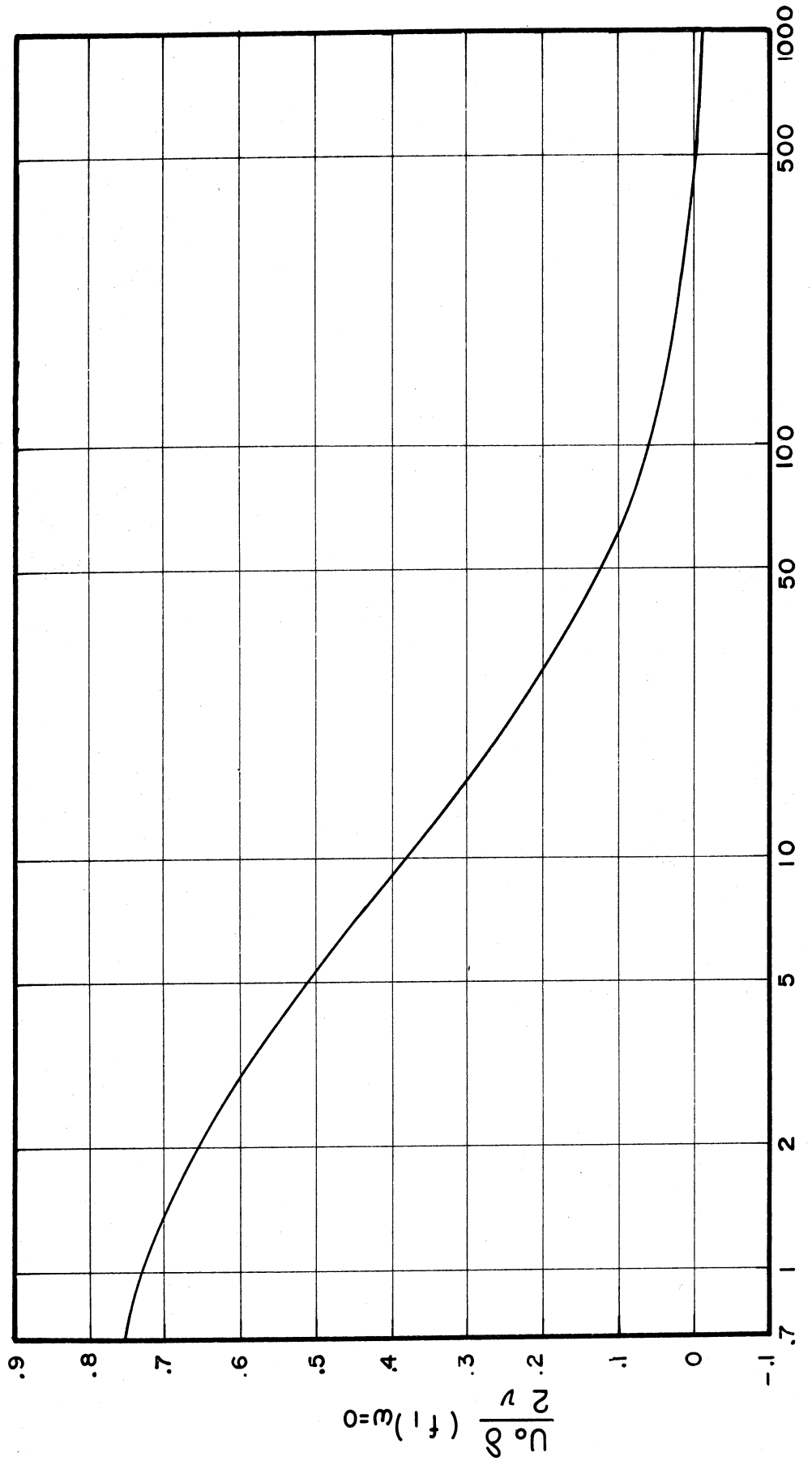

Figure 16. Quasi-Steady Friction Factor as a Function of Prandtl Number.

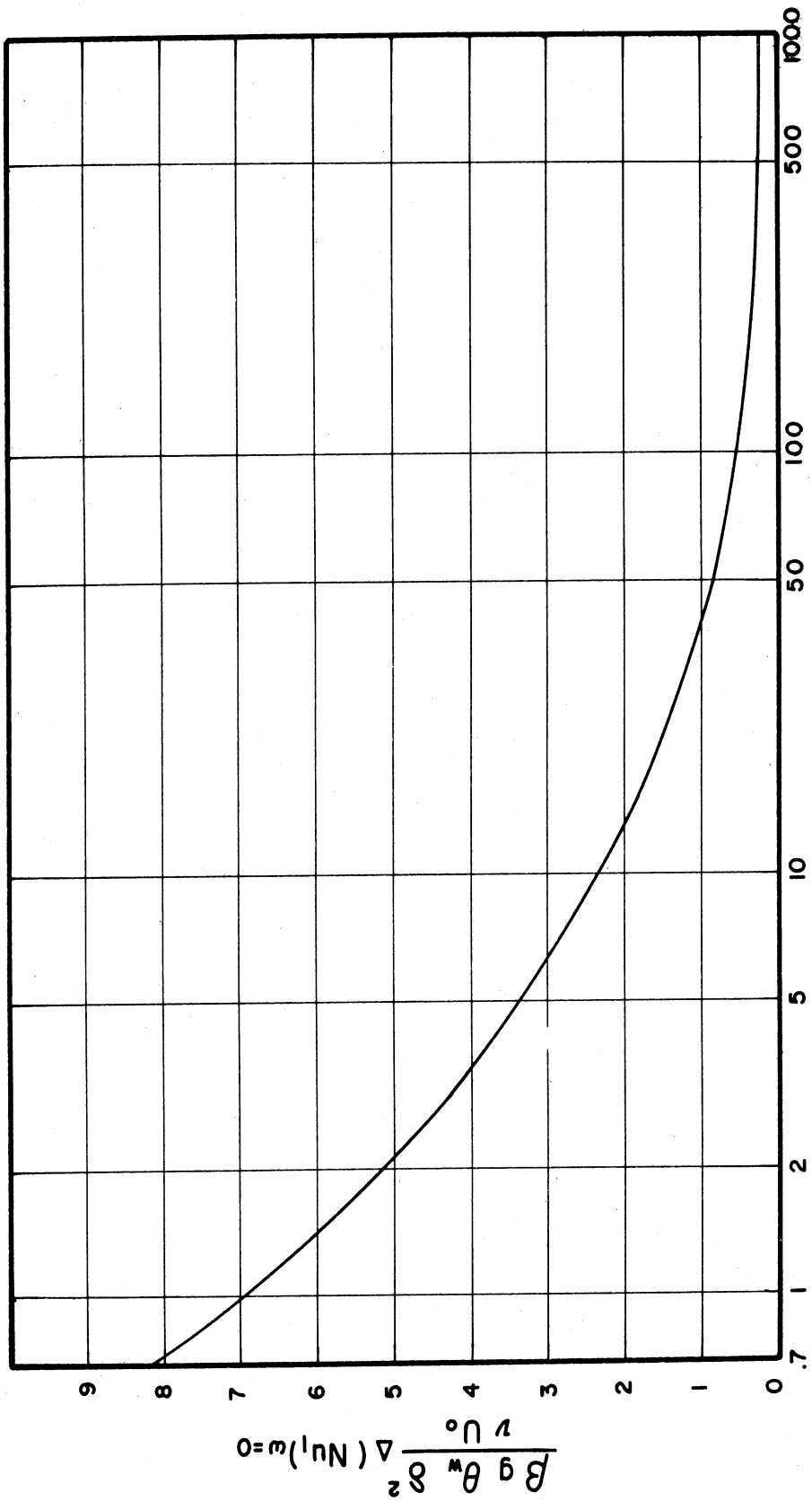

Figure 17. Quasi-Steady Nusselt Number as a Function of Prandtl Number.

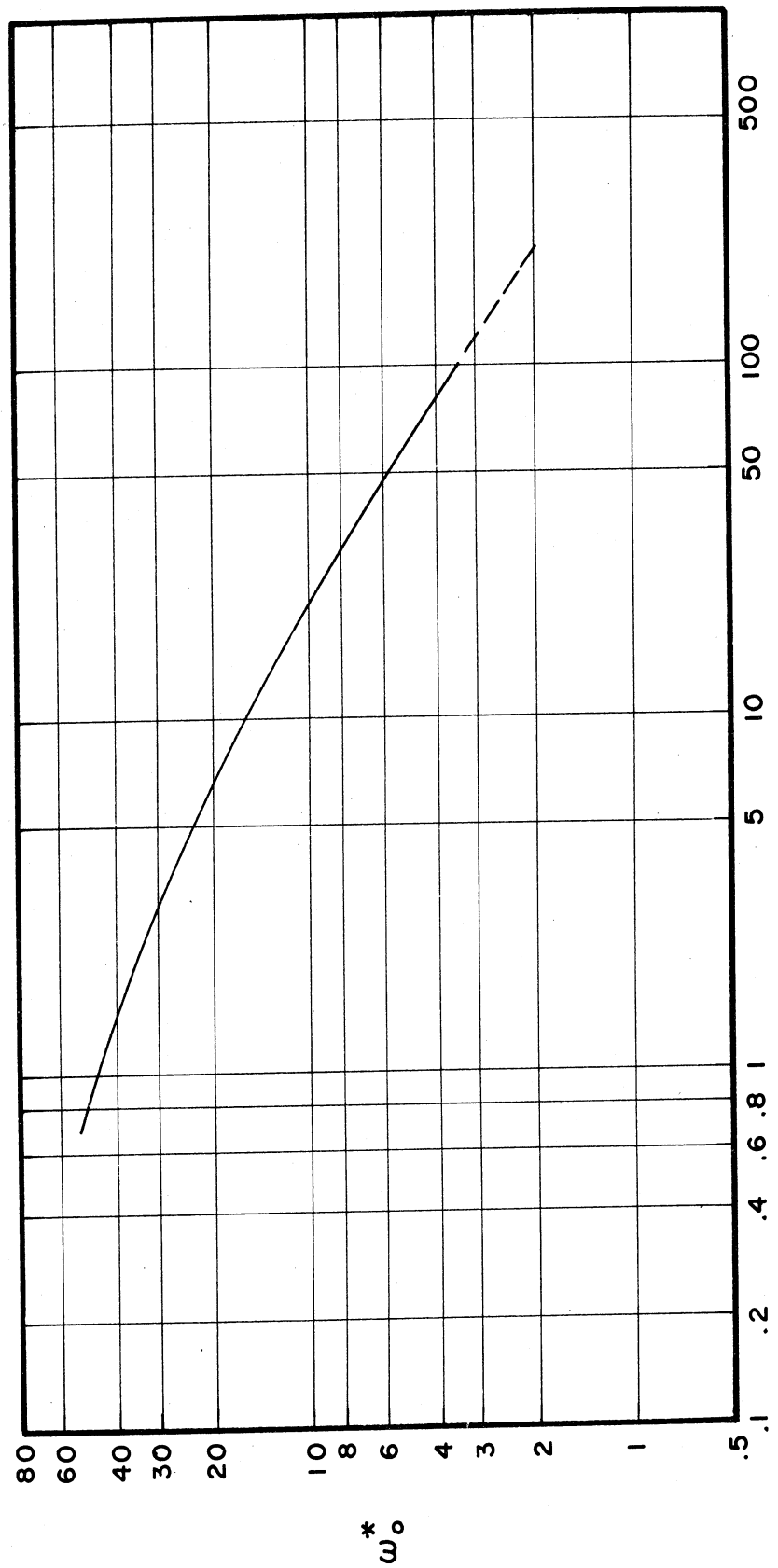

Figure 18. Critical Frequency Parameter as a Function of Prandtl Number.

frequency solutions of the third approximation; this would eliminate the necessity of carrying out a separate integral procedure. Therefore, only large frequency solutions will be obtained for the third approximation.

Solutions to the Third Approximation

As it was demonstrated in Equations (23), third approximation velocities and temperature consist of a term which is only a function of x and y, and another term which oscillates harmonically with a frequency of 2ω. The oscillating component that integrates to zero with respect to time, is of less importance compared to the non-oscillatory component which contributes to the steady phenomenon of flow and heat transfer. It is this component that results in a net change in friction and the rate of heat transfer. Therefore, attention is focused on these components that are governed by Equations (24), (25) and (26). Solutions are sought for large values of frequency and the region near the wall which allow simplification of the differential equations. Substituting Equation (31) into (24) and (26), gives,

$$u_o \frac{\partial u_{20}}{\partial x} + \frac{\partial u_o}{\partial x} u_{20} + v_o \frac{\partial u_{20}}{\partial y} + \frac{\partial u_o}{\partial y} v_{20} = \nu \frac{\partial^2 u_{20}}{\partial y^2} + \beta g \theta_{20}$$

$$u_o \frac{\partial \theta_{20}}{\partial x} + v_o \frac{\partial \theta_{20}}{\partial y} + u_{20} \frac{\partial \theta_o}{\partial x} + v_{20} \frac{\partial \theta_o}{\partial y} =$$

$$a \frac{\partial^2 \theta_{20}}{\partial y^2} - \frac{1}{4} \left(u_1 \frac{\overline{\partial \theta_1}}{\partial x} + \bar{u}_1 \frac{\partial \theta_1}{\partial x} \right) .$$

It should be noted that near the wall (small y),

$$u_0 \propto y \qquad \frac{\partial u_0}{\partial x} \propto y$$

$$u_{20} \propto y \qquad \frac{\partial u_{20}}{\partial x} \propto y$$

$$\frac{\partial \theta_0}{\partial x} \propto y \qquad \frac{\partial \theta_{20}}{\partial x} \propto y$$

$$v_0 \propto y^2 \qquad v_{20} \propto y^2 \quad ,$$

where $\propto$ signifies proportionality.

Near the wall and for large values of frequency, the differential equations can be simplified by retaining only the highest order terms.

Neglecting terms of the order of y^2 and smaller, the following differential equations are obtained.

$$\nu \frac{\partial^2 u_{20}}{\partial y^2} = -\beta g \theta_{20}$$

$$u_{20}(x, 0) = 0 \quad , \tag{69}$$

and,

$$a \frac{\partial^2 \theta_{20}}{\partial y^2} = \frac{1}{4}\left(u_1 \frac{\overline{\partial \theta_1}}{\partial x} + \bar{u}_1 \frac{\partial \theta_1}{\partial x} \right)$$

$$\theta_{20}(x, 0) = 0 \quad . \tag{70}$$

Equations (69) and (70) plus the condition of the boundedness of general solutions of the differential equations, are sufficient to obtain expressions for the rate of heat transfer and shear stress at the wall.

The value of $\theta_1(x,y)$ used in Equations (70) was expressed in Equation (34).

Defining

$$Nu_{20_x} \equiv -\frac{x}{\theta_w}\left(\frac{\partial \theta_{20}}{\partial y}\right)_w$$

and

$$f_{20} \equiv 2\frac{\nu}{U_o^2}\left(\frac{\partial u_{20}}{\partial y}\right)_w \quad ,$$

the final results of the third approximation are expressed as:

$$Nu_{20_x} = \frac{5}{32\sqrt{2}} H'(0) \frac{Pr}{(1+Pr)(1+\sqrt{Pr})^2} (Gr_x)^{1/4} \left(\frac{U_o}{\omega x}\right)^2$$

and, (71)

$$f_{20} = -\frac{5}{32\sqrt{2}} H'(0) \frac{Pr^2(5+Pr)}{(1+Pr)^3} (Gr_x)^{5/4} \left(\frac{\nu}{\omega x^2}\right)^3 .$$

Figures 19 and 20 show the Prandtl number dependency of N_{20_x} and f_{20}.

Summing up the results for large values of frequency,

$$Nu_x = Nu_{0x} + \epsilon \mathcal{R}\left\{Nu_{1x} e^{i\omega t}\right\} + \epsilon^2 Nu_{20x} + \epsilon^2 \mathcal{R}\left\{Nu_{21x} e^{2i\omega t}\right\} \quad , \quad (72)$$

and

$$f = f_o + \epsilon \mathcal{R}\left\{f_1 e^{i\omega t}\right\} + \epsilon^2 f_{20} + \epsilon^2 \mathcal{R}\left\{f_{21} e^{2i\omega t}\right\} .$$

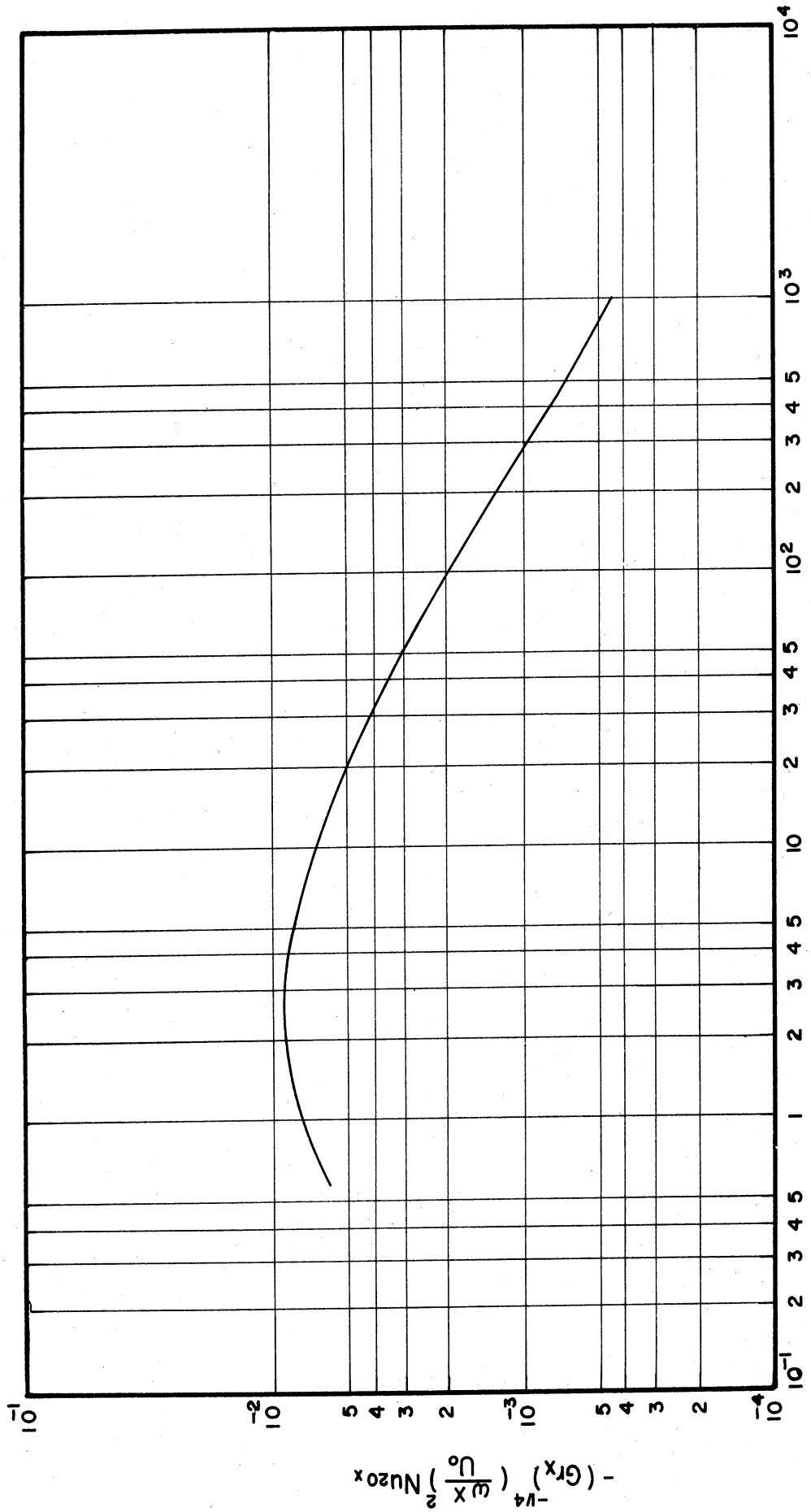

Figure 19. The Steady Decrease in Nusselt Number as a Function of Prandtl Number.

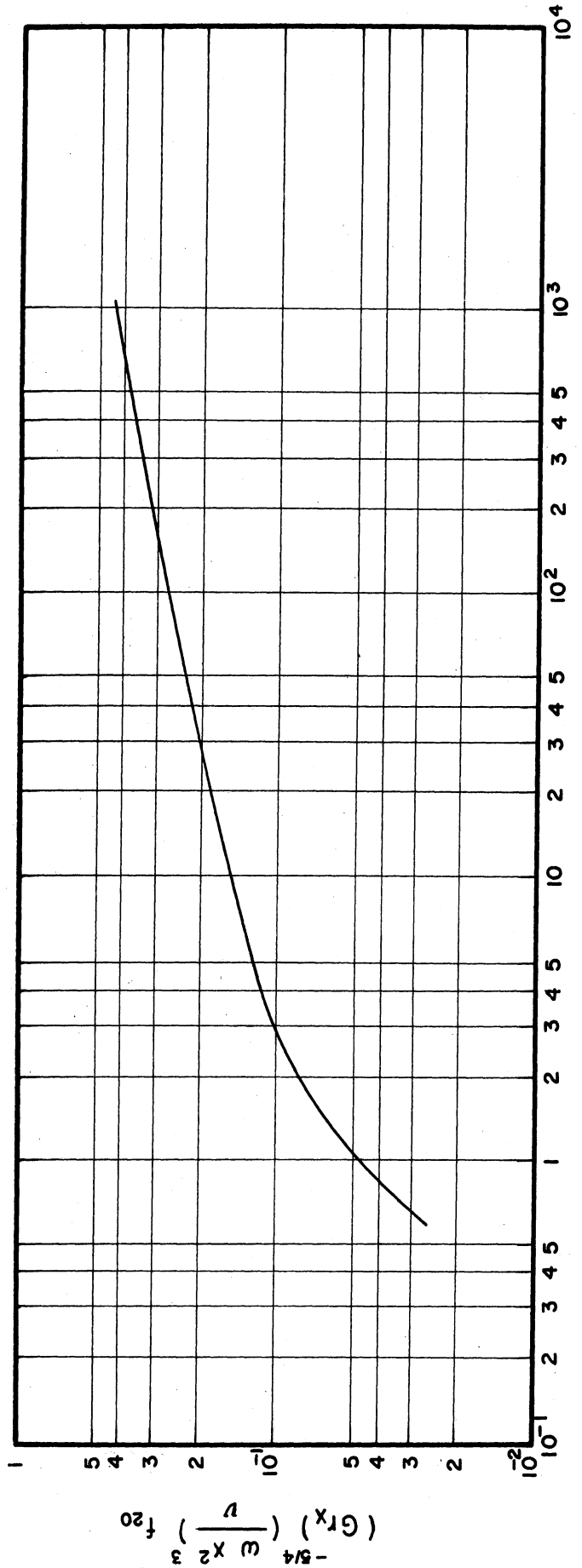

Figure 20. The Steady Increase in Friction Factor as a Function of Prandtl Number.

Substituting each term with its corresponding expression and retaining the first three terms, the following equations will be obtained.

$$Nu_x = -\frac{H'(0)}{\sqrt{2}}(Gr_x)^{1/4}\left[1+\frac{1}{4}\frac{1+2\sqrt{Pr}}{(1+\sqrt{Pr})^2}\frac{\epsilon U_o}{\omega x}\cos(\omega t-\frac{\pi}{2})-\right.$$

$$\left.\frac{5}{32}\frac{Pr}{(1+Pr)(1+\sqrt{Pr})^2}\left(\frac{\epsilon U_o}{\omega x}\right)^2\right] \qquad (73)$$

$$f = 2\sqrt{2}\left(\frac{\nu}{U_o x}\right)^2 (Gr_x)^{3/4}\left[F''(0)+\frac{1}{\sqrt{2}}(Gr_x)^{-3/4}\left(\frac{\omega x^2}{\nu}\right)^{1/2}\frac{\epsilon U_o x}{\nu}\cos(\omega t+\frac{\pi}{4})\right.$$

$$\left.-\frac{5}{128}H'(0)\frac{Pr^2(5+Pr)}{(1+Pr)^3}(Gr_x)^{1/2}\left(\frac{\omega x^2}{\nu}\right)^{-3}\left(\frac{\epsilon U_o x}{\nu}\right)^2\right] ,$$

Where $F(\eta)$ is the η dependency of the stream function in Ostrach's similarity solution[2] defined as

$$\psi(x,\eta) = 4\nu C x^{3/4} F(\eta) .$$

CHAPTER III

DISCUSSION OF THEORETICAL RESULTS

In the preceding chapter, the problem was stated, formulated, and treated analytically. The differential equations were perturbed for small oscillations and the first three terms calculated.

The first term is the steady free convection for which exist both numerical and integral solutions. However, an improved integral solution was obtained which agrees very well with the exact solution in the range of Pr from .7 to 200. According to these calculations, the Prandtl number at which the thermal boundary layer thickness equals the velocity boundary layer thickness is 0.757. This solution was necessary for the integral procedure used on the second approximation.

The differential equations for the second term were solved using the classical simplifications for large values of frequency. Expressions thus obtained for Nu_1 and f_1, show that heat transfer lags behind the plate oscillations by 90 degrees with an amplitude which decreases with frequency, and the shear stress at the wall leads the plate oscillations by 45 degrees with an amplitude which increases with increasing frequency. The heat transfer is a decreasing function and shear stress an increasing function of Prandtl number. In the small frequency region, the shear stress increases its amplitude with increasing frequency and always has a phase lead. This is the same trend that it possessed for large values of frequency. The heat transfer, however, experiences an increase in its amplitude and possesses a small phase lead at the beginning of the small frequency region. The phase angle after reaching a

peak lead, decreases to a lag for slightly higher frequencies. The amplitude of heat transfer should also begin to decrease but the present series solution fails to demonstrate this fact for Pr = 0.757 and 10. For Pr = 100, Figure 13, this decreasing effect does fall within the range in which the series solution is valid.

As mentioned in Chapter II, twice the value of ω_o^* is a good estimate of the lower limit of large frequency range. For an eight inch plate at 200°F, placed in air at 80°F, the boundary layer thickness at $x = 8"$ is 0.17 inches, $\omega_o^* = 51.5$ and the critical frequency ω_{crit} beyond which the large frequency solutions are valid, can be calculated as

$$\omega_{crit} = 2\nu\,\omega_o^*\,\delta^{-2} = 101 \quad rad/sec\ ,$$

which corresponds to 16 cycles per second. Therefore the assumption of large frequencies does not present too much of a restriction and can cover a wide range of frequencies.

The perturbation procedure shows that the functions of the order of ϵ^2, or the third approximation functions, must be composed, each, of two terms, a time-independent term, and an oscillating term. Calculations were carried out only for the time-independent, or the steady terms. The perturbation procedure alone predicts a steady change in heat transfer and shear stress due to a purely harmonic disturbance (plate oscillations). The question is, whether this steady change is zero, positive or negative. The results of the calculations presented in Equation (71) show that this steady change is positive for the shear stress and negative for the rate of heat transfer.

Any steady change in heat transfer coefficient, whether it is a decrease or an increase, will have valuable engineering applications provided the change is substantial. Although perturbation procedure involves small changes, it will be helpful to estimate the order of magnitude of these changes and compare them with relative intensity of the disturbance and namely, ϵ. For an eight inch plate at 200°F placed in air at 80°F,

$$Gr_x = 4.59 \times 10^7 \quad , \quad Nu_{o_x} = 29.36$$

and

$$u_{o_{max}} = U_o = 1.14 \ ft/sec \quad .$$

Taking $\epsilon = 0.2$ (this corresponds to an amplitude of 0.022" for a frequency of 20 cps) the steady change in the local Nusselt number will be

$$\epsilon^2 Nu_{20_x} = -0.0042 \quad ,$$

which is a decrease of 0.014%. This change compared to 20% is negligible. For all practical purposes, one may conclude that in the laminar region the rate of heat transfer is not disturbed by the oscillations of the plate.

It is interesting to note that the per cent decrease in Nusselt number is only a function of Prandtl number and $\frac{\epsilon U_o}{\omega x}$. By definition,

$$\epsilon U_o = A\omega \quad , \qquad (74)$$

where A is the amplitude of plate oscillations. But by (74), $\frac{\epsilon U_o}{\omega x} = \frac{A}{x}$ i.e., the per cent decrease in Nusselt number is only a function of Pr and $\frac{A}{x}$.

Per cent increase in friction factor, however, is an increasing function of local Grashof number as well as Prandtl number.

Although the expressions derived for the rate of heat transfer and shear stress at the wall are restricted to narrow regions and approximate, they have the important advantage of being in closed form. Furthermore, these expressions are simple and explicit with respect to all the parameters involved. This will best serve the study of qualitative behavior of the phenomenon in question.

CHAPTER IV

STEADY LAMINAR FREE-FORCED CONVECTION PHENOMENON

This chapter is based on a portion of the analysis in Chapter II herein discussed in detail. During the course of obtaining a solution for small values of frequency, expressions were derived for Nusselt number and friction factor for the case of zero frequency. These expressions added to their corresponding steady terms are solutions to the problem of steady free-forced convection from a vertical flat plate. Figure 21 shows the physical model where U_∞ is the free stream velocity and could be in either + x or - x direction.

Since the quasi-steady solutions are perturbations around steady free convection, the results discussed in this chapter will only represent the effect of a small free stream velocity on steady free convection heat transfer and will not cover the regions where forced convection predominates. The expression for local Nusselt number will be

$$Nu_x = D_1 (Gr_x)^{1/4} + D_2 (Gr_x)^{-1/4} Re_x \quad , \tag{75}$$

where

$$Re_x = \frac{U_\infty x}{\nu}$$

and

$$D_2 = \frac{0.004875\ \lambda_0}{\Delta (1.8\Delta - 1)^{3/4}} \quad .$$

Values of D_1 are tabulated in Appendix II. The second term on the right of Equation (75) can be integrated over a finite length of the plate giving the average change in Nusselt number.

$$Nu_\ell = \frac{4}{3} D_1 (Gr_\ell)^{1/4} + 4 D_2 (Gr_\ell)^{-1/4} Re_\ell \tag{76}$$

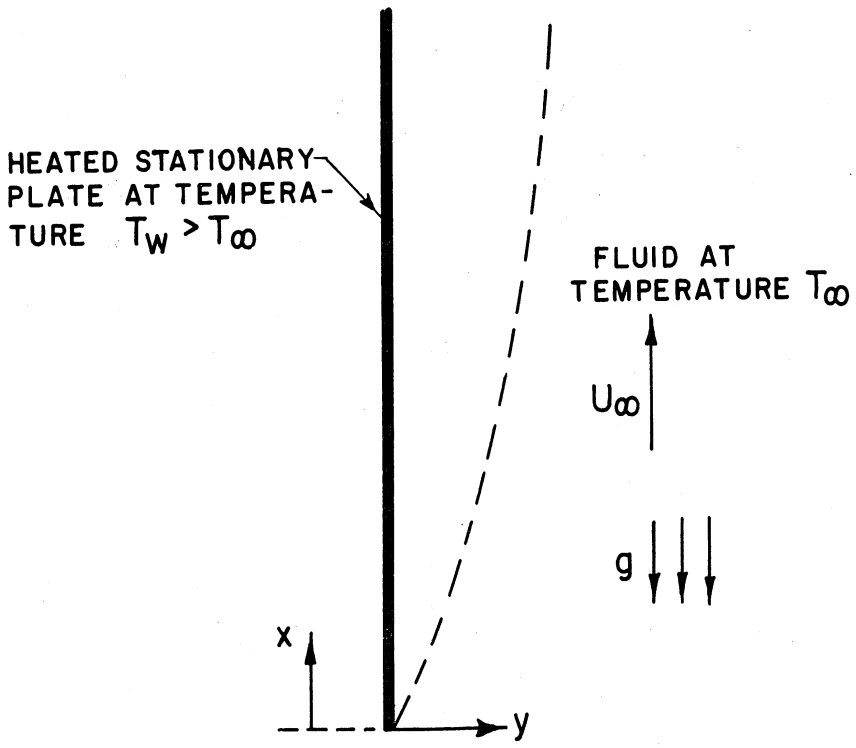

Figure 21. Physical Model for the Zero-Frequency Case.

The above expression will hold as long as

$$(Gr_\ell)^{-1/2} Re_\ell < D_3(Pr) \quad ,$$

where $D_3(Pr) = (\beta g \theta_w x)^{-1/2} u_{o_{max}}$ has been plotted versus Pr in Figure 3, and also tabulated in Appendix II. For a gas, (Pr = 0.76), in free convection, with $Gr_\ell = 10^8$, a free stream flow with $Re = 10^3$, will give rise to a change of 3.8% in the average Nusselt number — an increase if U_∞ is in + x direction and a decrease otherwise. The use of Equation (76) is recommended for predicting changes in average Nusselt number up to about 10%.

CHAPTER V

EXPERIMENTAL WORK

Introduction

An experimental program has been conducted as suggested by the analysis of Chapter II. Before the final design of the test section, a number of preliminary isothermal tests were made in water of different geometrical configurations. The purpose of these tests was to seek an experimental model that would closely approximate the analytical model of Chapter II. These visual studies were carried out on a plate 1/16 of an inch thick and on a cylinder one inch in diameter. The cylinder was oscillated once with its spherical end open and once with its end projected through a large plate. It was noted that vortices produced in the wake of the plate and the open-end cylinder, would disturb the flow around the test section. By introducing the large plate mentioned above, these disturbances were eliminated. A slight disturbance, however, was introduced at the intersection of the plate and the cylinder but was of a local nature. Based on these observations it was decided to use a cylinder, with a diameter many times greater than the steady boundary layer thickness, and to project it through two large plates one on each end, heating it only in a section away from the two end plates.

All the experiments have been made in an enclosure containing atmospheric air. Measurements were made of the mean coefficient of heat transfer. For small values of velocity amplitude, slight decreases were noticed which confirm the results of the analysis in Chapter II. At

higher velocity amplitudes increases were observed which were assumed to have been caused by transition to turbulent flow. This was confirmed by a series of smoke studies. The maximum decrease observed in the coefficient of heat transfer is 1.2% at a frequency of 10 cycles per second, which is of the same order of magnitude as the prediction of the theoretical analysis.

The Test Apparatus

The assembly drawing of the test section and other mechanical components of the test apparatus are shown in Figure 22. At the bottom of the drawing, the vibrator has been shown schematically. The vibration equipment is built by the MB Manufacturing Company. The vibrator is a model C-5B and its control unit is a model T-51D. The vibrator together with its control unit can be seen in Figure 24. As it is shown in Figure 22, the moving horizontal plate is connected to a steel rod (item 4) through a flexible connector (item 11). This is the driving rod which in turn is connected to the bottom end cylinder (item 2) and the test section (item 1). This driving mechanism will cause the oscillation of test package (items 1, 2 and 3) through two bearings provided by teflon O-rings. These O-rings serve both as bearings and seals. The test section is made of Aluminum tube, eight inches long which is highly polished on the outside. The outside diameter is 4.870 inches and the wall is 0.310 inches thick. Ring heaters are provided at either end of the test section and serve as guard heaters. The ends are closed by aluminum disks fastened to flanges welded to the cylinder wall. All the threaded joints are secured by double-nuts or slotted nuts held with wire. The

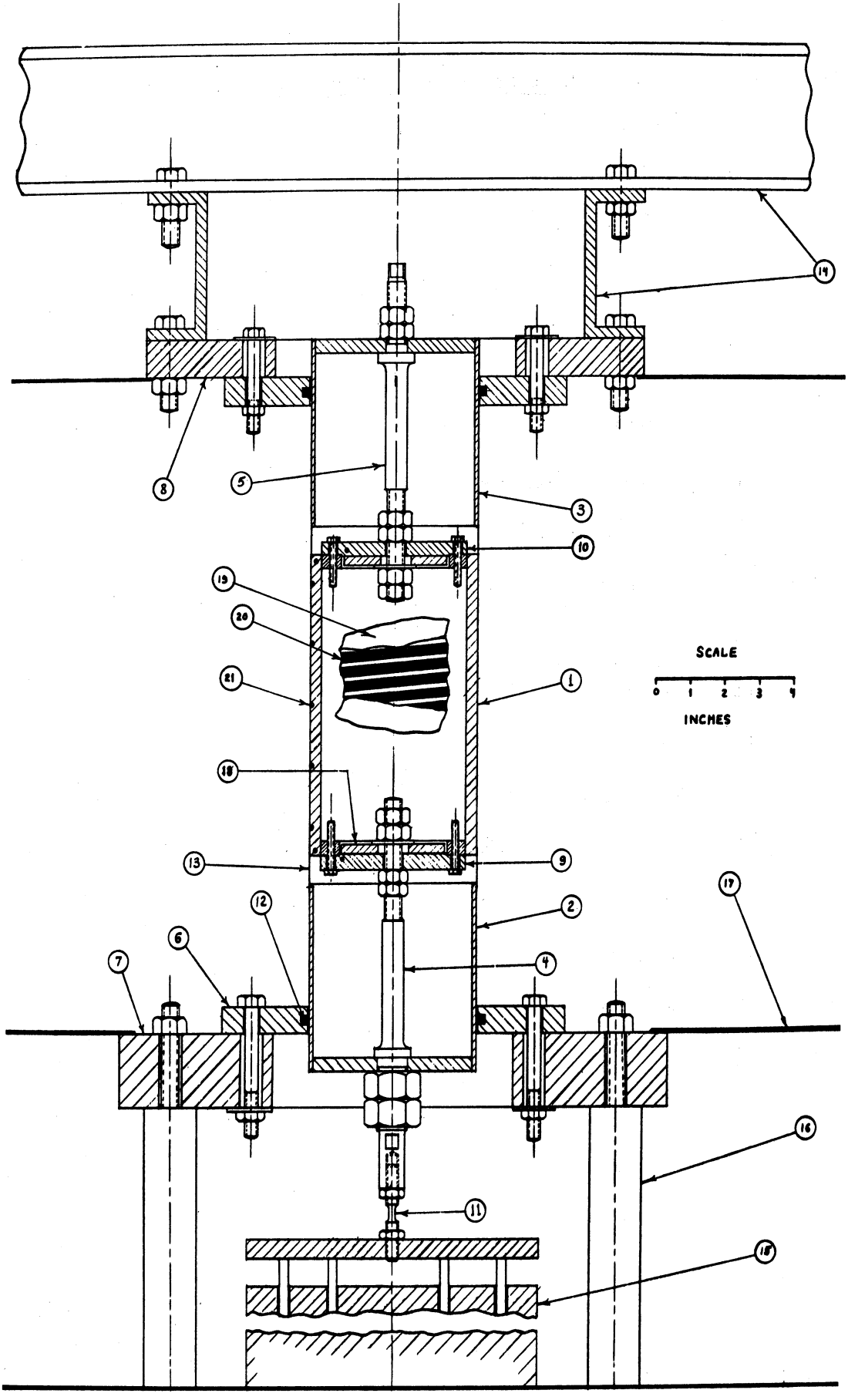

Figure 22. A Sketch of the Test Section Assembly.

List of Items in Figure 22

1	Test section
2	Lower cylinder
3	Upper cylinder
4	Driving rod
5	Upper rod
6	O-Ring supports
7	Lower bearing support
8	Upper bearing support
9	Lower cover
10	Upper cover
11	Flexible connector
12	O-Rings
13	Insulating tape
14	Supporting structure
15	Vibration exciter
16	Supporting rods
17	Enclosure walls
18	Ring heaters
19	Electric tape
20	Heater ribbon
21	Thermocouples

gaps on either end of test section are covered with a strip of electrical tape to secure a continuous surface on the outside. A view of the test section and the end cylinders is shown in Figure 23. Also shown in this figure and in Figure 24, is the masonite enclosure 4 feet by 4 feet by 1.5 feet surrounding the test area. Its function is to insure that the measurements are not influenced by drafts and air currents produced by the ventilating system of the building or the cooling fan on the vibrator.

The energy input to the main heater and the guard heaters is supplied by a 120 volt AC line. The line power is passed through a voltage regulator and then to three separate variacs each controlling the voltage across their corresponding heater element. The voltage regulator is a Sornesen 0.5 KVA Model 500. This device will minimize any voltage changes that may occur in the line.

The smoke studies made use of a smoke generator built by Blankenship.(15) A schematic diagram of the smoke generator is shown in Figure 25. The smoke from cigars soaked in oil was used as the indicating medium. The smoke was generated by blowing compressed air down over two cigars in a copper tube. The smoke from the cigars was then bubbled through a layer of water in the bottom of a glass container. This layer of water would filter the unburned oil and tar from the cigars. The smoke then filtered out through a steel wool filter to go to the injecting nozzles located on a fixed plate at the bottom end of the test section. The injectors consisted of ten small nozzles of approximately 0.032 inches diameter. However, only three of them were used for visual studies.

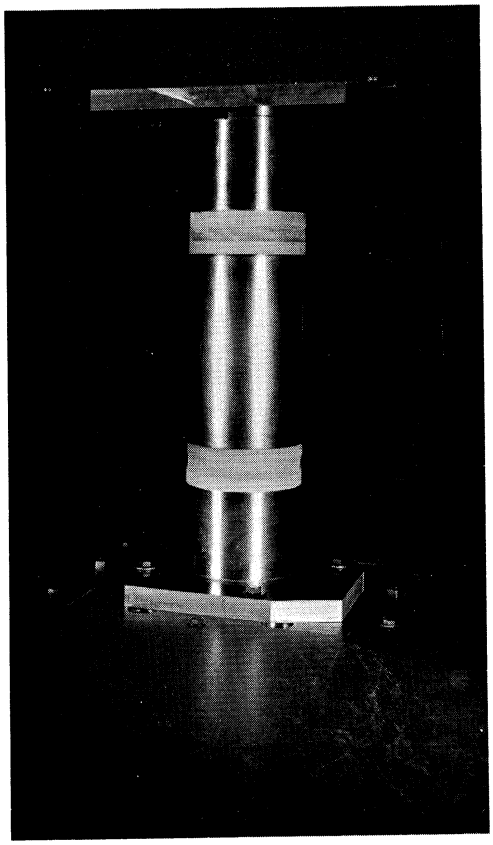

Figure 23. A View of the Test Section and End Cylinders.

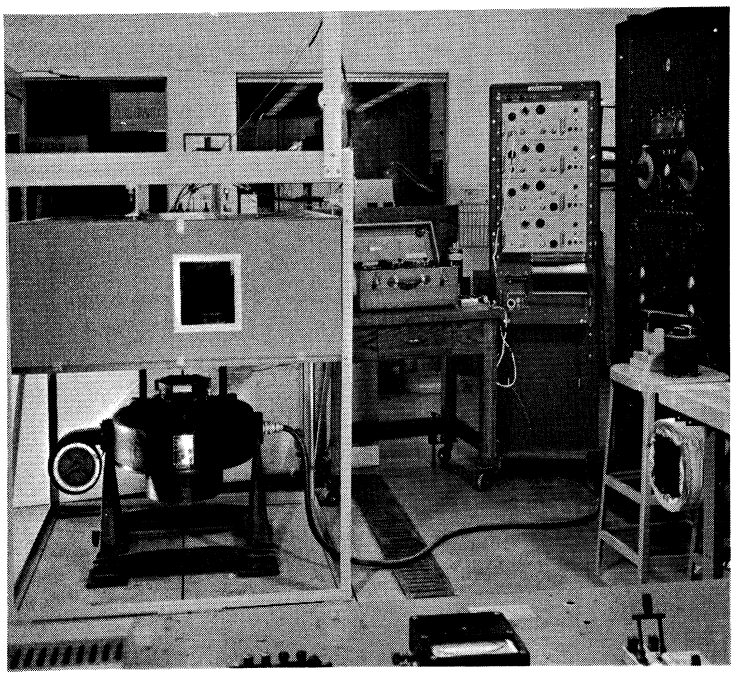

Figure 24. General View of the Test Apparatus.

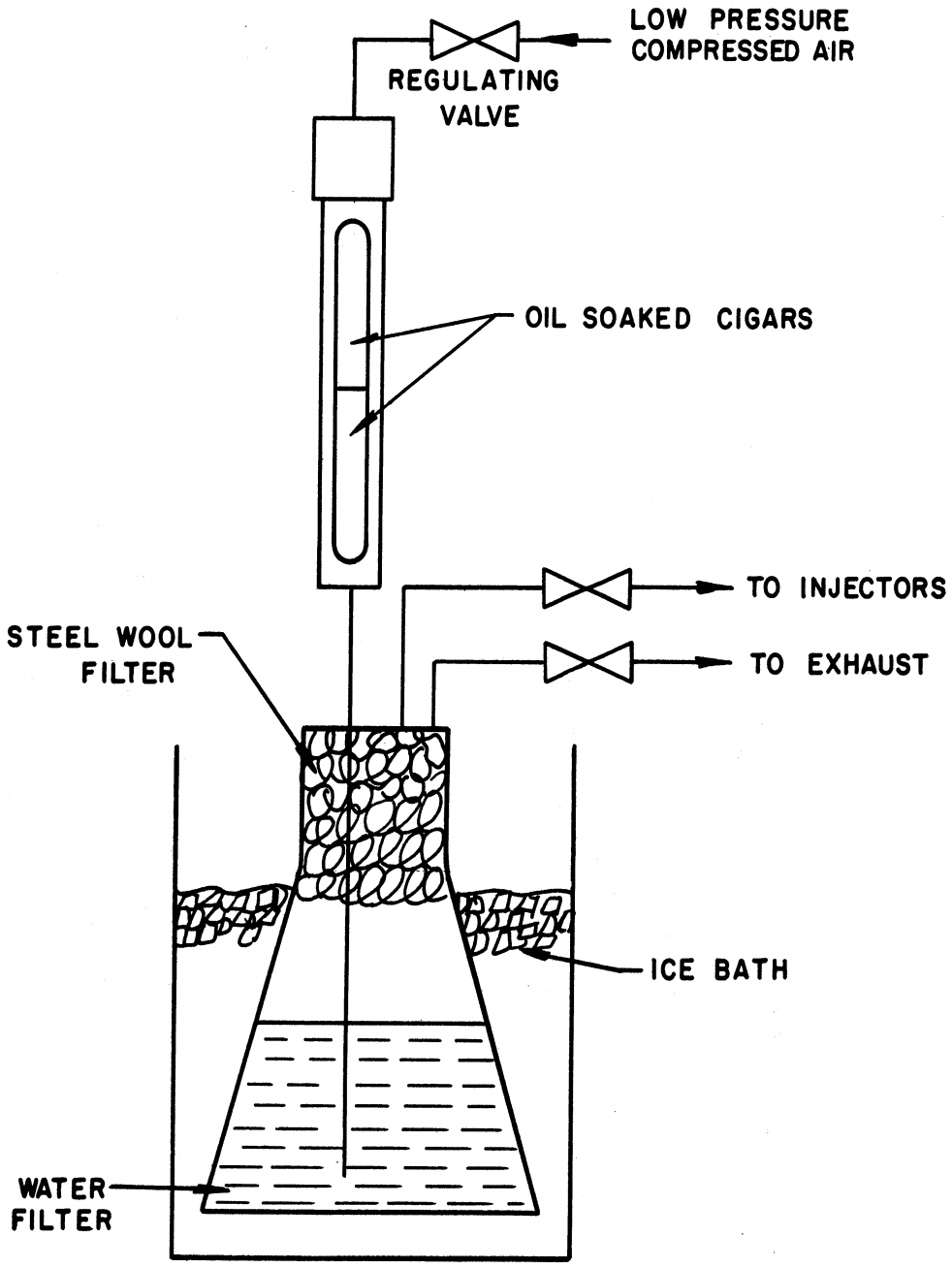

Figure 25. Sketch of the Smoke Generator.

Instrumentation of the Test Section

The test section is heated by Chromel-A heater ribbon 1/4 of an inch wide by 0.002 inches thick wrapped uniformly on the inner surface of the test section. The ribbon is sandwiched between two layers of Scotch No. 69 electrical tape to provide both electrical insulation from the wall and maintaining the relative position of sections of the ribbon. This tape is thermosetting and can withstand a maximum temperature of 356°F. The resistance of the main heater is about 18 ohms. Two guard heaters are provided on either end of the cylinder. The purpose of guard heaters is to prevent the leakage of any part of the main heater energy from the ends. These are Chromalox ring heaters each with a capacity of 100 watts at 120 volts.

Chromel-Constantan thermocouples have been used for temperature measurements consisting of 30 guage twin wires insulated individually and placed in fiber glass insulation. The thermocouples used for measuring surface temperature, are installed in 1/32 of an inch holes in the wall and are secured in place by filling the holes with aluminum cement such that the tip of each thermocouple is almost in the same level as the outer surface of the cylinder. A total of eighteen thermocouples have been used, thirteen of which are installed in the test section, four in the walls of the end cylinders and one within the masonite enclosure for measuring ambient temperature.

Measuring Instruments

Thermocouple wires are connected to a system of rotary switches making it possible to switch to any single thermocouple and read its

indicated output voltage using a Leeds and Northrup Model 8662 portable precision potentiometer. An ice bath is used for the reference junction and the thermocouple wire has been calibrated in the laboratory. Sometimes a Sanborn four-channel recorder was used during the initial transient period in order to observe the approach to equilibrium. However, all the actual temperature measurements were made by the potentiometer mentioned above. These measuring devices can be seen in Figure 24.

Figure 26 shows a diagram of the heating circuit. The energy input to the main heater is measured by reading the current and voltage drop across the heating element at all times. The current is measured by a Westan Model 904 AC ammeter and the voltage by a Westan Model 155 AC voltmeter.

In evaluating heat transfer measurements it is important to know the magnitude of the radiation losses from the outer surface of the test section. For this reason the emissivity of the polished aluminum cylinder was measured using a Model 810C69 Cenco Thermopile. The output of the thermopile was measured by a precision potentiometer. A black body constructed by Schoenhals[23] was used as an essential device for measuring emissivities. This and the thermopile can be seen in Figure 24. The procedure for obtaining the emissivity of the aluminum surface was to focus the thermopile on the surface of the aluminum cylinder and to record the output of the thermopile for each surface temperature. This was done after every run. This process was repeated for the black body in a wide range of black body temperatures. The ratio of the thermopile outputs at a given temperature, then, would give the emissivity of the aluminum surface. The emissivity of the polished aluminum surface of the test section

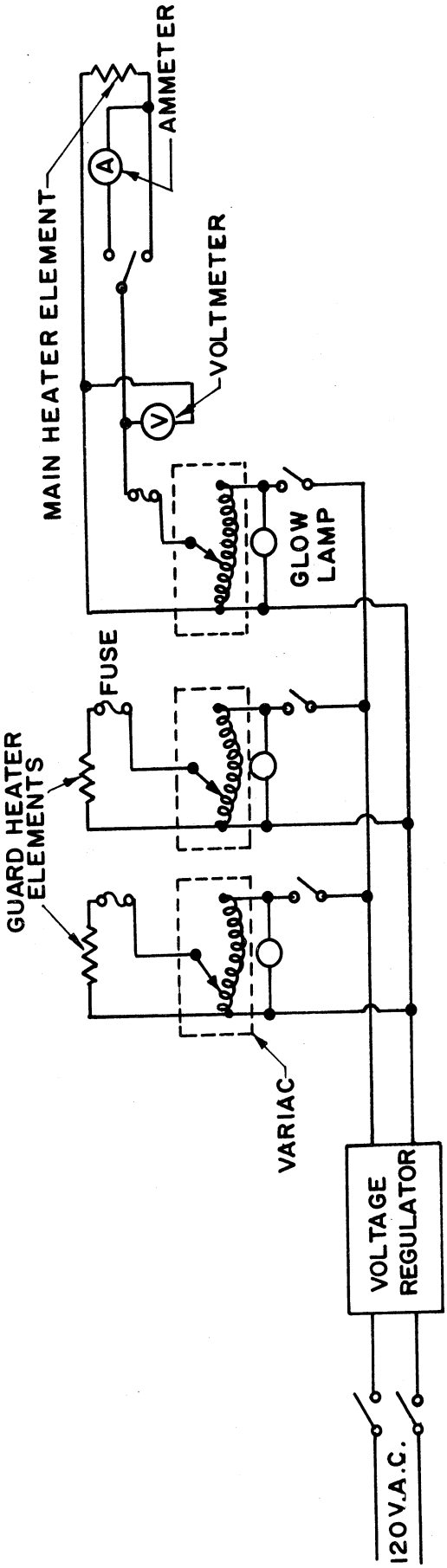

Figure 26. Electrical Diagram for Measurement and Control of Energy Input to the Heater Elements.

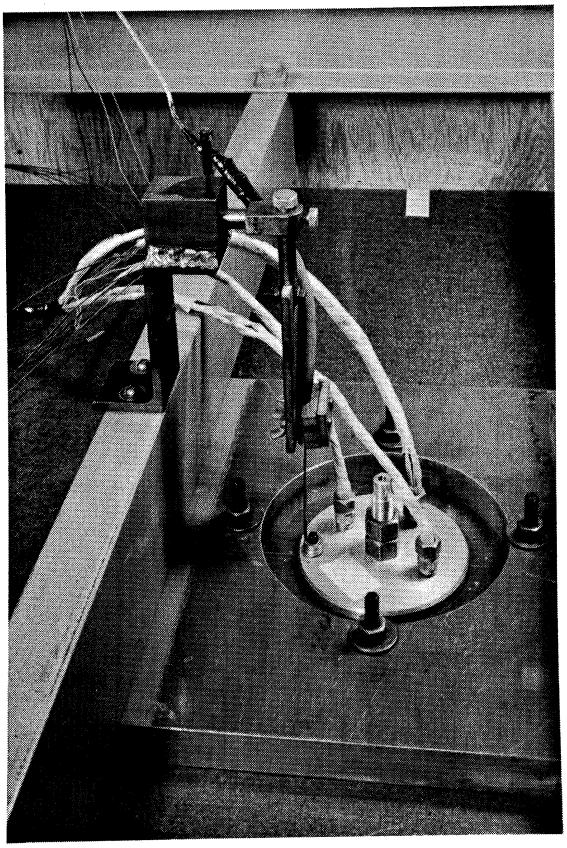

Figure 27. A View of the Amplitude Pick-up.

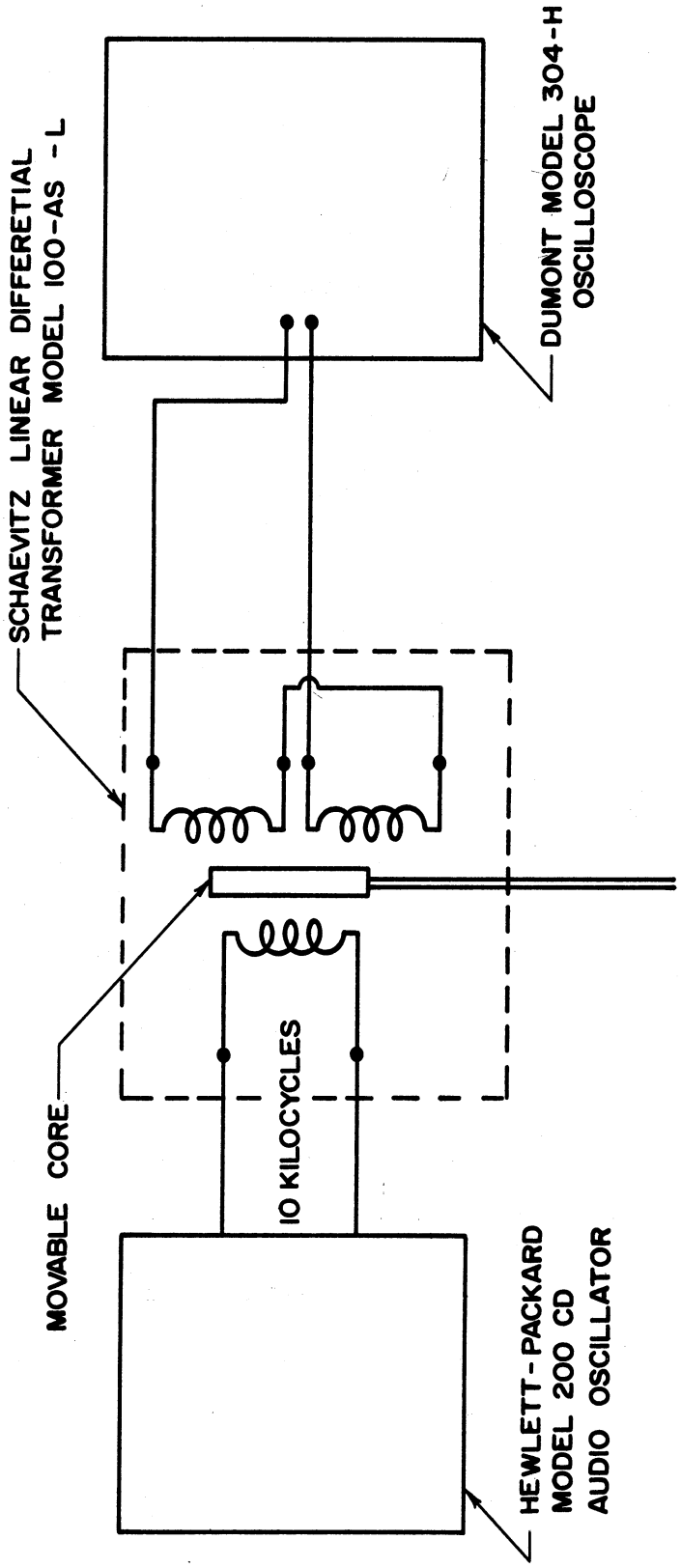

Figure 28. Linear Differential Transformer Circuit for Measurement of Vibration Amplitude.

varied between 0.062 and 0.074 for surface temperatures ranging from 120-270°F.

The frequency of oscillation is set on the frequency dial of the vibrator control unit ranging from 5 to 500 cycles per second. This frequency was measured by a Model 631-BL Strobotac manufactured by General Radio Company. The results of strobatac measurements agreed closely with the numbers indicated on the frequency dial of the control unit.

The amplitude of oscillation is monitored by means of a Schaevitz Linear Differential Transformer Model 100-AS-L and a movable core attached to the top of the top end cylinder with a small brass rod. The transformer has a stationary mounting, built by Schoenhals,[23] provided with fine position adjustment by means of a sliding memeber controlled by a threaded shaft. The transformer and movable core system can be seen in Figure 27. A Hewlett-Packard Model 200 CD Audio Oscillator is used for an imput to the transformer. The output is displayed on a Model 304H Dumont Oscilloscope. A diagram of this system is shown in Figure 28. In order to calibrate the system, the transformer is first placed in its null position with respect to core, by moving it until a zero signal is shown on the scope. Then the sliding member of the transformer mounting system is moved against a spacer having the same thickness as the amount of the desired amplitude to be measured. The spacer is placed in a slot provided for this purpose. This displaces the transformer by the amount desired, with respect to the core, away from the null position so that the high carrier frequency causes a blurred signal on the scope as shown in Figure 29. The oscillator output or scope gain

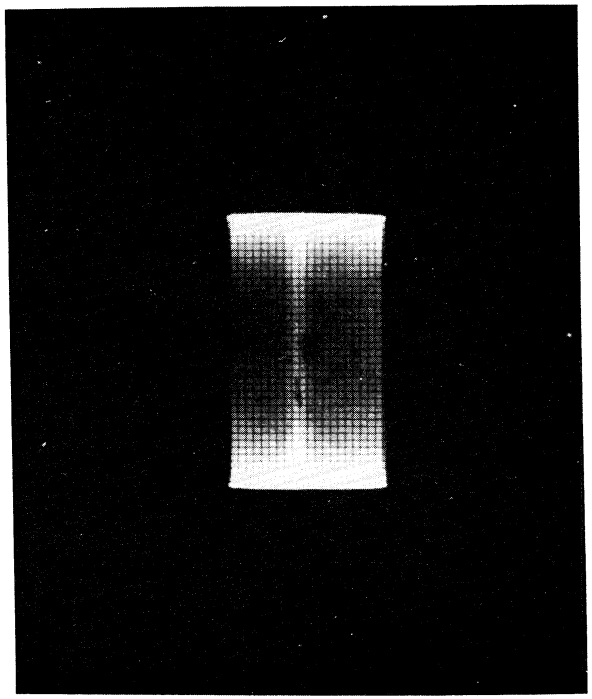

Figure 29. Output Signal of the Linear Differential Transformer with the Core Displaced from the Null Position as Displayed on an Oscilloscope.

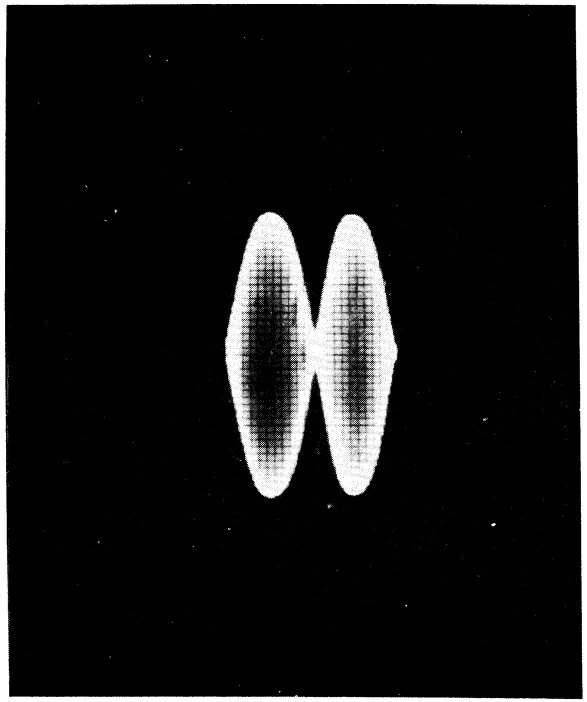

Figure 30. Output Signal of the Linear Differential Transformer under Vibratory Conditions as Displayed on an Oscilloscope.

is then adjusted until the signal occupies the full scale of the scope screen. This calibrates the system so that the full scale corresponds to the same displacement as the thickness of the spacer. During vibratory conditions the sweep frequency on the scope is set equal to the frequency of vibration. The signal appears as the envelope of a sine wave as shown in Figure 30. Then the amplitude is increased by turning the amplitude knob on the control unit such that the image on the scope covers full scope; now the vibrator is oscillating with the desired frequency.

A view of some of the instruments is shown in Figure 31. The black body is shown on the lower left corner.

Procedure and Results of Heat Transfer Measurements

The procedure for temperature measurements and the determination of the total heat input have been discussed earlier. Based on these two measurements and knowing the heat transfer area (0.85 square feet), a total heat transfer coefficient can be defined as

$$\bar{h}_T \equiv \frac{(q/A_T)}{T_w - T_\infty} \quad ,$$

where q is the main heater wattage in its proper units. In order to correct for radiation losses, a radiation heat transfer coefficient $\bar{h}_r$ may be defined as

$$\bar{h}_r \equiv \epsilon_m \sigma \frac{T_w^4 - T_\infty^4}{T_w - T_\infty} \quad .$$

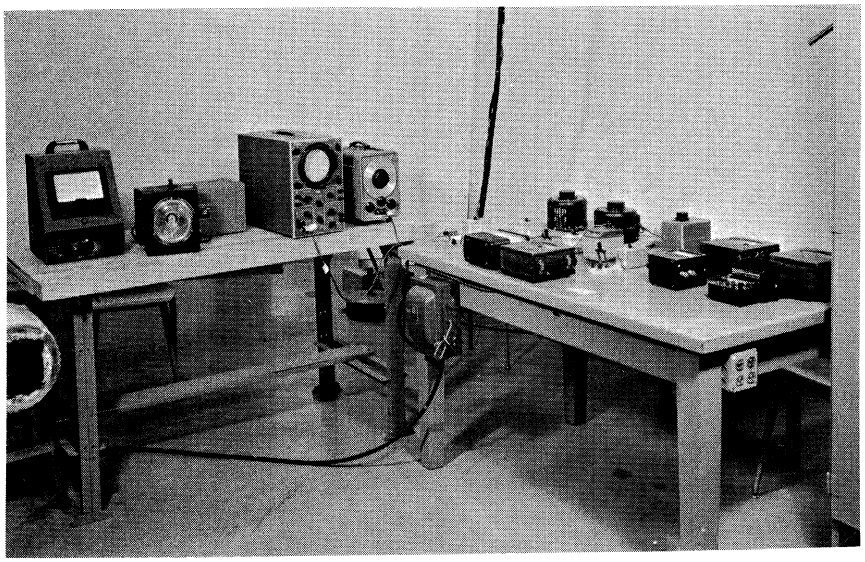

Figure 31. A View of Some of the Instruments.

Then the average convection coefficient $\bar{h}_c$ would be the difference

$$\bar{h}_c = \bar{h}_T - \bar{h}_r \quad .$$

A series of steady heat transfer measurements were made which correspond closely to the free convection correlation given in Reference 22. Figure 32 shows the experimental data obtained for Nusselt number plotted against the product of Grashof and Prandtl numbers. The solid line is a plot of the correlation equation in Reference 22.

The same procedure was used for measuring heat transfer coefficient while the cylinder was oscillating. The test section was allowed to come to equilibrium condition under nonoscillatory conditions. The guard heaters were carefully adjusted so as to prevent end losses. At this time the temperature distribution in the cylinder wall was essentially uniform. The test package was then vibrated at a known frequency and with a desired amplitude. The wall temperature difference $(T_w - T_\infty)$ was carefully observed on the precision potentiometer and the guard heaters monitored at all times.

For small values of velocity amplitude, the wall temperature difference rose slightly in all the experimental runs. The guard heaters, under these conditions, did not require any further adjustment. At higher velocity amplitudes, however, an abrupt decrease was noticed in the wall temperature and the guard heaters required further adjustment. This abrupt decrease in wall temperature was attributed to transition to turbulent flow.

Figure 33 shows two sets of experimental data obtained at a frequency of 15 cycles per second. The Nusselt number based on total

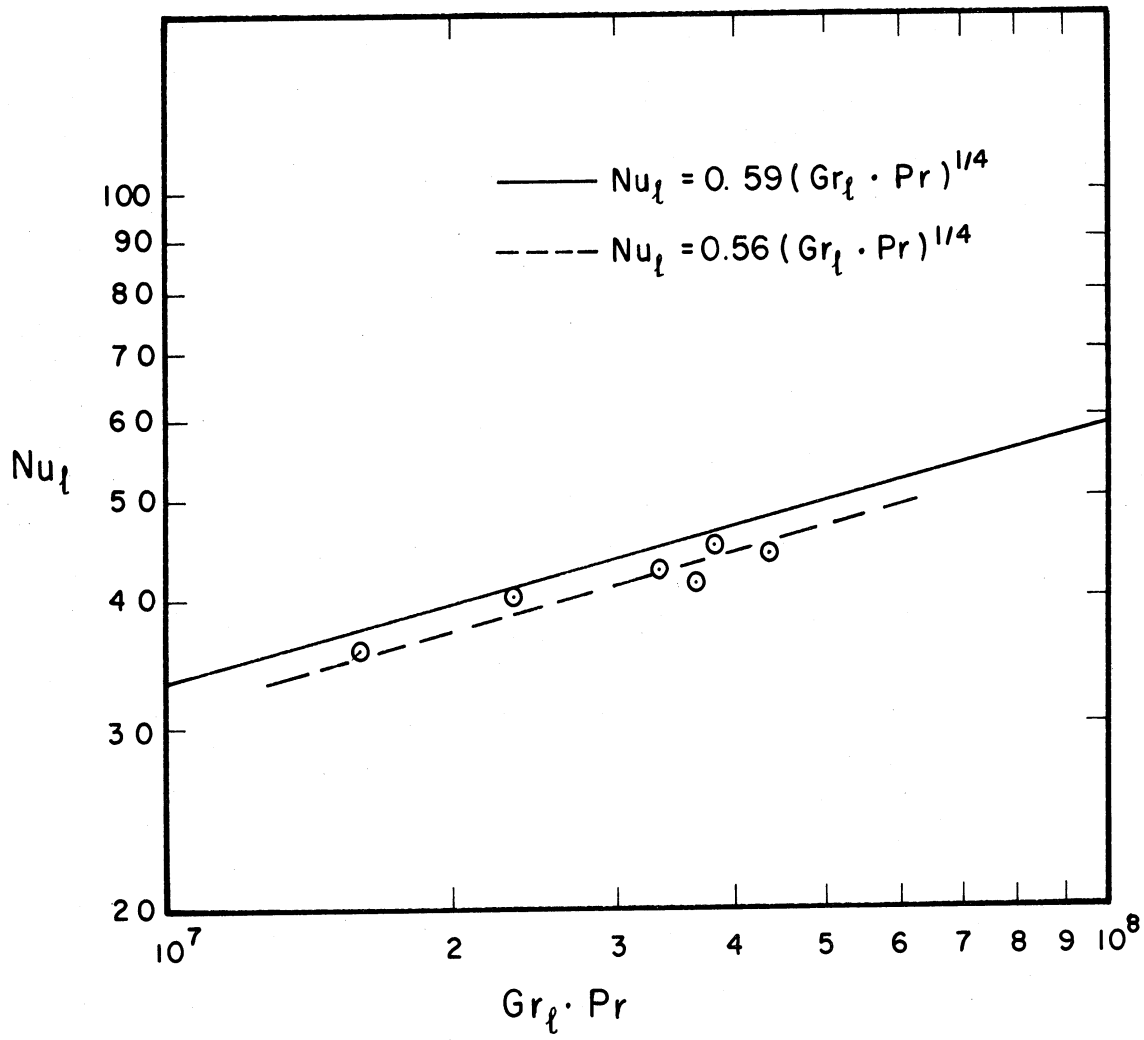

Figure 32. Steady Free Convection Data.

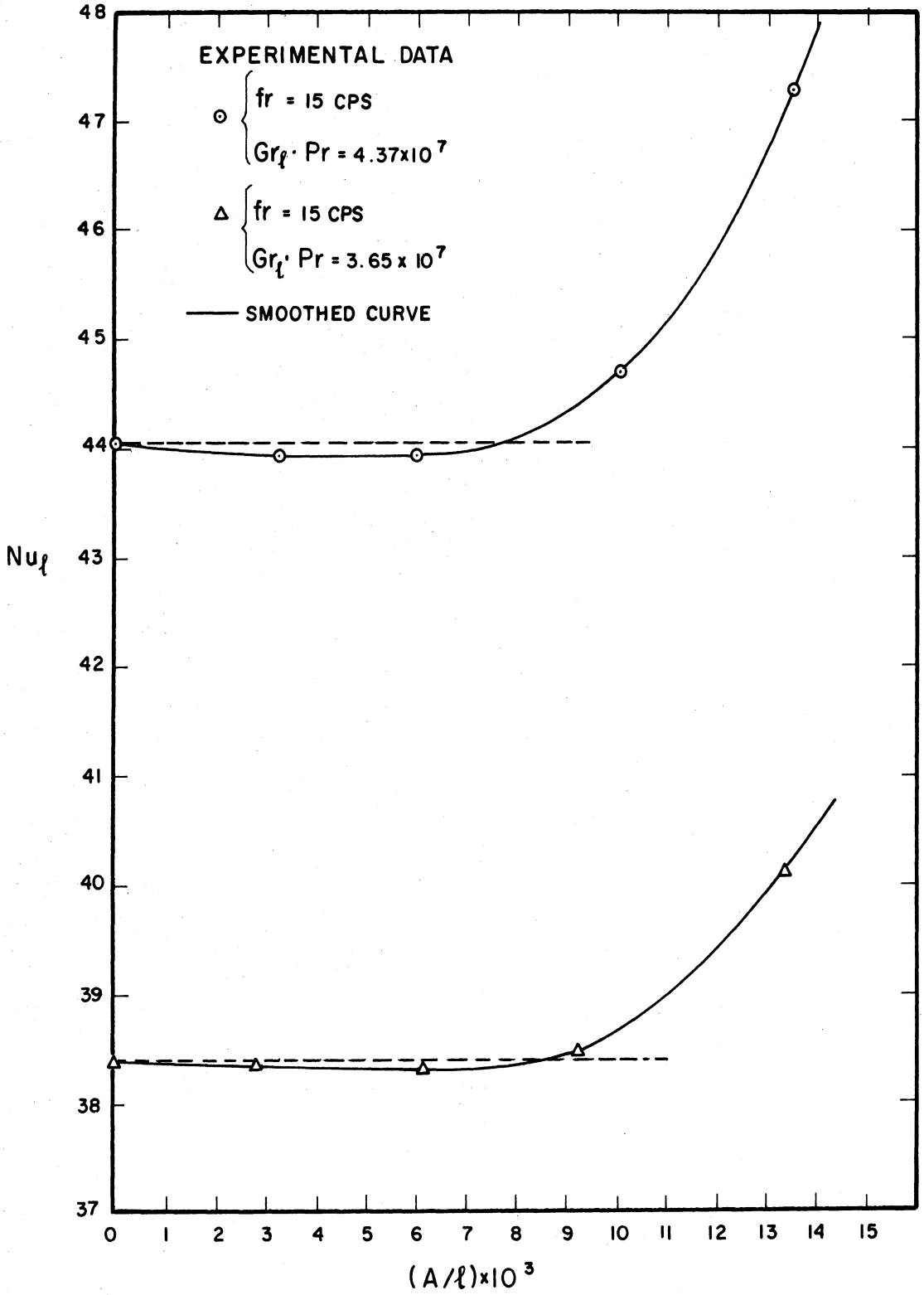

Figure 33. Typical Data Showing Nusselt Number Versus Vibration Amplitude Ratio.

length of the cylinder, decreases slightly with increasing values of A/ℓ, reaches a minimum and then reversing its trend, increases abruptly over its steady state value. The solid lines in Figure 33 are curves best fitted through the experimental points. Each of these curves crosses its steady state value at an amplitude ratio whose magnitude is a decreasing function of Grashof number. The curve for Gr. Pr = 3.65×10^7, crosses at $A/\ell = 8.6 \times 10^{-3}$ whereas the one for Gr. Pr = 4.37×10^7 crosses at $A/\ell = 7.6 \times 10^{-3}$. Also the rise in Nu_ℓ is sharper for the higher value of Gr. Pr.

Figure 34 contains data obtained for different frequencies and a constant Grashof number. Heat transfer data has been presented in terms of per cent change in Nusselt number caused by oscillations of the test section.

Smoke studies revealed that all the experimental points on Figures 33 and 34 that represent a decrease in heat transfer coefficient are in laminar region. The procedure for smoke studies consisted of permitting the test section to achieve different temperatures for different power inputs. Once the test section reached equilibrium, the smoke generator was started. An optimum smoke exit velocity was found by adjusting the compressed air and the various valves. Two Plexiglass windows were provided on two of the enclosure walls, one for lighting purposes and the other for observing the smoke patterns. The criterion for smoke exit velocity adjustment was to obtain the minimum velocity possible for the smoke filaments to be stable and clearly visible. Then the flow patterns were observed for different values of frequency and amplitude.

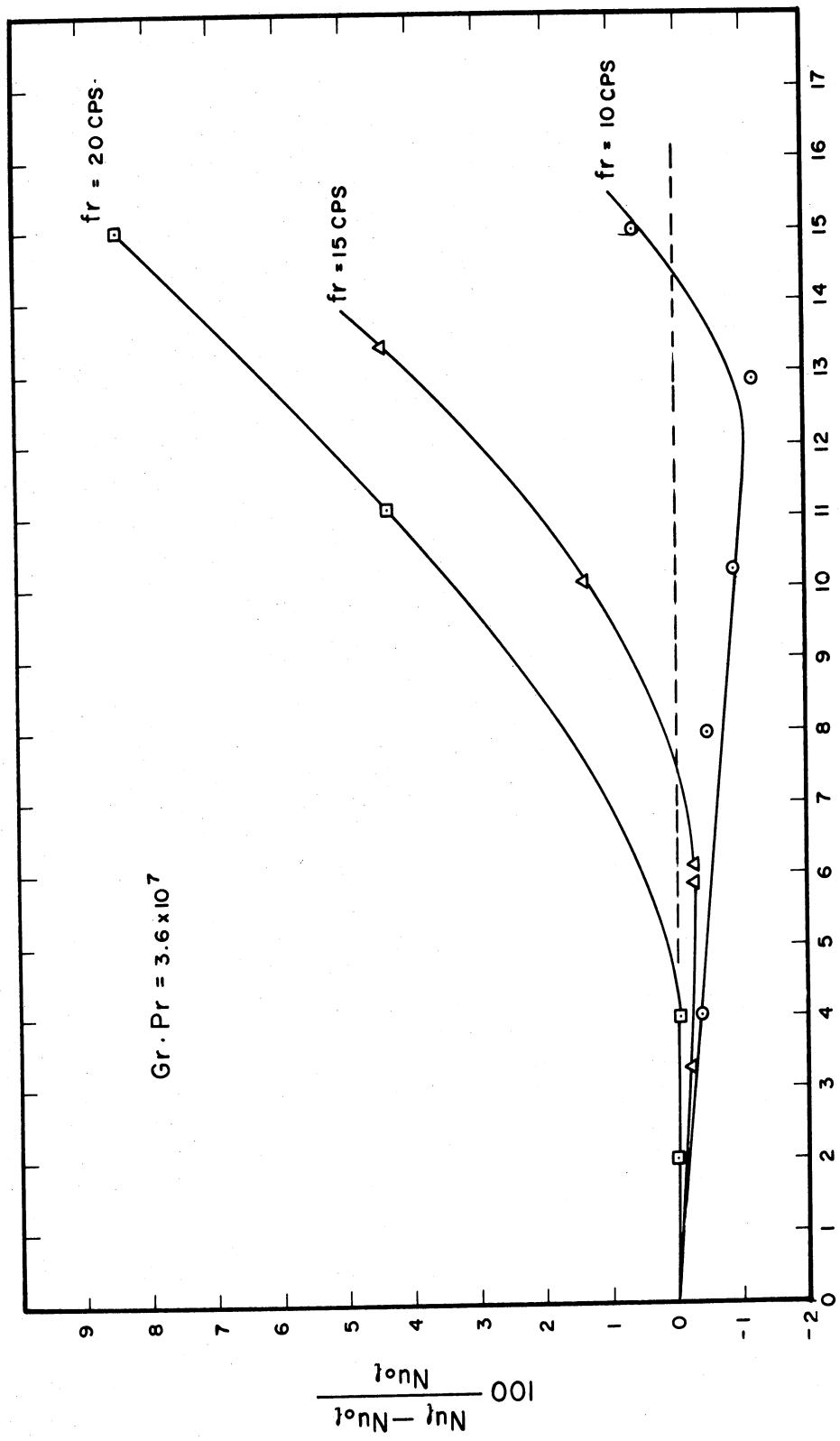

Figure 34. Experimental Data Showing Per Cent Change in Nusselt Number Resulting from Oscillations.

For small values of velocity amplitude the smoke filaments retained their streamline shape as in the case of no oscillations. For larger values of velocity amplitude, however, a mixing action was observed on the upper portion of the test cylinder. The region where the smoke was mixed rather than streamlined, would move downward when the amplitude of oscillation was further increased. It was concluded that this mixing action was due to turbulence. In each run the length of the cylinder in turbulent regime was measured by means of a scale mounted on the test section.

Figures 35 through 37 show the results of smoke studies shown schematically for the data presented in Figure 34.

Figures 38 through 42 are photographs of the smoke studies. These photographs are representative of what was seen without a camera. Figure 38 represents the smoke pattern in steady state case (A = 0). In Figure 39 the cylinder is oscillating with a small amplitude, however, the smoke patterns are identical to the steady state case. In Figure 40, where the cylinder is oscillating with a higher velocity amplitude, a change is noticed in shape of the smoke filaments. Within the top three inches of the test section the smoke is slightly mixed which signifies transition to turbulence. In Figures 41 and 42 the cylinder is oscillating under more severe vibratory conditions. The mixing action is stronger and it covers a wider region along the length of the cylinder.

All the photographs were taken by a Graflex f/4.7 camera using Polaroid Land 4 x 5 type 57 film. This type of film has an ASA equivalent exposure index of 3200. This film was used with a setting of 1/200 second at f/4.7.

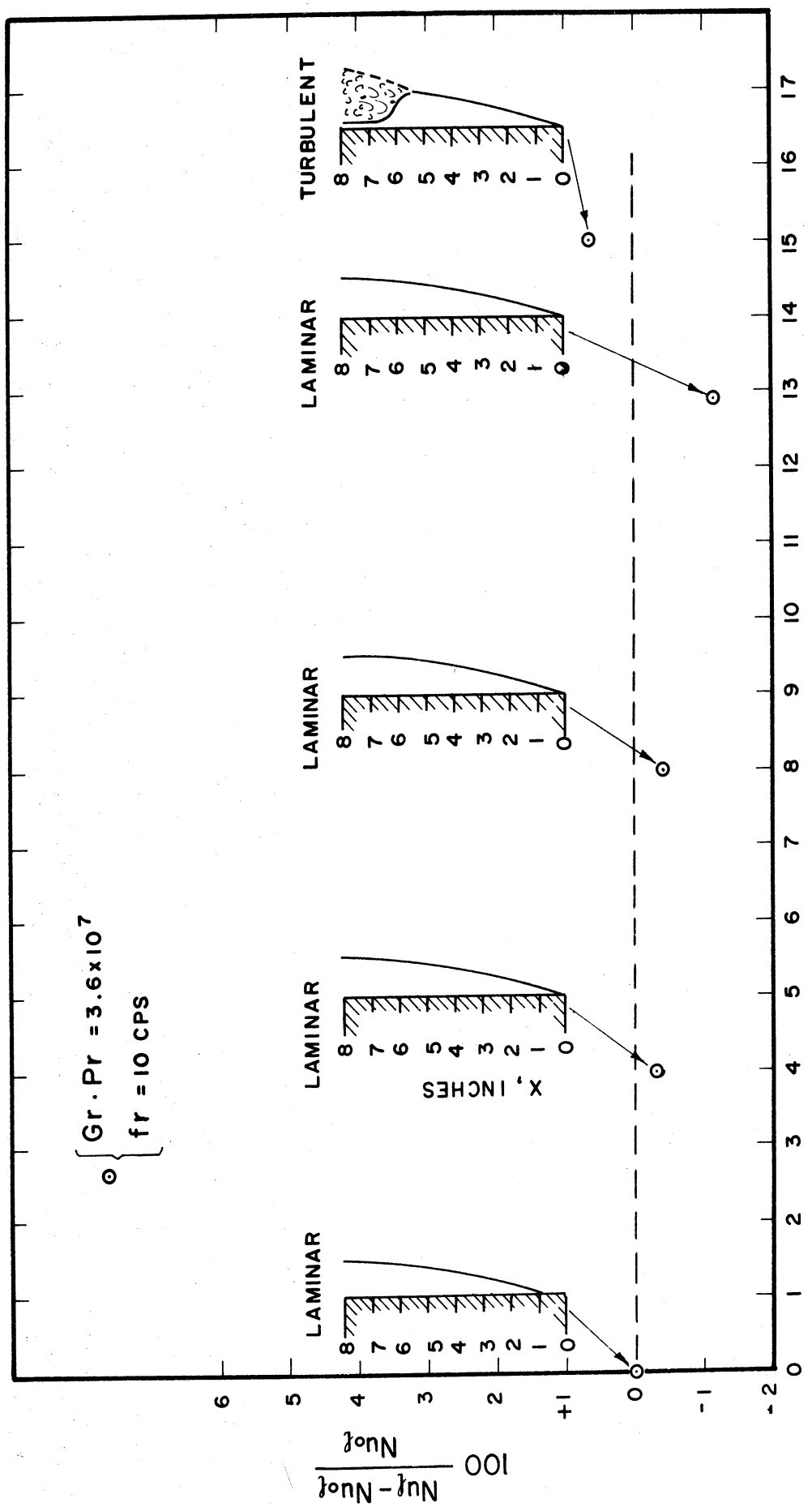

Figure 35. Smoke Study Data Showing the Nature of Flow Regime Along the Length of the Cylinder for Various Heat Transfer Measurements.

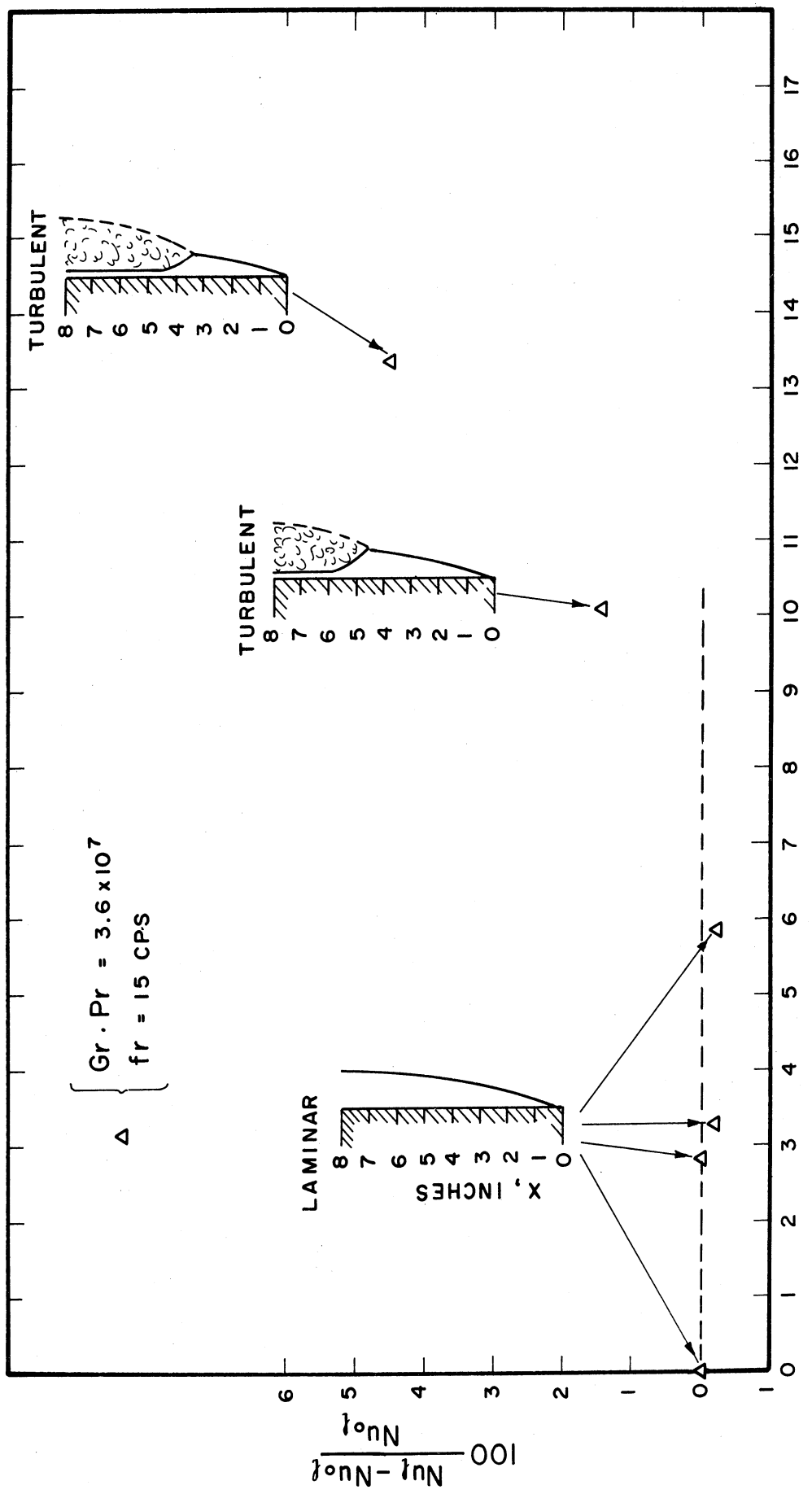

Figure 36. Smoke Study Data Showing the Nature of Flow Regime Along the Length of the Cylinder for Various Heat Transfer Measurements.

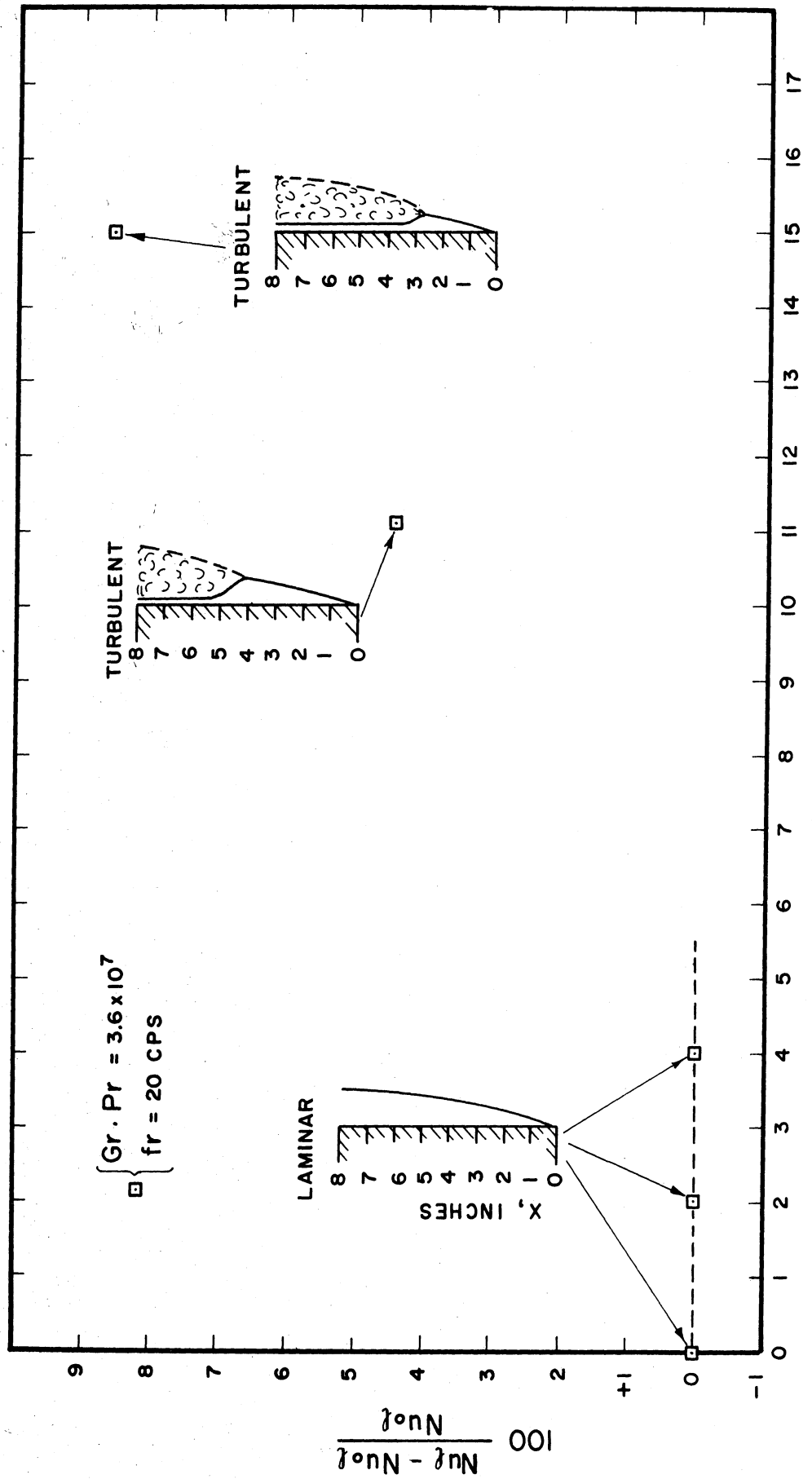

Figure 37. Smoke Study Data Showing the Nature of Flow Regime Along the Length of the Cylinder for Various Heat Transfer Measurements.

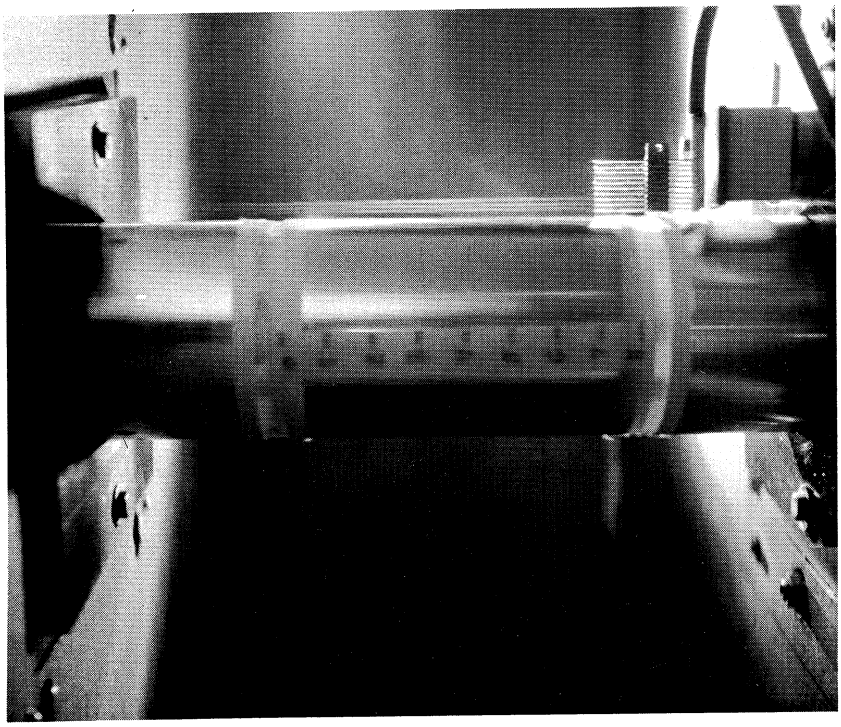

Figure 39. Smoke Photograph for $T_w - T_\infty = 139°F$, A = 0.05 inches and fr = 16 cps.

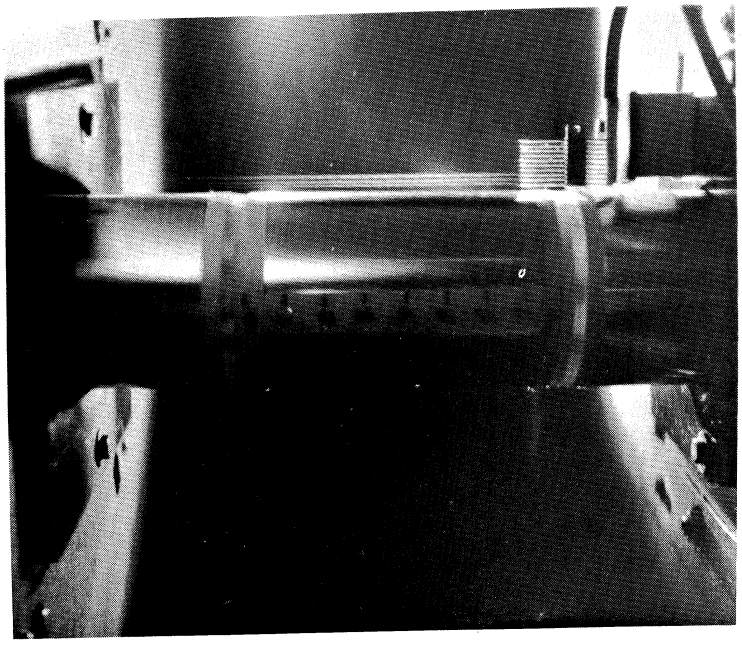

Figure 38. Smoke Photograph for $T_w - T_\infty = 139°F$, and No Oscillation.

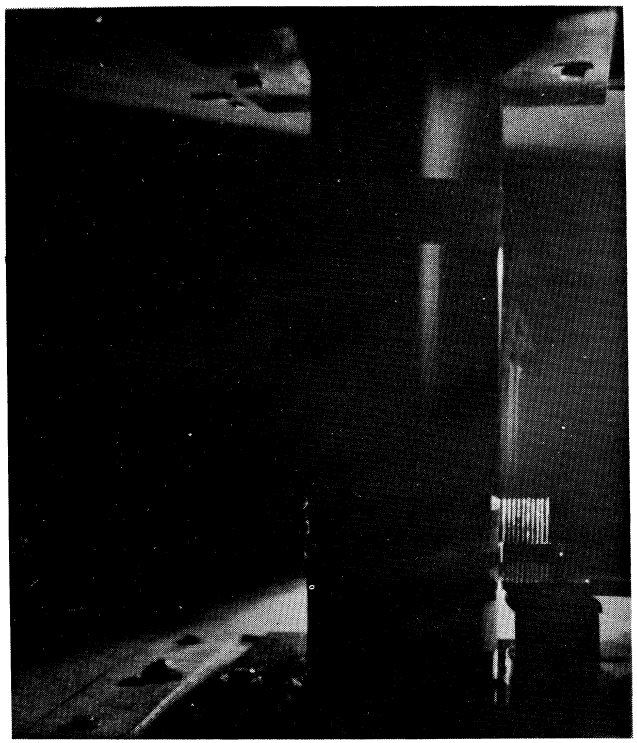

Figure 40. Smoke Photograph for $T_w - T_\infty = 176°F$, A = 0.11 inches and fr = 16 cps.

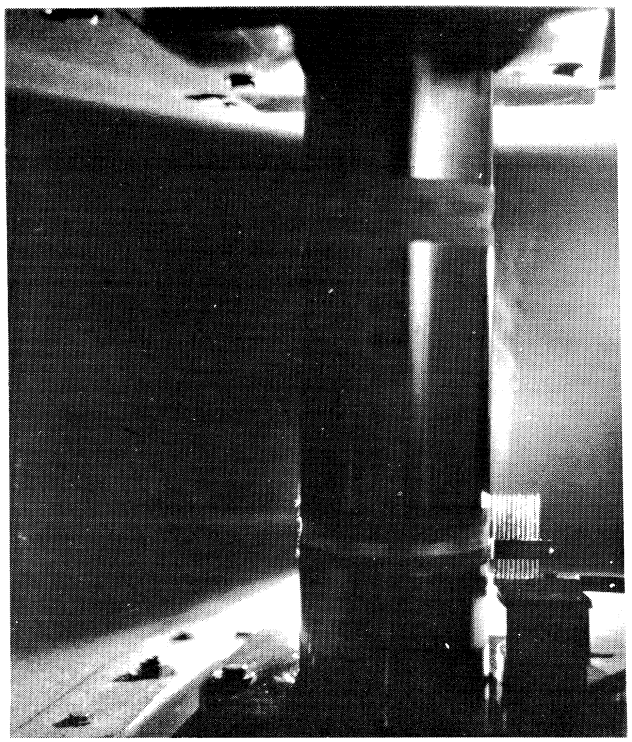

Figure 41. Smoke Photograph for $T_w - T_\infty = 176°F$, A = 0.07 inches and fr = 45 cps.

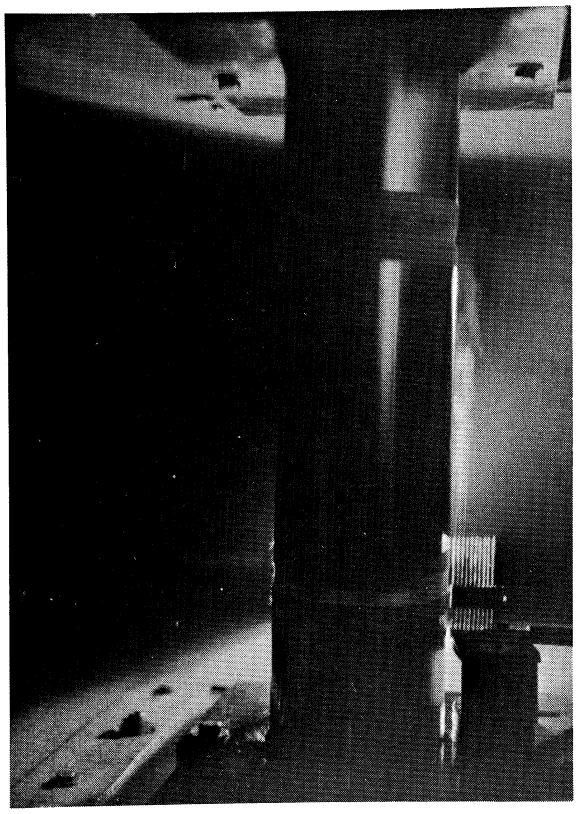

Figure 42. Smoke Photograph for $T_w - T_\infty = 176°F$, A = 0.005 inches and fr = 200 cps.

Another set of heat transfer data has been presented in Figure 43 for a frequency of 12 cycles per second. Each experimental measurement shown in Figure 43 has been accompanied with a photograph indicating the flow regime for exactly the same conditions. The experimental points in Figure 43 which correspond to Figures 44 - 47 are definitely in laminar region and represent decreases in the coefficient of heat transfer. A slight undulation can be seen in Figure 49 on top of the test section. This implies that at these conditions a very small portion of the test section is experiencing minute turbulence whose gross effect on the average coefficient of heat transfer is to nullify the decrease which prevails in the portion of the test cylinder still in laminar region. The measurements relating to Figures 50 and 51 show increases in the coefficient of heat transfer. There is a definite disturbance in the smoke filaments near the top of the test cylinder which is interpreted as the start of transition to turbulent flow. The smoke patterns in Figure 48 indicate a slight waviness on the outer filament suggesting that transition to turbulent flow starts from the outside.

The over-all study of the smoke photographs brings about a gross indication of transition to turbulence as a consequence of longitudinal oscillation of the test cylinder the mechanism of which is to be determined by further research.

Correlation of Experimental Data

It was pointed out earlier that for high values of velocity amplitude the coefficient of heat transfer under vibratory conditions experiences an increase over its steady state value. It was also established

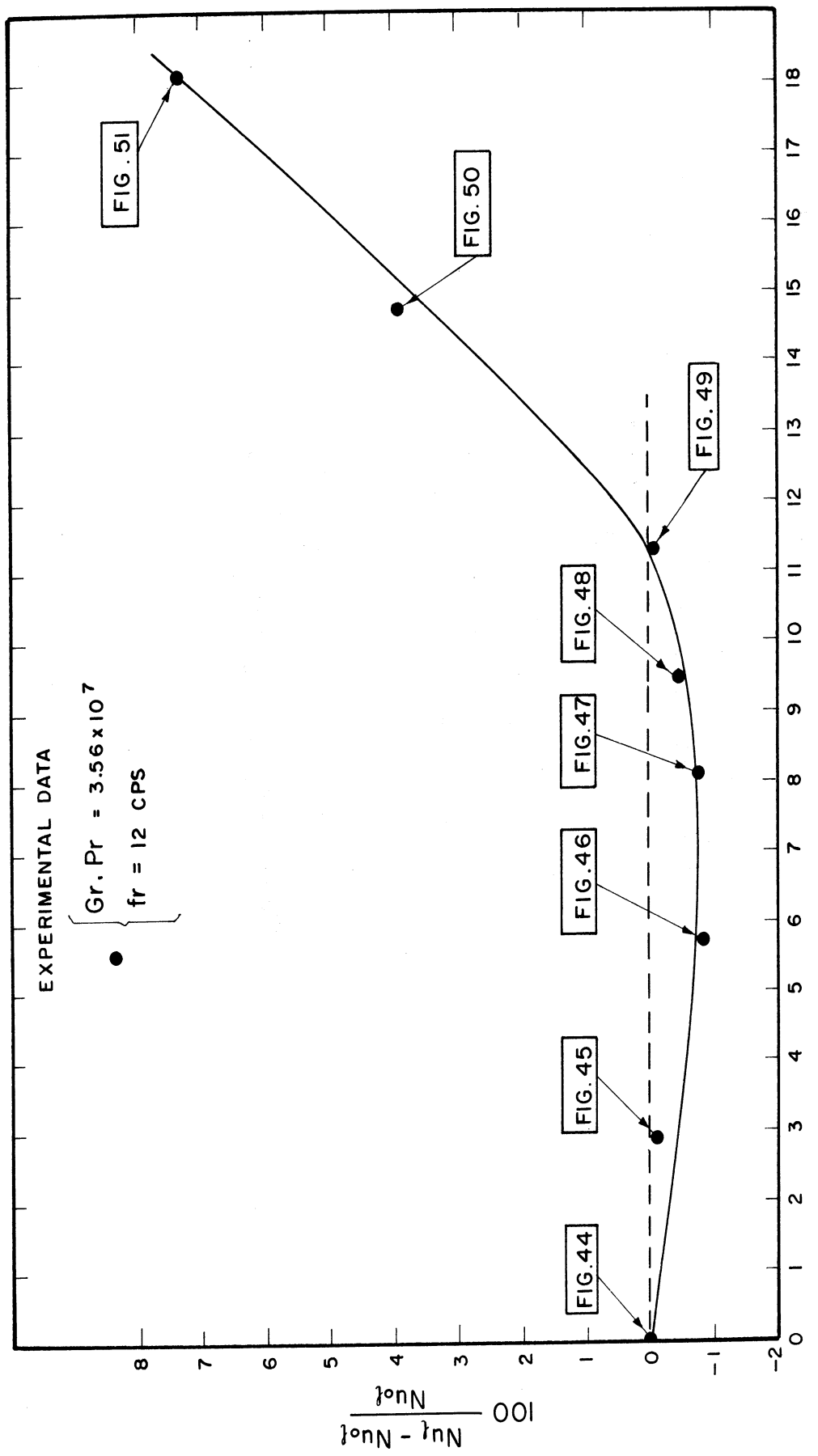

Figure 43. Per Cent Change in Nusselt Number Resulting from Oscillations as a Function of Amplitude.

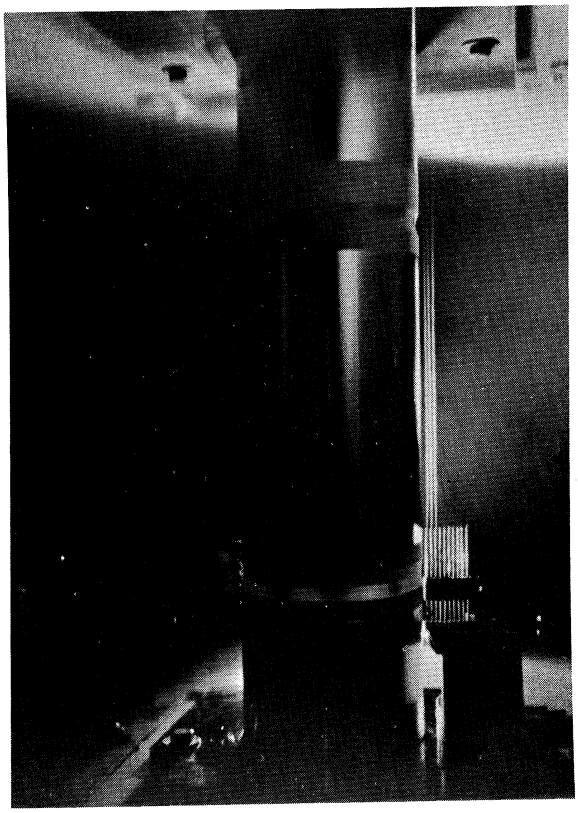

Figure 44. Smoke Photograph for Gr. Pr = 3.56×10^7, and No Oscillation.

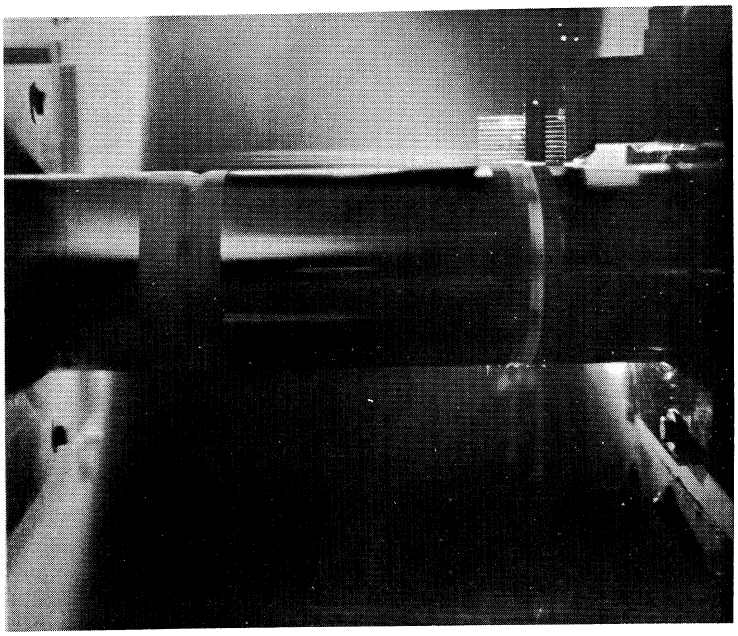

Figure 46. Smoke Photograph for Gr. Pr = 3.56 x 10^7, A/ℓ = 5.7 x 10^{-3} and fr = 12 cps.

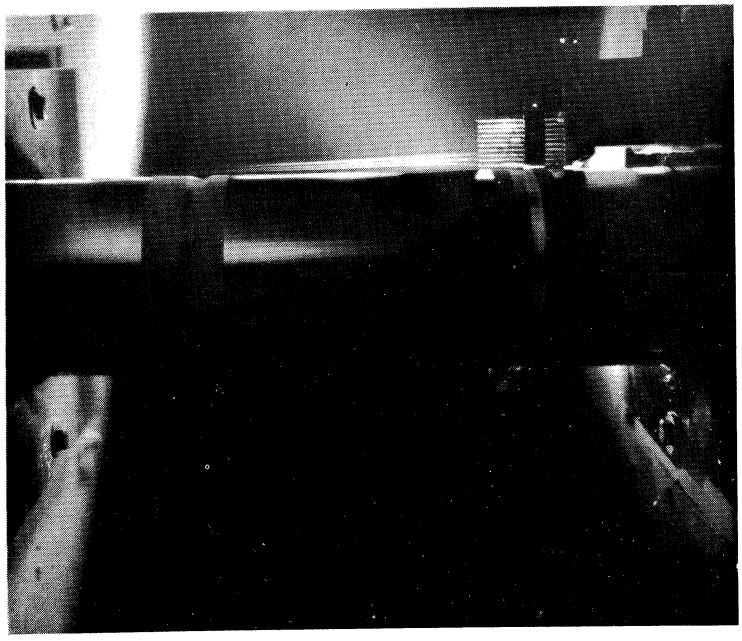

Figure 45. Smoke Photograph for Gr. Pr = 3.56 x 10^7, A/ℓ = 2.9 x 10^{-3} and fr = 12 cps.

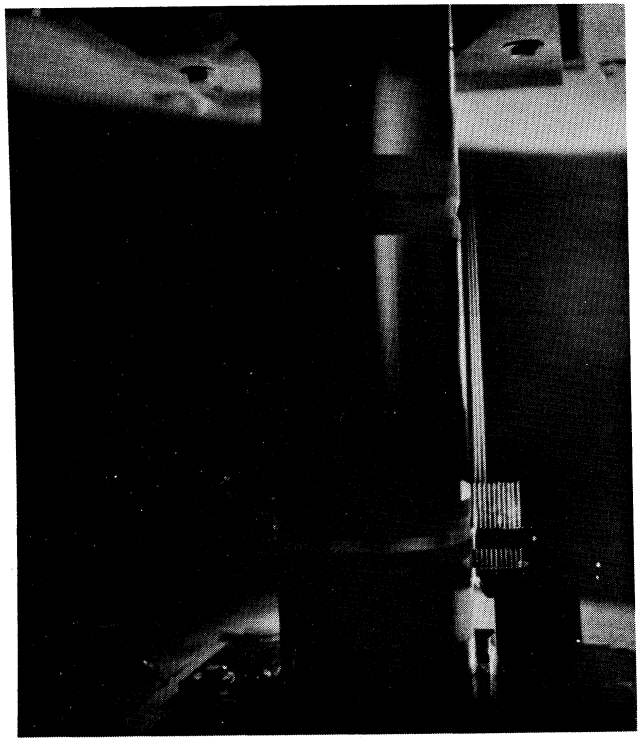

Figure 47. Smoke Photograph for Gr. Pr = 3.56 x 107, A/ℓ = 8.1 x 10^{-3} and fr = 12 cps.

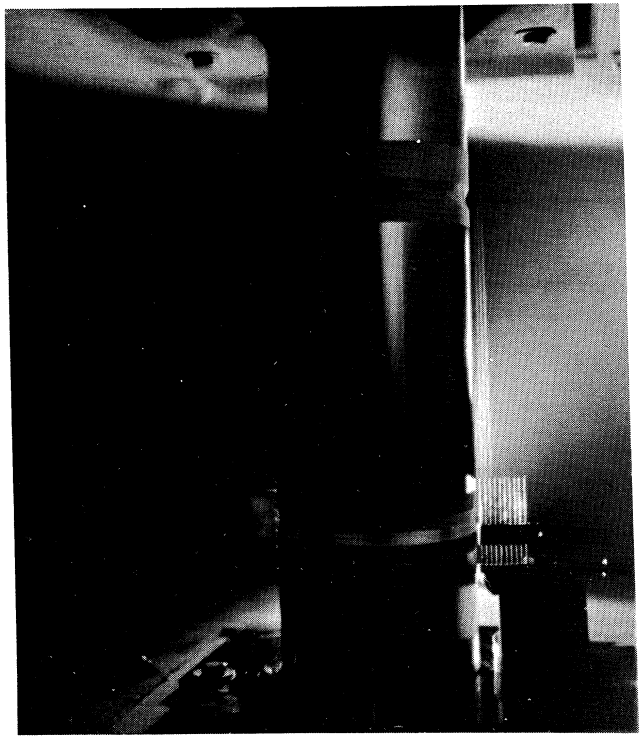

Figure 48. Smoke Photograph for Gr. Pr = 3.56 x 107, A/ℓ = 9.5 x 10^{-3} and fr = 12 cps.

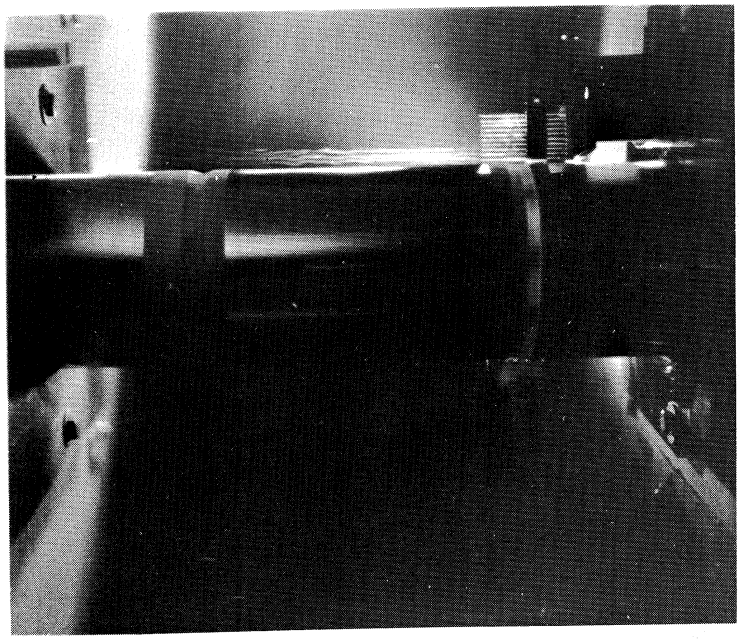

Figure 50. Smoke Photograph for Gr. Pr = 3.56 x 10^7, A/ℓ = 14.7 x 10^{-3} and fr = 12 cps.

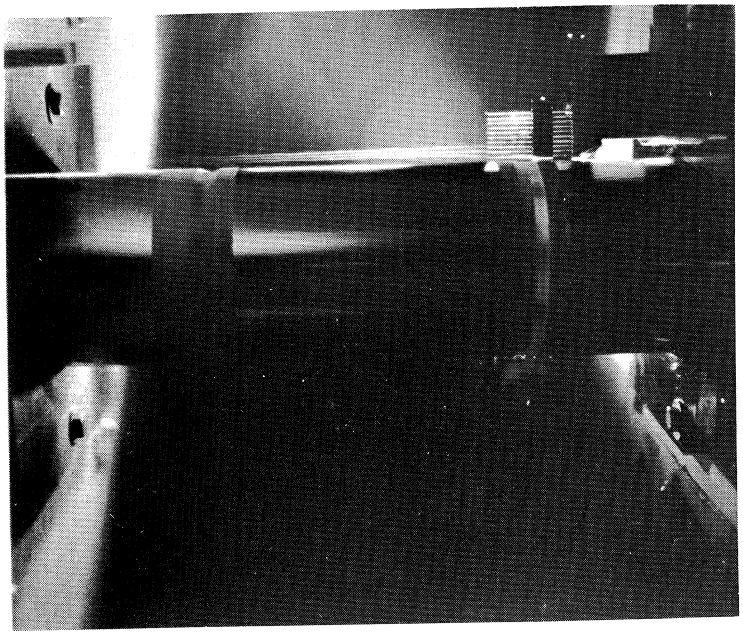

Figure 49. Smoke Photograph for Gr. Pr = 3.56 x 10^7, A/ℓ = 11.3 x 10^{-3} and fr = 12 cps.

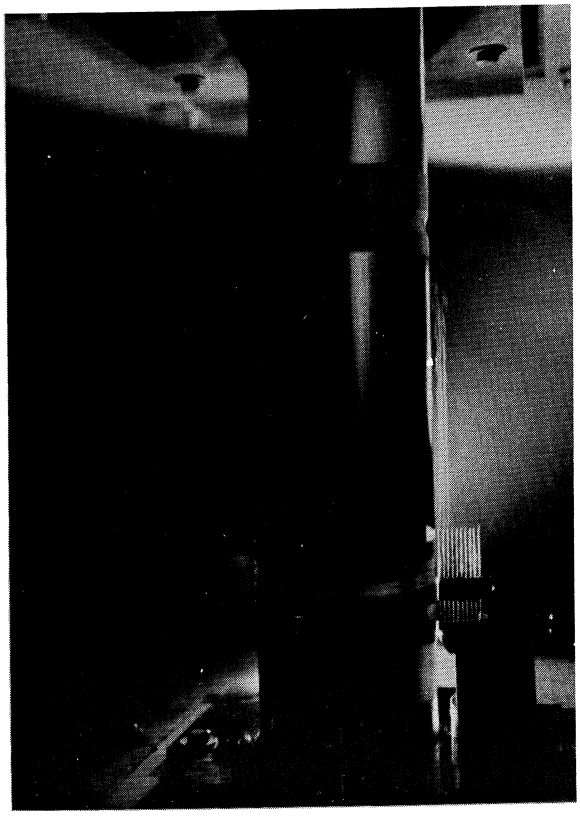

Figure 51. Smoke Photograph for Gr. Pr = 3.56×10^7, $A/\ell = 18.1 \times 10^{-3}$ and fr = 12 cps.

that in such cases the flow is in turbulent region. An attempt has been made to correlate this data in terms of a suitable parameter which would take into account both the free convective effect and the influence of oscillations. Figures 33 and 34 indicate that the Nusselt number increases with increasing Gr_ℓ, A/ℓ and ω. This was the criterion for defining a modified Grashof number Gr_{cv} which would have the above-mentioned characteristics. It was found that Nu_ℓ could be correlated as a function of Gr_{cv} defined as

$$Gr_{cv} \equiv Gr_\ell + 2\frac{A\omega\ell}{\nu}(Gr_\ell)^{1/2}(Pr)^{1/3}$$

Figure 52 is a plot of Nu_ℓ versus $Gr_{cv} \cdot Pr$ where the solid line is the best curve fitted through the data points. The experimental measurements presented in Figure 52 do not test the Prandtl number dependencies since all the data is for air with Pr = 0.72. The Prandtl number appearing in the definition of Gr_{cv}, however, has been extracted from theoretical analysis of steady free convection and it is expected to apply to fluids other than air.

No attempt has been made to present a correlation equation because of the limited range of the vibratory as well as thermal and geometrical parameters. More data in a wider range of parameters is necessary if a meaningful correlation equation is to be obtained. Nevertheless, within the limits of this work an equation of the form

$$Nu_\ell = K(Gr_{cv}\, Pr)^{1/3}$$

appears to correlate the turbulent data.

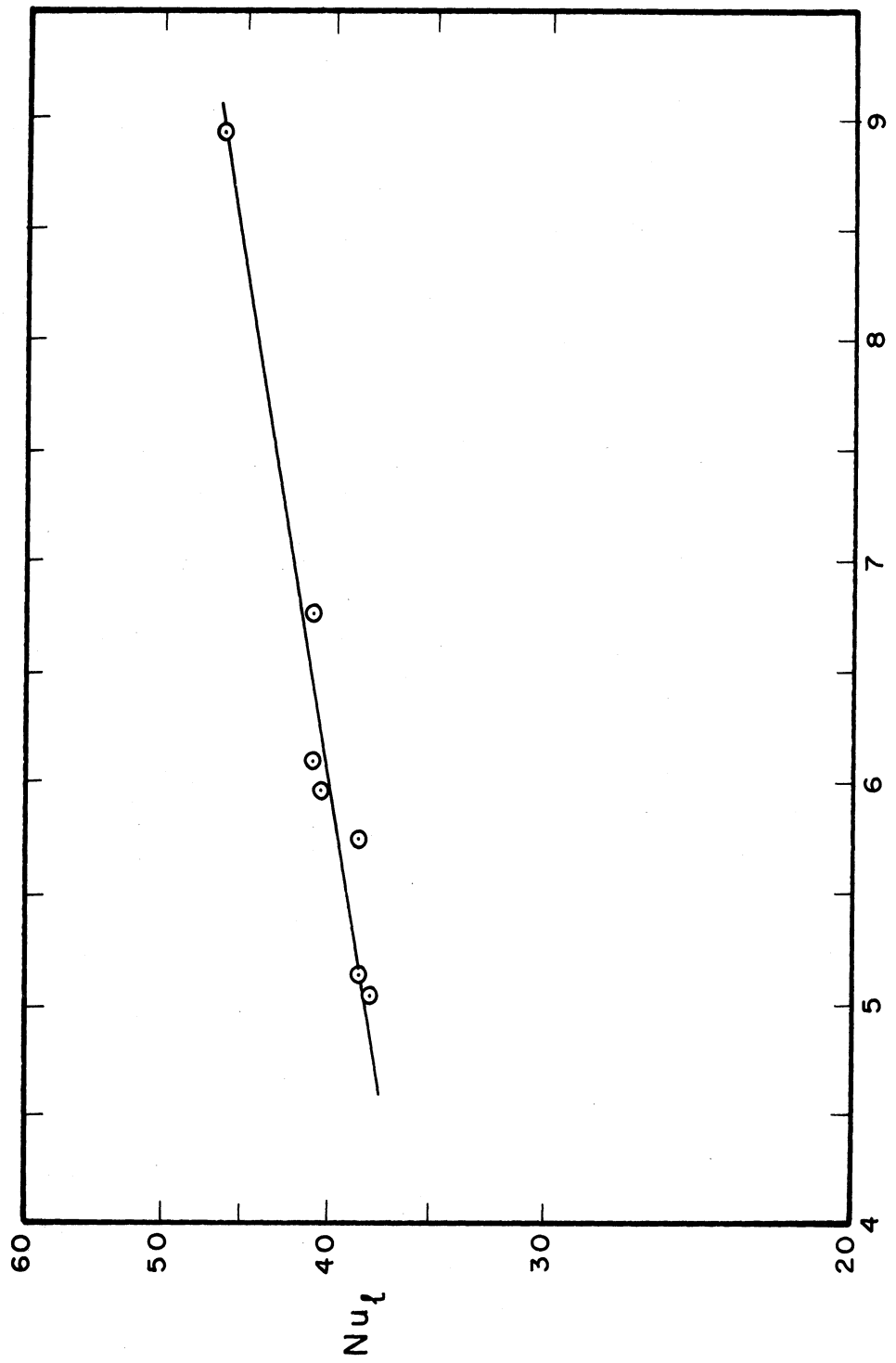

Figure 52. Correlation of Turbulent, Oscillatory, Free Convection Data.

The heat transfer data obtained in laminar region under vibratory conditions indicate that the average coefficient of heat transfer falls slightly below its steady state value. The analysis of Chapter II shows the same trend. Equation (73) determines the local Nusselt number and is valid as long as ω^* is greater than $2\,\omega_o^*$. Since ω^* is proportional to $\omega x^{1/2}$ then the use of Equation (73), for a fixed value of ω, restricts the lower limit of x. In other words, for finite ω, x cannot arbitrarily approach zero if Equation (73) is to be used. This implies that the local Nusselt number cannot be integrated over the total length of the heated section to yield an expression for the average Nusselt number. Considering the fact that the experimental measurements include not local coefficients but the average coefficients of heat transfer, a direct comparison between theory and experiment is not possible. It is intended, however, to make use of Equation (73) in order to obtain a semi-empirical expression for per cent change in Nusselt number caused by oscillations. It was pointed out, in Chapter III, that the relative change in Nusselt number is a function only of Pr and A/x, for large values of ω^*. This suggests that an attempt could be made to correlate the experimental data using A/ℓ as the main parameter describing relative change in Nusselt number for laminar heat transfer phenomenon. The expression in Equation (73), for Nu_x, could be integrated, for each frequency ω, from a point $x = x_o$ where $\omega^* = 2\,\omega_o^*$ up to the point where $x = \ell$. Then from $x = 0$ to $x = x_o$, it is conceivable to assume a distribution for relative change in Nusselt number that is similar in nature to its functionality in the range $x = x_o$ to $x = \ell$. A two region integration over the length of the heated section will then lead into a

semi-empirical equation. This procedure has been carried out for air (Pr = 0.72); the following equation is obtained

$$100\,\frac{Nu_\ell - Nu_{o\ell}}{Nu_{o\ell}} = -1.433\left\{\frac{4}{5}\left(\frac{A}{\ell}\right)^2\left[\left(\frac{\ell}{X_o}\right)^{5/4} - 1\right] + \frac{1}{0.75-p_1}\left(\frac{A}{X_o}\right)^{p_1}\left(\frac{X_o}{\ell}\right)^{3/4}\right\} \qquad (77)$$

In the above equation

$$X_o = 4.315\,\frac{\theta_w}{T_f}\cdot\frac{1}{fr^2}\,, \qquad (78)$$

and p_1 is a constant that should be determined experimentally for each set of conditions excluding the parameter A/ℓ.

In Equation (78) x_o is in feet, fr in cycles per second and $T_f = \frac{1}{2}(T_w + T_\infty)$ is the film temperature in degrees absolute. The expression in Equation (77) has been worked out for two sets of conditions and the results are presented in Figures 53 and 54 together with the experimental data obtained for the same conditions. The plots in Figures 53 and 54 indicate that as long as the flow is in laminar region Equation (77) agrees with the data as expected, deviations for larger values of A/ℓ being a consequence of transition to turbulence.

Summary of Experimental Results

A vertical heated cylinder with a diameter many times greater than the steady-state boundary layer thickness was oscillated vertically

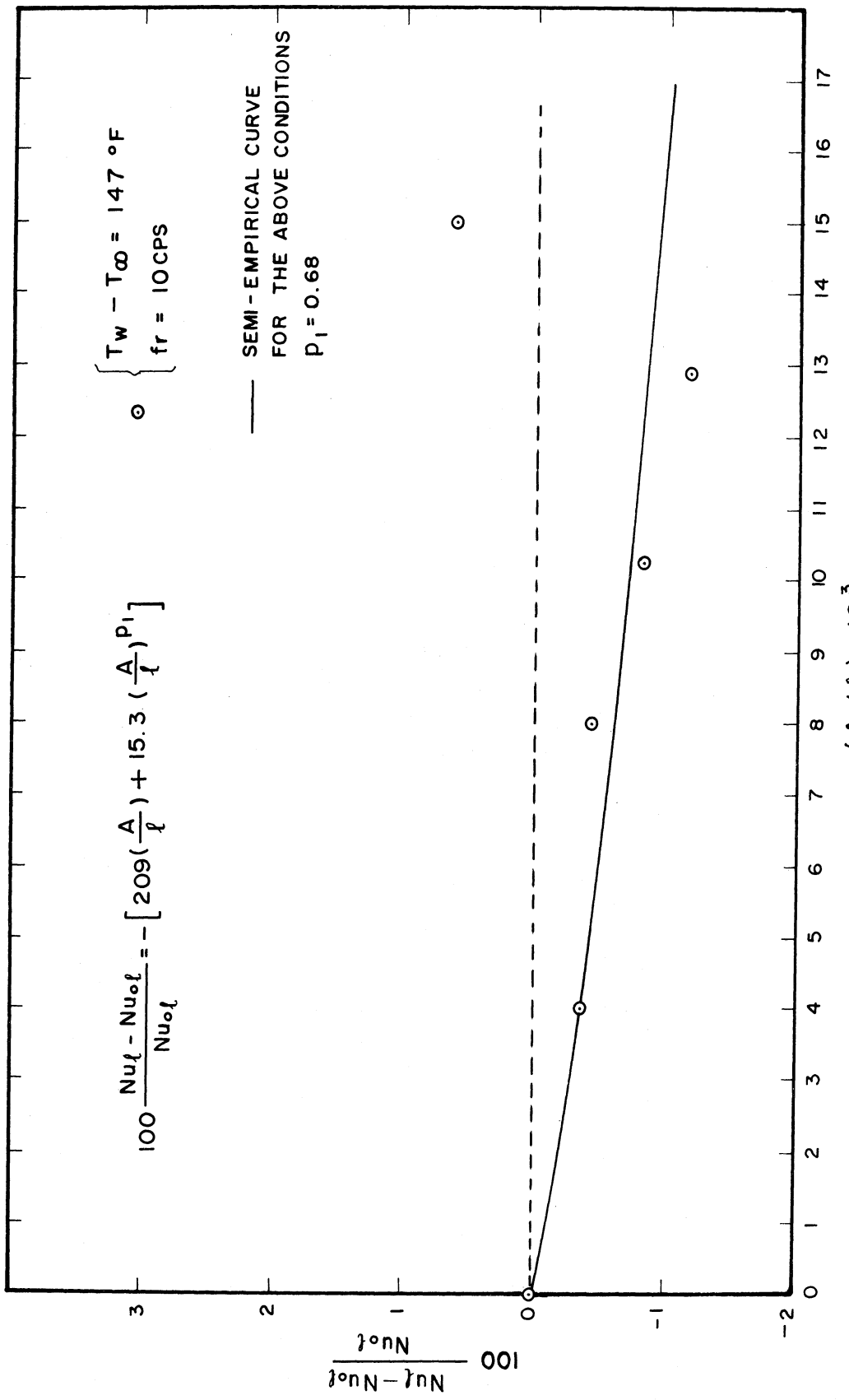

Figure 53. Correlation of Laminar Data.

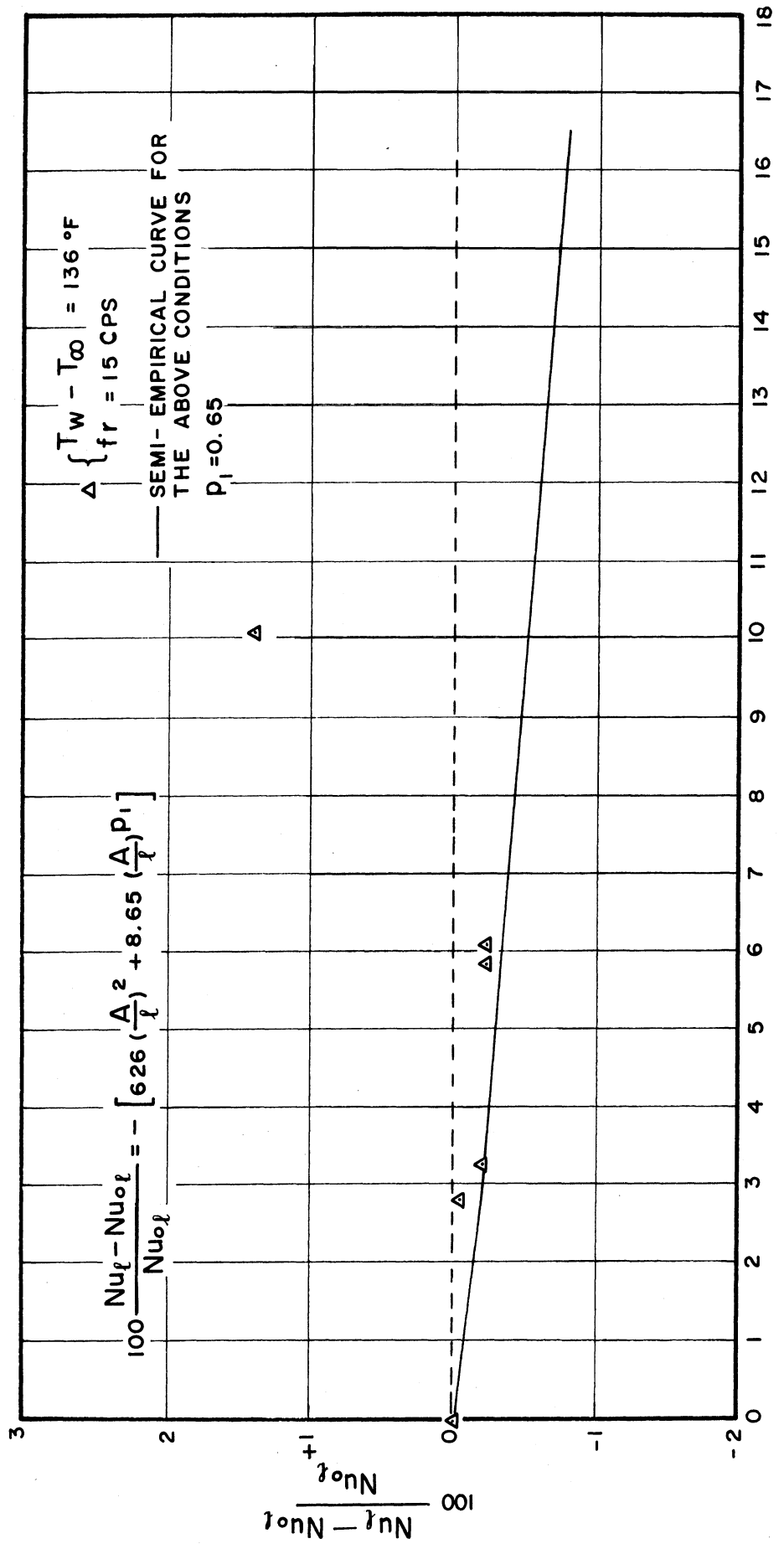

Figure 54. Correlation of Laminar Data.

in atmospheric air and heat transfer measurements were made. The changes in the coefficient of heat transfer under oscillatory conditions were compared to their measured values in the case of no oscillations. It was found that for small values of oscillatory velocity amplitude there was a small decrease in the coefficient of heat transfer. For higher values of velocity amplitude, however, increases were observed in the average coefficients over their measured steady state values. This reversal in the behavior of heat transfer coefficient was attributed to a transition phenomenon from laminar to turbulent flow. Smoke studies were carried out and evidence of a transition to turbulence was observed.

Semi-empirical equations were devised for the flow region associated with decreases in the heat transfer coefficient which are of a monotonically increasing character, in absolute value, with respect to the amplitude ratio defined as the ratio of oscillation amplitude to the heated length of the cylinder. The data in the turbulent region was correlated in terms of a modified Grashof number defined such that it is a superposition of the free convective and forced oscillation effects. Furthermore, a correlation equation was suggested that has to be verified by more extensive data.

REFERENCES

1. Schmidt, E. and Beckmann, W. "Das Temperature und Geschwindighetsfeld von einer Warme abgebenden Senkrechten platte bei naturlicher Konvektion." Technische Mechanik und Thermodynamik, (October 1930), 341-349, (November 1930), 391-406.

2. Ostrach, S. "Analysis of Laminar Free-Convection Flow and Heat Transfer about a Flat Plate Parallel to the Direction of the Generating Body Force." U.S. NACA Report TN2635, 1952.

3. Sparrow, E. M. and Gregg, J. L. "Laminar Free Convection from a Vertical Plate with Uniform Surface Heat Flux." Trans. ASME, 78 (1956), 435-440.

4. Sparrow, E. M. and Gregg, J. L. "Similar Solutions for Free Convection from a Nonisothermal Vertical Plate." Trans. ASME, 80 (1958), 379-386.

5. Finston, M. "Free Convection Past a Vertical Plate." ZAMP, 7 (1956), 527-529.

6. Millsaps, K. and Pohlhausen, K. "The Laminar Free-Convection Heat Transfer from the Outer Surface of a Vertical Circular Cylinder." Journal of the Aeronautical Science, 25 (1958), 357-360.

7. Yang, Kwang-Tzu. "Possible Similarity Solutions for Laminar Free Convection on Vertical Plates and Cylinders." J. of Applied Mechanics, (June 1960), 230-236.

8. Sugawara, S. and Michiyoski, I. "The Heat Transfer by Natural Convection in the Unsteady State on a Vertical Flat Wall." Proc. of the First Japan National Congress for Applied Mechanics, 1951.

9. Siegel, Robert. "Transient Free Convection from a Vertical Flat Plate." Trans. ASME, 80 (1958), 347-359.

10. Chung, P. M. and Anderson, A. D. "Unsteady Laminar Free Convection." Journal of Heat Transfer (November 1961) 473-478.

11. Lighthill, M. J. "The Response of Laminar Skin Friction and Heat Transfer to Fluctuations in the Stream Velocity." Proc. Roy. Soc., A224 (1954) 1-23.

12. Illingworth, C. R. "The Effect of a Sound Wave on the Compressible Boundary Layer on a Flat Plate." J. of Fluid Mechanics, 3 (1958), 471-493.

13. Kestin, J., Maeder, P. F., and Wang, H. E. "On Boundary Layers Associated with Oscillating Streams." Appl. Sci. Res., Sec. A, 10, 1960.

14. Schoenhals, R. J. and Clark, J. A. "Laminar Free Convection Boundary-Layer Perturbations Due to Transverse Wall Vibration." Journal of Heat Transfer (August 1962), 225-234.

15. Blankenship, V. D. "The Influence of Transverse Harmonic Oscillations on the Heat Transfer from Finite and Infinite Vertical Plates in Free Convection." Ph.D. Thesis, The University of Michigan, 1962.

16. Chamberlin, G. B., Jr. "Heat Transfer by Free Convection from a Longitudinally Oscillating Cylinder in Air." M.S. Thesis, Air Force Inst. of Tech., 1957.

17. Sprott, A. L., Holman, J. P. and Durand, F. L. "An Experimental Study of the Interaction of Strong Sound Fields with Free Convection Boundary Layers." WADC Technical Report 59-717, November 1959.

18. Holman, J. P., Gartrell, H. E. and Soehngen, E. E. "A Study of Free Convection Boundary Layer Oscillations and Their Effects on Heat Transfer." WADC Tech. Report 59-3, December 1959.

19. Soehngen, E. E. and Holman, J. P. "Experimental Studies on the Interaction of Strong Sound Fields with Free Convection Boundary Layers." ARL Tech. Report 60-323, October 1960.

20. Goldstein, S. "Modern Developments in Fluid Dynamics." Oxford University Press, Vol. II (1938), 641-643.

21. Eckert, E. R. G. and Drake, R. M., Jr. Heat and Mass Transfer. McGraw-Hill, (1959) 312-315.

22. McAdams, W. H. Heat Transmission. McGraw-Hill, 1954.

23. Schoenhals, R. J. "The Response of Laminar Incompressible Fluid Flow and Heat Transfer to Transverse Wall Vibration." Thesis, The University of Michigan, 1960.

APPENDIX I

EQUIVALENCE OF THE CASE OF AN OSCILLATING PLATE IN A STAGNANT AMBIENT TO THE CASE OF A FIXED PLATE IN AN OSCILLATING POTENTIAL FLOW

The terms in the energy equation will retain the same form whether the system of coordinates is fixed or accelerating. The boundary layer equation, however, being the x-component of momentum equation would undergo some changes.

Let us first consider the case where the plate moves in the x-direction with a velocity $-U(t)$ relative to a fixed coordinate axis. In this case, the boundary layer equations become,

$$\begin{cases} \dfrac{Du}{Dt} = \nu \dfrac{\partial^2 u}{\partial y^2} - \dfrac{1}{\rho}\dfrac{\partial p}{\partial x} - g + \dfrac{d}{dt}\left[U(t)\right] \\ \dfrac{dU}{dt} = -\dfrac{1}{\rho}\dfrac{\partial p}{\partial x} - g + \dfrac{dU}{dt} \\ u(x,0,t) = v(x,0,t) = 0 \;\; ; \;\; u(x,\infty,t) = U(t) \end{cases}$$

$$\therefore \; -\frac{\partial p}{\partial x} = \rho_\infty g \quad ,$$

and finally,

$$\frac{Du}{Dt} = \nu \frac{\partial^2 u}{\partial y^2} + \beta g (T - T_\infty) + \frac{dU}{dt}$$

$$u(x,0,t) = v(x,0,t) = 0 \;\; ; \;\; u(x,\infty,t) = U(t) \; .$$

In the other case where the plate and consequently the system of coordinates are fixed, there are no inertia forces present and the equations take their classical form of

$$\begin{cases} \dfrac{Du}{Dt} = \nu \dfrac{\partial^2 u}{\partial y^2} - \dfrac{1}{\rho} \dfrac{\partial p}{\partial x} - g \\ \dfrac{dU}{dt} = -\dfrac{1}{\rho} \dfrac{\partial p}{\partial x} - g \\ u(x,0,t) = v(x,0,t) = 0 \;\; ; \; u(x,\infty,t) = U(t) \end{cases}$$

$$\therefore \quad -\frac{\partial p}{\partial x} = \rho_\infty g + \rho \frac{dU}{dt} \quad ,$$

and finally

$$\frac{Du}{Dt} = \nu \frac{\partial^2 u}{\partial y^2} + \beta g (T - T_\infty) + \frac{dU}{dt}$$

$$u(x,0,t) = v(x,0,t) = 0 \;\; ; \; u(x,\infty,t) = U(t) \quad ,$$

which are exactly the same as the equations obtained for the first case.

In conclusion, the term $\frac{dU}{dt}$ appears in the first case as an inertia force (body force) and in the second case as a pressure force.

APPENDIX II

TABULATION OF THE RESULTS OF THE STEADY STATE INTEGRAL SOLUTION

Pr	Δ	$D_1 = \frac{Nu_x}{(Gr_x)^{1/4}}$	$D_3 = \frac{u_{max}}{(\beta g \Theta_w x)^{1/2}}$
0.005	6.03117	0.03173	1.91931
0.010	4.44177	0.04695	1.61694
0.02	3.31645	0.07849	1.36287
0.03	2.81689	0.08476	1.23342
0.60	1.05914	0.32816	0.58206
0.70	1.01935	0.34805	0.55859
0.72	1.01237	0.35178	0.55437
0.733	1.00799	0.35417	0.55170
25/33 = 0.7575	1.00000	0.35859	0.54681
1	0.93727	0.39742	0.50676
2	0.81129	0.50749	0.41478
10	0.64106	0.84461	0.23984
50	0.57733	1.32017	0.12104
100	0.56692	1.58179	0.08744
1000	0.55674	2.83381	0.02825
10000	0.555674	5.04329	0.00895
∞	5/9 = 0.5555	-	-

In Chapter II, the functions H'(0) and F"(0) from Ostrach's numerical solution,[2] have been refered to. These functions are tabulated below for different Prandtl numbers.

Pr	0.01	0.72	0.733	1	2	10	100	1000
-H'(0)	0.0812	0.5046	0.5080	0.5671	0.7165	1.1694	2.191	3.966
F"(0)	0.9862	0.6760	0.6741	0.6421	0.5713	0.4192	0.2517	0.1450

APPENDIX III

DEFINITION OF α's AND β's

For $\Delta \leq 1$

$$\alpha_7 = 1.8\Delta - 1$$

$$\alpha_0 = \frac{1}{93}\Delta^{-1}$$

$$\alpha_1 = 3 + \frac{25}{31\alpha_7}$$

$$\alpha_2 = \frac{5}{93}\Delta^{-1} + \frac{5\Delta}{31\alpha_7}$$

$$\alpha_3 = \frac{150}{31}$$

$$\alpha_4 = \frac{1}{93}$$

$$\alpha_5 = \frac{5}{93} + \frac{5}{31\alpha_7}$$

$$\alpha_6 = \frac{5}{2232\alpha_7}$$

$$\alpha_8 = \alpha_6\left(\Delta^{-1} + \Delta^{3}Pr\right)$$

$$\alpha_9 = \frac{45}{62} + \frac{50}{93\alpha_7}$$

$$\alpha_{10} = \frac{5}{186\alpha_7}$$

$$\alpha_{11} = -39.407\, H'(0)(\alpha_7)^{5/4}\frac{\Delta}{\lambda_0}\frac{1+2\sqrt{Pr}}{(1+\sqrt{Pr})^2}$$

$$\beta_1 = 3 + \frac{5}{252\,Pr\,\Delta\,\alpha_7\,S(\Delta)}$$

$$\beta_2 = 6\,\frac{Z(\Delta)}{S(\Delta)}$$

$$\beta_3 = 6\,\frac{W(\Delta)}{S(\Delta)}$$

$$\beta_4 = \frac{1}{6}\,Pr\,\frac{Y(\Delta)}{S(\Delta)}$$

$$\beta_5 = \frac{\Delta}{252\,\alpha_7\,S(\Delta)} + \frac{5\,Pr\,Y(\Delta)}{6\,S(\Delta)}$$

$$\beta_6 = \frac{\Delta^3\,Pr}{18144\,\alpha_7\,S(\Delta)}$$

$$\beta_7 = 6\,\frac{V(\Delta)}{S(\Delta)}$$

$$\beta_8 = 3\,\beta_7$$

$$\beta_9 = 18\,\frac{X(\Delta)}{S(\Delta)}$$

Also values of α_{11} have been tabulated for some Prandtl numbers.

Pr	0.757	1	2	10	100
α_{11}	1.490	1.4068	1.0999	0.5088	0.1225

APPENDIX IV

TABULATION OF γ_n AND λ_n FOR DIFFERENT VALUES OF PRANDTL NUMBER

Pr	0.757		1		10		100	
n	γ_n	λ_n	γ_n	λ_n	γ_n	λ_n	γ_n	λ_n
0	.74794	$.78715 \times 10^{1}$	.73349	$.69854 \times 10^{1}$	.37987	$.23661 \times 10^{1}$	$.56817 \times 10^{-1}$	.53633
1	.18106	.31442	.18641	.37052	.28860	.92735	.43318	$.13451 \times 10^{1}$
2	$.31654 \times 10^{-2}$	$.54153 \times 10^{-1}$	$.31562 \times 10^{-2}$	$.69534 \times 10^{-1}$	$-.53343 \times 10^{-3}$	.54463	-.21293	$.43567 \times 10^{1}$
3	$.78520 \times 10^{-4}$	$-.46146 \times 10^{-2}$	$.14668 \times 10^{-3}$	$-.70231 \times 10^{-2}$	$.79701 \times 10^{-2}$	-.22632	.61514	$-.11422 \times 10^{2}$
4	$.16995 \times 10^{-4}$	$-.27537 \times 10^{-3}$	$.28467 \times 10^{-4}$	$-.54613 \times 10^{-3}$	$.34067 \times 10^{-2}$	$-.85837 \times 10^{-1}$	$.12067 \times 10^{1}$	$-.30228 \times 10^{2}$
5	$-.14461 \times 10^{-5}$	$.70913 \times 10^{-5}$	$-.26907 \times 10^{-5}$	$.30398 \times 10^{-4}$	$-.10876 \times 10^{-2}$	$.31609 \times 10^{-1}$	$-.22374 \times 10^{1}$	$.85018 \times 10^{2}$
6	$-.72051 \times 10^{-7}$	$-.98765 \times 10^{-6}$	$-.16433 \times 10^{-6}$	$.44027 \times 10^{-6}$	$-.28118 \times 10^{-3}$	$.11767 \times 10^{-1}$	$-.41383 \times 10^{1}$	$.26029 \times 10^{3}$
7	$-.97839 \times 10^{-9}$	$.19626 \times 10^{-6}$	$.15736 \times 10^{-8}$	$.15484 \times 10^{-6}$	$.52779 \times 10^{-4}$	$-.46448 \times 10^{-2}$	$.80018 \times 10^{1}$	$-.87964 \times 10^{3}$
8	$-.74057 \times 10^{-9}$	$.19879 \times 10^{-7}$	$-.12763 \times 10^{-8}$	$.20331 \times 10^{-7}$	$.25515 \times 10^{-5}$	$-.20503 \times 10^{-2}$	$.17806 \times 10^{2}$	$-.33018 \times 10^{4}$
9	$.10071 \times 10^{-9}$	$-.10423 \times 10^{-8}$	$.20824 \times 10^{-9}$	$-.18604 \times 10^{-9}$	$.30956 \times 10^{-5}$	$.10462 \times 10^{-2}$	$-.52411 \times 10^{2}$	$.13755 \times 10^{5}$
10	$.77962 \times 10^{-11}$	$.60197 \times 10^{-10}$	$.16748 \times 10^{-10}$	$.44023 \times 10^{-9}$	$.12459 \times 10^{-5}$	$.61173 \times 10^{-3}$	$-.21454 \times 10^{3}$	$.63254 \times 10^{5}$
11	$-.66362 \times 10^{-13}$	$-.23074 \times 10^{-10}$	$.33604 \times 10^{-12}$	$-.11193 \times 10^{-9}$	$.26228 \times 10^{-6}$	$-.39576 \times 10^{-3}$	$.11098 \times 10^{4}$	$-.31869 \times 10^{6}$
12	$.94308 \times 10^{-13}$	$-.30780 \times 10^{-11}$	$.37768 \times 10^{-12}$	$-.18108 \times 10^{-10}$	$.78923 \times 10^{-6}$	$-.27454 \times 10^{-3}$	$.65377 \times 10^{4}$	$-.17458 \times 10^{7}$
13	$-.18354 \times 10^{-13}$	$.17376 \times 10^{-12}$	$-.74089 \times 10^{-13}$	$.21235 \times 10^{-11}$	$-.82176 \times 10^{-6}$	$.20088 \times 10^{-3}$	$-.41781 \times 10^{5}$	$.10329 \times 10^{8}$
14	$-.19841 \times 10^{-14}$	$-.26008 \times 10^{-13}$	$-.84330 \times 10^{-14}$	$.15532 \times 10^{-12}$	$-.71434 \times 10^{-6}$	$.15420 \times 10^{-3}$	$-.28497 \times 10^{6}$	$.65612 \times 10^{8}$
15	$.67903 \times 10^{-16}$	$.96663 \times 10^{-14}$	$.23813 \times 10^{-15}$	$.22653 \times 10^{-14}$	$.61152 \times 10^{-6}$	$-.12411 \times 10^{-3}$	$.20622 \times 10^{7}$	$-.44526 \times 10^{9}$
16	$-.25376 \times 10^{-16}$	$.16774 \times 10^{-14}$	$-.15851 \times 10^{-15}$	$.27139 \times 10^{-14}$	$.54876 \times 10^{-6}$	$-.10475 \times 10^{-3}$	$.15781 \times 10^{8}$	$-.32141 \times 10^{10}$
17	$.72365 \times 10^{-17}$	$-.17526 \times 10^{-15}$	$.48670 \times 10^{-16}$	$-.35144 \times 10^{-15}$	$-.52409 \times 10^{-6}$	$.92687 \times 10^{-4}$	$-.12734 \times 10^{9}$	$.24586 \times 10^{11}$
18	$.11141 \times 10^{-17}$	$-.15447 \times 10^{-17}$	$.88915 \times 10^{-17}$	$.28028 \times 10^{-16}$	$-.52930 \times 10^{-6}$	$.85878 \times 10^{-4}$	$-.10806 \times 10^{10}$	$.19862 \times 10^{12}$
19	$-.90401 \times 10^{-19}$	$-.42466 \times 10^{-17}$	$-.10956 \times 10^{-17}$	$-.24538 \times 10^{-16}$	$.55947 \times 10^{-6}$	$-.83206 \times 10^{-4}$	$.96200 \times 10^{10}$	$-.16896 \times 10^{13}$
20	$.77193 \times 10^{-20}$	$-.11637 \times 10^{-17}$	$-.55454 \times 10^{-19}$	$-.67779 \times 10^{-17}$	$.61458 \times 10^{-6}$	$-.84181 \times 10^{-4}$	$.89638 \times 10^{11}$	$-.15095 \times 10^{14}$
21	$-.49414 \times 10^{-20}$	$.18990 \times 10^{-18}$	$-.14355 \times 10^{-19}$	$.11906 \times 10^{-17}$	$-.69915 \times 10^{-6}$	$.88811 \times 10^{-4}$	$-.87246 \times 10^{12}$	$.14128 \times 10^{15}$
22	$-.12051 \times 10^{-20}$	$.16328 \times 10^{-19}$	$-.48769 \times 10^{-20}$	$.10418 \times 10^{-18}$	$-.82243 \times 10^{-6}$	$.97583 \times 10^{-4}$	$-.88535 \times 10^{13}$	$.13822 \times 10^{16}$
23	$.20156 \times 10^{-21}$	$.17328 \times 10^{-20}$	$.64467 \times 10^{-21}$	$.18712 \times 10^{-19}$	$.99970 \times 10^{-6}$	$-.11154 \times 10^{-3}$	$.93510 \times 10^{14}$	$-.14109 \times 10^{17}$
24	$.21571 \times 10^{-22}$	$.11309 \times 10^{-20}$	$-.67403 \times 10^{-22}$	$.11954 \times 10^{-19}$	$.12551 \times 10^{-5}$	$-.13247 \times 10^{-3}$	$.10263 \times 10^{16}$	$-.14998 \times 10^{18}$
25	$.16160 \times 10^{-24}$	$-.29201 \times 10^{-21}$	$.69194 \times 10^{-22}$	$-.35907 \times 10^{-20}$	$-.16267 \times 10^{-5}$	$.16331 \times 10^{-3}$	$-.11689 \times 10^{17}$	$.16576 \times 10^{19}$

APPENDIX V

COMPUTATION PROCEDURE

All the expressions derived for large values of frequency in Chapter II were simple and explicit in all the parameters involved and therefore, did not require extensive computation. The integral procedures, however, did involve some numerical evaluation. For this part of the analysis, the IBM 7090 Electronic Computer of the University of Michigan Computing Center was utilized. Three sets of computer programs were written for different stages of the computation.

The first program was used to obtain a numerical solution to Equation (41) of Chapter II. This resulted in tabulation of Δ for different Prandtl numbers (Appendix II). Newton's iteration process was used and the initial values of Δ, for each Pr, were estimated by a rough plot of Pr versus Δ.

The second program was written for the evaluation of the first three terms of the series solution for B and B_1, i.e., γ_0 through γ_2 and λ_0 through λ_2. This program was simple in nature and involved only evaluation of a set of formulas for a few values of Prandtl number.

The third program was set up to calculate coefficients γ_n and λ_n for the values of n greater than two for which generalized expressions were derived in Equation (58) of Chapter II. These are the coefficients listed in Appendix IV.

The series themselves, however, were calculated on a desk calculator. This would allow one to observe the convergence behavior of the

series and does not present any problem concerning the order of magnitude of the numbers involved.

All the programs were written in MAD (Michigan Algorithm Decoder).

```
$ COMPILE MAD,EXECUTE,PRINT OBJECT,PUNCH OBJECT,DUMP                    04/18/62

MAD (12 MAR 1962 VERSION) PROGRAM LISTING ... ... ...

                PRINT FORMAT F1                                          *001
                VECTOR VALUES F1=$///S10,35HFOR PRANDTL NUMBERS LESS THAN 0.7
               157///S5,85HSIGMA        I        DELTA        I        CONST
               2  I        ERRDEL       I        UMAX/S2,91H***********     I
               3 ***********     I     ***********     I     ***********     I
               4*************$                                            *002
      BASE2     READ FORMAT F2,SIGMA,DELTA                               *003
                VECTOR VALUES F2=$2F15.5*$                               *004
                WHENEVER SIGMA.G.0.757,TRANSFER TO BASE5                 *005
                THROUGH BASE1,FOR I=0,1,(.ABS.(2.52-8.316*DELTA-1./SIGMA+0.15
               1/(DELTA.P.3)-0.81/(DELTA.P.2)+0.972/DELTA+6.804*(DELTA.P.2)).
               2L.1E-6).OR.I.G.15                                        *006
      BASE1     DELTA=DELTA+(1./SIGMA-2.52+8.316*DELTA-6.804*(DELTA.P.2)-0.15
               1/(DELTA.P.3)+0.81/(DELTA.P.2)-0.972/DELTA)/(-8.316+13.608*DEL
               2TA-0.972/(DELTA.P.2) +1.62/(DELTA.P.3)-0.45/(DELTA.P.4))  *007
                WHENEVER SIGMA.L.0.757,TRANSFER TO BASE4                 *008
      BASE5     PRINT FORMAT F4                                          *009
                VECTOR VALUES F4=$///S10,35HFOR PRANDTL NUMBERS MORE THAN 0.7
               157///S5,85HSIGMA        I        DELTA        I        CONST
               2  I        ERRDEL       I        UMAX/S2,91H***********     I
               3 ***********     I     ***********     I     ***********     I
               4*************$                                            *010
      BASE6     READ FORMAT F2,SIGMA,DELTA                               *011
                THROUGH BASE7,FOR J=0,1,(.ABS.(-1./SIGMA-5.04*(DELTA.P.3)+14.
               1472*(DELTA.P.4)-12.15*(DELTA.P.5)+4.794*(DELTA.P.6)-0.756*(DE
               2LTA.P.7)).L.1E-7).OR.J.G.15                              *012
      BASE7     DELTA=DELTA+(1./SIGMA+5.04*(DELTA.P.3)-14.472*(DELTA.P.4)+12.
               115*(DELTA.P.5)-4.794*(DELTA.P.6) +0.756* (DELTA.P.7))/(-15.12
               2*(DELTA.P.2)+57.888*(DELTA.P.3)-60.75*(DELTA.P.4)+28.764*(DEL
               3TA.P.5)-5.292*(DELTA.P.6))                               *013
      BASE4     CONST=1./(DELTA*(75.6*(1.8*DELTA-1.)).P.0.25)            *014
                WHENEVER SIGMA.L.0.757                                   *015
                ERRDEL=1.E-6/(-8.316+13.608*DELTA-0.972/DELTA.P.2.+1.62/DELTA
               1.P.3.-0.45/DELTA.P.4.)                                   *016
                OTHERWISE                                                *017
                ERRDEL=1.E-7/(-15.12*DELTA.P.2.+57.888*DELTA.P.3.-60.75*DELTA
               1.P.4.+28.764*DELTA.P.5.-5.292*DELTA.P.6.)                *018
                END OF CONDITIONAL                                       *019
                UMAX=(9./128.)*(75.6*(1.8*DELTA-1.)).P.0.5               *020
                PRINT FORMAT F3,SIGMA,DELTA,CONST,ERRDEL,UMAX            *021
                VECTOR VALUES F3=$S2,F10.4,S5,1HI,S2,F13.8,S4,1HI,S4,F11.6,S4
               1,1HI,S4,E11.4,S4,1HI,S4,F11.6/*$                         *022
                WHENEVER SIGMA.L.0.757,PRINT FORMAT F5,I                 *023
                VECTOR VALUES F5=$S114,I3*$                              *024
                WHENEVER SIGMA.G.0.757,PRINT FORMAT F6,J                 *025
                VECTOR VALUES F6=$S114,I3*$                              *026
                WHENEVER SIGMA.L.0.757,TRANSFER TO BASE2                 *027
                WHENEVER SIGMA.G.0.757,TRANSFER TO BASE6                 *028
                INTEGER I,J                                              *029
                END OF PROGRAM                                           *030
```

```
      $ COMPILE MAD,EXECUTE ,PRINT OBJECT,DUMP                                  000036

MAD (16 APR 1962 VERSION) PROGRAM LISTING ... ... ...

                PRINT FORMAT F2                                                 *001
                VECTOR VALUES F2=$//S9,5HSIGMA,S12,5HALPH8,S12,5HALPH9,S12,6H   *002
               1ALPH14,S12,6HALPH15,S12,6HALPH16,S12,6HALPH17*$                 *002
                ALPH3=4.8387097                                                 *003
                ALPH4=1./93.                                                    *004
      BASE1     READ FORMAT F1, SIGMA, DELTA                                    *005
                VECTOR VALUES F1=$2F20.5*$                                      *006
                ALPH7=1.8*DELTA-1.                                              *007
                ALPH0=1./93./DELTA                                              *008
                ALPH1=3.+25./31./ALPH7                                          *009
                ALPH2=5./93./DELTA+5.*DELTA/31./ALPH7                           *010
                ALPH5=5./93.+5./31./ALPH7                                       *011
                ALPH6=5./2232./ALPH7                                            *012
                ALPH10=(5./2232.)*(1./DELTA/ALPH7+SIGMA/ALPH7*DELTA.P.3.)       *013
                ALPH11=45./62.+50./93./ALPH7                                    *014
                ALPH13=5./186./ALPH7                                            *015
                S=(DELTA.P.2.)*(2./21.-6./35.*DELTA+1./9.*DELTA.P.2.            *016
               1 -8./315.*DELTA.P.3.)                                           *016
                W=(DELTA.P.2.)*(1./15.-1./45.*DELTA.P.3.+1./105.                *017
               1 *DELTA.P.4.)                                                   *017
                V=DELTA.P.4.*(1./560.-1./540.*DELTA+1./1890.*DELTA.P.2.)        *018
                X=DELTA.P.3.*(-1./84.+1./120.*DELTA.P.2.-1./315.*DELTA.P.3.)    *019
                Y=DELTA.P.4.*(1./105.-1./56.*DELTA+1./84.*DELTA.P.2.-1./360.*   *020
               1DELTA.P.3.)                                                     *020
                Z=(DELTA.P.5.)*(1./36.-4./315.*DELTA)                           *021
                BETA1=3.+(5./252.)/(SIGMA*DELTA*S*ALPH7)                        *022
                BETA2=6.*Z/S                                                    *023
                BETA3=6.*W/S                                                    *024
                BETA4=SIGMA*Y/6./S                                              *025
                BETA5=DELTA/252./S/ALPH7+5.*SIGMA*Y/6./S                        *026
                BETA6=SIGMA*DELTA.P.3./18144./S/ALPH7                           *027
                BETA7=6.*V/S                                                    *028
                BETA8=3.*BETA7                                                  *029
                BETA9=18.*X/S                                                   *030
                ALPH8=(ALPH3*BETA3+ALPH1*BETA2)/(ALPH2*BETA3+ALPH1*BETA1        *031
               1-2.*ALPH0*BETA3-2.*ALPH1)                                       *031
                ALPH9=(1./ALPH1)*(ALPH3+ALPH8*(2.*ALPH0-ALPH2))                 *032
                ALPH14=(BETA1*(ALPH11-ALPH10*ALPH8-ALPH5*ALPH9)+ALPH2*(ALPH8*   *033
               1(BETA5-2.*BETA4)-ALPH9*BETA8-BETA9))/(2.*BETA1+ALPH1*BETA1+     *033
               23.*ALPH2*BETA3)                                                 *033
                ALPH15=(ALPH8*(BETA5-2.*BETA4)-BETA8*ALPH9-BETA9-3.*BETA3*      *034
               1ALPH14)/BETA1                                                   *034
                ALPH16=((4.+ALPH1)*(2.*BETA5*ALPH15-2.*BETA6*ALPH8+             *035
               12.*ALPH14*(BETA8+2.*BETA7))-5.*BETA3*(2.*ALPH6*ALPH9-2.*       *035
               2ALPH13+2.*ALPH14*(ALPH5+2.*ALPH4)-2.*ALPH10*ALPH15))/(5.*      *035
               3BETA3*(ALPH2+2.*ALPH0)+(4.+ALPH1)*(2.+BETA1))                   *035
                ALPH17=(2.*BETA5*ALPH15-2.*ALPH8*BETA6+ALPH14*(4.*BETA7+2.*BE   *036
               1TA8)-ALPH16*(2.+BETA1))/5./BETA3                                *036
                PRINT FORMAT F3,SIGMA,ALPH8,ALPH9,ALPH14,ALPH15,ALPH16,ALPH17   *037
                VECTOR VALUES F3=$7E17.8*$                                      *038
                TRANSFER TO BASE1                                               *039
                END OF PROGRAM                                                  *040
```

```
$ COMPILE MAD,EXECUTE ,PRINT OBJECT,DUMP                                    057458

MAD (16 APR 1962 VERSION) PROGRAM LISTING ... ... ...

                PRINT FORMAT F2                                             *001
                VECTOR VALUES F2=$///S10,1HN,S10,5HSIGMA,S10,8HGAMMA(N),S10,9 *002
               1HLAMBDA(N)*$                                                *002
                J=1                                                         *003
                DIMENSION GAMMA(100),LAMBDA(100)                            *004
                ALPH4=1./93.                                                *005
BASE1           READ FORMAT F1,SIGMA,DELTA,N1,N2,    GAMMA(1),GAMMA(2),LAMBDA( *006
               11),LAMBDA(2)                                                *006
                VECTOR VALUES F1=$2F20.5/2I5/4F15.5*$                       *007
                ALPH7=1.8*DELTA-1.                                          *008
                ALPH0=1./93./DELTA                                          *009
                ALPH1=3.+25./31./ALPH7                                      *010
                ALPH2=5./93./DELTA+5.*DELTA/31./ALPH7                       *011
                ALPH5=5./93.+5./31./ALPH7                                   *012
                ALPH6=5./2232./ALPH7                                        *013
                ALPH10=(5./2232.)*(1./DELTA/ALPH7+SIGMA/ALPH7*DELTA.P.3.)   *014
                S=(DELTA.P.2.)*(2./21.-6./35.*DELTA+1./9.*DELTA.P.2.        *015
               1 -8./315.*DELTA.P.3.)                                       *015
                W=(DELTA.P.2.)*(1./15.-1./45.*DELTA.P.3.+1./105.            *016
               1 *DELTA.P.4.)                                               *016
                V=DELTA.P.4.*(1./560.-1./540.*DELTA+1./1890.*DELTA.P.2.)    *017
                Y=DELTA.P.4.*(1./105.-1./56.*DELTA+1./84.*DELTA.P.2.-1./360.* *018
               1DELTA.P.3.)                                                 *018
                BETA1=3.+(5./252.)/(SIGMA*DELTA*S*ALPH7)                    *019
                BETA3=6.*W/S                                                *020
                BETA4=SIGMA*Y/6./S                                          *021
                BETA5=DELTA/252./S/ALPH7+5.*SIGMA*Y/6./S                    *022
                BETA6=SIGMA*DELTA.P.3./18144./S/ALPH7                       *023
                BETA7=6.*V/S                                                *024
                BETA8=3.*BETA7                                              *025
                THROUGH  BA&E2,FOR N=N1,N2,.ABS.LAMBDA(N-1).LE.1.E-36.OR.   *026
               1.ABS.GAMMA(N-1).LE.1.E-36.OR..ABS.LAMBDA(N-1).GE.1.E+36.OR. *026
               2 .ABS.GAMMA(N-1).GE.1.E+36                                  *026
                A1=-N*(ALPH5+2.*(N-1.)*ALPH4)*(-J).P.N                      *027
                A2=N*(N-1.)*ALPH6                                           *028
                A3=2.*(N-1.)*ALPH0+ALPH2                                    *029
                A4=-N*ALPH10*(-J).P.N                                       *030
                A5=2.*N+ALPH1                                               *031
                C1=-N*(2.*(N-2.)*BETA4+BETA5)*(-J).P.N                      *032
                C2=N*(N-1.)*BETA6                                           *033
                C3=(2.*N+1.)*BETA3                                          *034
                C4=-N*(2.*(N-1.)*BETA7+BETA8)*(-J).P.N                      *035
                C5=2.*(N-1.)+BETA1                                          *036
                LAMBDA(N)=(1./(C5*A5+A3*C3))*(A5*(-C1*LAMBDA(N-1)+C2*LAMBDA(N *037
               1-2)+C4*GAMMA(N-1))+C3*(A2*GAMMA(N-2)-A1*GAMMA(N-1)-A4*LAMBDA( *037
               2N-1)))                                                      *037
                GAMMA(N)=(A2*GAMMA(N-2)-A1*GAMMA(N-1)-A4*LAMBDA(N-1)-A3*LAMBD *038
               1A(N))/A5                                                    *038
BASE2           PRINT FORMAT F3,N,SIGMA,GAMMA(N),LAMBDA(N)                  *039
                VECTOR VALUES F3=$S11,I3,S12,E7.3,2E20.6*$                  *040
                TRANSFER TO BASE1                                           *041
                INTEGER N,N1,N2,N3,J                                        *042
                END OF PROGRAM                                              *043
```

APPENDIX VI

EXPERIMENTAL DATA

A	fr	$T_w - T_\infty$	T_∞	$\overline{h_T}$	$\overline{h_r}$	$\overline{h_c}$
in.	cps	°F	°F	$\frac{BTU}{hr\text{-}ft^2\text{-}°F}$	$\frac{BTU}{hr\text{-}ft^2\text{-}°F}$	$\frac{BTU}{hr\text{-}ft^2\text{-}°F}$
0.035	10	147.3	79.1	1.1172	0.0998	1.0170
0.082	10	147.5	82.2	1.1160	0.1013	1.0150
0.103	10	147.8	82.4	1.1138	0.1015	1.0120
0.032	10	150.9	82.8	1.0962	0.1127	0.9835
0.064	10	151.0	83.4	1.0955	0.1130	0.9825
0.120	10	149.6	83.6	1.1057	0.1127	0.9930
0.0225	15	135.6	76.1	1.0393	0.1026	0.9367
0.049	15	135.8	76.4	1.0377	0.1029	0.9348
0.074	15	132.2	78.5	1.0660	0.1029	0.9631
0.107	15	130.3	79.0	1.0815	0.1027	0.9788
0.047	15	150.7	83.6	1.0977	0.1131	0.9846
0.083	15	142.3	84.8	1.1624	0.1113	1.0511
0.026	15	187.3	83.6	1.2433	0.1271	1.116
0.048	15	187.3	84.0	1.2433	0.1273	1.116
0.081	15	185.1	83.6	1.2581	0.1264	1.132
0.108	15	177.6	84.9	1.3112	0.1248	1.186
0.0162	20	150.1	79.6	1.0994	0.0982	1.0012
0.0325	20	150.2	79.8	1.0986	0.0983	1.0003
0.061	20	142.6	80.0	1.1572	0.0964	1.0608
0.089	20	142.0	82.2	1.1593	0.1175	1.0418
0.120	20	138.1	83.2	1.1920	0.1168	1.0752
0.033	50	139.8	83.1	1.1775	0.0997	1.0778
0.080	50	173.5	86.0	1.3422	0.1191	1.223
0	-	157.1	83.6	1.1526	0.1305	1.0221
0.023	12	157.3	83.0	1.1511	0.1302	1.0209
0.045	12	158.4	81.7	1.1431	0.1298	1.0133
0.064	12	158.2	83.0	1.1446	0.1305	1.0141
0.076	12	157.7	83.5	1.1482	0.1307	1.0175
0.090	12	157.2	83.8	1.1519	0.1307	1.0212
0.118	12	152.1	84.5	1.2040	0.1288	1.0620
0.145	12	147.8	84.6	1.2251	0.1280	1.0971